DISS ETH NO. 19491

Non-invasive assessment of sensory and nociceptive processing in mice using functional MRI

A dissertation submitted to
ETH ZURICH

for the degree of
DOCTOR OF SCIENCES

presented by
SIMONE CLAUDIA BOSSHARD
Dipl. Natw. ETH, ETH Zürich

born January 29, 1982
citizen of Zürich, Switzerland

accepted on the recommendation of

Prof. Markus Rudin, examiner
Prof. Hanns Ulrich Zeilhofer, co-examiner
Prof. John N. Wood, co-examiner

2011

Table of Contents

Summary

Magnetic resonance imaging has become a powerful tool in both clinical and preclinical research to non-invasively assess brain structure and function. Its application to animals has opened new possibilities to perform longitudinal studies in order to investigate anatomical or functional plasticity of the brain e.g. after injuries of the nervous system. Functional MRI (fMRI) allows assessing activation of brain areas in response to a stimulus by measuring local changes of the vascular system associated with neuronal activation. fMRI is also playing an important role in pain research. Chronic pain is a major issue in our society and much research is done in order to reveal its underlying mechanisms and develop potent new drugs. (Functional) MRI provides a way to assess the network of brain areas involved in pain perception and processing, and to reveal potential changes associated with pathological pain. The method, originally applied in human studies, has been translated back to small animals, which allows performing basic research on animal models of different pain pathologies. Most of these studies have been performed in rats. In view of the many transgenic mouse lines available it would be advantageous to transfer the method to mice.

The establishment of mouse fMRI to assess sensory and nociceptive processing by measuring changes in blood oxygenation (BOLD, blood oxygen level dependent contrast) was one of the main goals of this thesis. In a first study described in Chapter 2, an electrical forepaw stimulation paradigm was implemented. The resulting changes in BOLD signal were assessed using a cryogenically cooled radiofrequency (RF) coil (CryoProbe) in a small-animal 9.4 T system. BOLD signal changes in response to four different stimulation amplitudes were measured using a gradient-echo echo-planar imaging (GE-EPI) sequence. The signal changes observed correlated well with the stimulation amplitude and were located in the brain areas associated with somatosensory and nociceptive processing. The BOLD signals were analyzed in terms of amplitude and signal decay to better understand the signal dynamics and its underlying mechanisms.

The forepaw stimulation paradigm has been used to assess the performance of the CryoProbe in comparison with a conventional room temperature (RT) coil for fMRI applications. The use of the CryoProbe yielded a gain in signal-to-noise ratio (SNR) as compared with the RT coil. This gain in sensitivity allows acquiring sequences with high spatial and temporal resolution, which are important prerequisites in small animal imaging. In addition to the comparison in terms of sensitivity, the influence of different shield surface temperatures on the BOLD signal and the cerebral blood volume (CBV) was investigated. The heated ceramic shield of the CryoProbe protects the mouse head from the cooled RF coil and can be adjusted to different temperatures. Four different temperatures in the range of 22-38 °C were analyzed and found to significantly influence baseline CBV and stimulus-induced BOLD signal changes.

The electrical stimulation paradigm was then applied to pharmacologically pretreated mice. The animals received forepaw injections of very low concentrations of the local anesthetic lidocaine prior to electrical stimulation. This pretreatment led to an increase in BOLD signal changes as compared with untreated mice. The detailed mechanisms of the lidocaine-induced hyperalgesia still remain unclear, but experiments using global cannabinoid-receptor 1 (CB_1) knock-out mice or a CB_1-blocking drug in wild type animals suggest an involvement of the CB_1 receptor.

Another application used electrical stimulation to investigate nociceptor-specific $Na_V1.7R^{-/-}$ mice. These mice are lacking a sodium channel important for the propagation of action potentials in nociceptors, leading to insensitivity to noxious stimuli. In the fMRI experiment, this led to a significant decrease of the BOLD signal in response to electrical stimulation as compared with wild type mice.

As electrical stimulation may not always be suitable to assess nociceptive processing due to reasons outlined in Chapter 6, we aimed at developing a strictly nociceptive stimulation. High (noxious) temperatures activate specific thermoreceptors located on C-fiber sensory afferents, rendering it a true physiological stimulus. The heat stimulation paradigm using infrared laser diodes with a temperature-controlling feedback loop was tested for 45 and 46

°C. Specificity of the paradigm for nociceptive signaling was demonstrated by pharmacological modulation of the response via TRPV1 receptor-mediated blockage of sodium channels. Combined administration of the TRPV1 agonist capsaicin and the lidocaine derivative QX-314 has been shown to induce a C-fiber specific block, inhibiting the transmission of activation elicited by noxious heat stimulation. In the fMRI experiments using thermal stimulation, this pretreatment led to an abolishment of the BOLD signal, demonstrating the nociceptive-specific action of the stimulation paradigm.

In summary, two stimulation paradigms to assess processing of innocuous and/or noxious peripheral input in mice using BOLD fMRI have been established. Both paradigms have been validated and applied to different models. The application of the CryoProbe allowed for sufficiently high SNR, temporal and spatial resolution to detect BOLD changes of a few percent in very small brain areas. This provides a tool for different applications to investigate pain processing in mouse models of different pain pathologies. The non-invasive nature of the method allows for longitudinal studies to follow changes in structure and/or function of the brain over time.

Zusammenfassung

Kernspintomographie (magnetic resonance imaging, MRI) ist ein modernes bildgebendes Verfahren, das eine immer wichtigere Rolle in der Diagnostik sowie in der klinischen und präklinischen Forschung spielt. Mittels starken Magnetfeldern und Radiofrequenz-Wellen werden magnetische Eigenschaften von Materie, z.B. von Wasser im Gewebe, erfasst, was die nicht invasive Untersuchung von Struktur und Funktion des Gehirns oder anderer Organe ermöglicht. Die Übertragung der Technik auf Tierexperimente eröffnet neue Möglichkeiten im Bereich der Grundlagenforschung. Sie erlaubt es, Veränderungen in Struktur oder Funktion des Gehirns z.B. nach Verletzungen des Nervensystems über längere Zeit im gleichen Tier zu verfolgen. Neuronale Aktivität im Gehirn kann mittels funktionellem MRI (fMRI) gemessen werden. Dabei werden lokale Änderungen des vaskulären Systems, die im Zusammenhang mit neuronaler Aktivierung stehen, gemessen. In der Schmerzforschung spielt fMRI eine wichtige Rolle, da es erlaubt, das Netzwerk von Hirnstrukturen, die durch einen Schmerzreiz aktiviert werden, zu ermitteln. Chronischer Schmerz ist ein medizinisches Problem von zunehmender Bedeutung unserer Gesellschaft, wobei es für viele pathologische Schmerzen noch keine zufriedenstellende Therapie gibt. Intensive Forschung bemüht sich, die Mechanismen, die für die pathologischen Schmerzen verantwortlich sind, aufzuklären und wirksame Medikamente mit geringen Nebenwirkungen dagegen zu entwickeln. (Funktionelles) MRI wird dabei eingesetzt, um mögliche Veränderungen der Hirnstruktur oder –funktion, die bei chronischen Schmerzen auftreten können, zu messen. Die Anwendung der Methode bei Kleintieren erlaubt es, Grundlagenforschung an verschiedenen Modellen für krankhafte Schmerzleiden zu betreiben. Bis jetzt wurden die meisten Studien an Ratten durchgeführt. Die Übertragung der Methoden auf die Maus wäre jedoch wichtig, um einen Nutzen aus den zahlreichen transgenen Mausmodellen zu ziehen.

Eines der Hauptziele dieser Arbeit bestand darin, ein zuverlässiges Stimulationsparadigma zu entwickeln, um damit die Schmerzverarbeitung in der Maus zu untersuchen. In einer ersten Studie stimulierten wir die Vorderpfote der Maus elektrisch. Die davon ausgelöste Aktivität im Hirn wurde über Änderungen der Blutoxygenierung (blood oxygen level dependent

contrast, BOLD) in einem MRI System mit 9.4 T Magnetfeldstärke gemessen. Um die Sensitivität zu steigern, wurde eine Tieftemperatur-Radiofrequenzspule (CryoProbe) verwendet. Die durch die Stimulation ausgelösten BOLD-Signaländerungen in den aktivierten Regionen korrelierten stark mit den verwendeten Stromstärken; die stärkste Stimulation löste die grösste Signaländerung aus. Die Signale traten zudem in den Hirnarealen auf, die bekannterweise in die Schmerzverarbeitung involviert sind. Um die Dynamik des Signals besser zu verstehen, wurde der zeitliche Verlauf der BOLD-Signaländerungen bezüglich der maximalen Amplitude und des Signalzerfalls analysiert.

Das entwickelte Stimulationsparadigma wurde gebraucht, um die Detektionsempfindlichkeit der CryoProbe mit der einer konventionellen Raumtemperatur-Spule zu vergleichen. In diesen Experimenten zeigte die CryoProbe eine wesentlich höhere Sensitivität, die mit einem besseren Signal zu Rauschen-Verhältnis einherging. Die erhöhte Sensitivität konnte eingesetzt werden, um die räumliche und zeitliche Auflösung im Vergleich zu der Raumtemperatur-Spule zu steigern, was bei Mausstudien von erheblichem Vorteil ist.

Die elektrische Stimulation wurde angewendet, um den Effekt von pharmakologischen Interventionen auf die Signaltransmission zu untersuchen. Den Mäusen wurde vor der Stimulation ein Lokalanästhetikum (Lidocain) in geringer Konzentration in die Pfote gespritzt. Entgegen der Erwartung führte dies zu einer erhöhten BOLD-Signaländerung, was auf eine Hyperalgesie (übermässiges Schmerzempfinden) hinweist. Die genauen Mechanismen, die zu dieser Hyperalgesie führten, sind noch nicht geklärt. Experimente mit Mäusen, denen der Cannabinoidrezeptor 1 (CB_1) fehlt, sowie Experimente, bei denen der CB_1-Rezeptor pharmakologisch blockiert wurde, lassen darauf schliessen, dass der CB_1-Rezeptor dabei eine Rolle spielt.

Genetisch veränderte Mäuse, bei denen die Expression eines Natriumkanals auf den Schmerzrezeptoren unterdrückt wurde, verspüren keinen Schmerz. Das Fehlen des Kanals hat zur Folge, dass die Signale nicht via Aktionspotenzial zu höheren Zentren der Schmerzmatrix weitergeleitet werden. In den fMRI Experimenten zeigten die genetisch

veränderten Mäuse eine verminderte BOLD Signaländerung als Reaktion auf die elektrische Stimulation. Diese Resultate bestätigen die Relevanz des elektrischen Stimulationsparadigma.

Da die elektrische Stimulation aus verschiedenen Gründen (s. Kapitel 6) nicht für alle Schmerzstudien geeignet ist, wurde eine thermische Stimulation entwickelt. Hohe Temperaturen aktivieren direkt Thermorezeptoren, die sich auf so genannten C-Fasern befinden. Dadurch erhält man einen physiologischen Stimulus. Die hohen Temperaturen wurden mit einem auf die Vorderpfoten gerichteten Laserstrahl erzielt und über ein automatisches Regelsystem kontrolliert. Die Stimulation wurde bei 45 und 46 °C durchgeführt und ihre Spezifität pharmakologisch getestet. Frühere Studien haben gezeigt, dass Capsaicin, ein Agonist der TRPV1-Rezeptoren, zusammen mit dem Lidocainderivat QX-314 spezifisch die C-Fasern hemmt. Die aktivierten und geöffneten TRPV1-Rezeptoren ermöglichen das Eindringen von QX-314 in die Zellen, wo es die Natriumkanäle blockiert. In der fMRI-Studie brachte die Verabreichung der zwei Substanzen die BOLD-Signaländerung zum Verschwinden, was bestätigt, dass durch die thermale Stimulation spezifisch die C-Fasern aktiviert werden.

In der vorliegenden Arbeit wurden zwei Stimulationsparadigmen entwickelt, die es erlauben, Schmerzverarbeitung bei Mäusen mittels fMRI zu untersuchen. Beide Stimulationen wurden validiert und für unterschiedliche Modelle angewendet. Durch die Verwendung der CryoProbe waren die Messungen genügend sensitiv, um Signaländerungen von nur wenigen Prozenten in kleinen Hirnarealen zu messen.

1. Introduction

1.1 Magnetic Resonance Imaging (MRI)

Historical Overview

Magnetic resonance imaging (MRI) is a relatively new imaging technique which founds on the independent discovery of the nuclear magnetic resonance phenomenon by Edward Purcell (Harvard University) and Felix Bloch (Stanford University) in 1946 [1, 2]. This discovery led to the development of NMR spectroscopy, which soon became an important method to study the structure of chemical compounds. Bloch and Purcell were awarded the Nobel Prize in Physics in 1952.

In 1966, Richard Ernst found a way to increase the sensitivity of NMR by replacing the traditionally used slow passage NMR of sweeping a radiofrequency wave across the spectrum, by Fourier NMR using short intense pulses [3]. A few years later, Ernst developed a technique that enabled high resolution, two-dimensional NMR spectroscopy of large molecules. For his achievements in NMR, Richard Ernst was awarded the Nobel Prize in Chemistry in 1991.

Around the same time, Paul Lauterbur moved from the single dimension of NMR spectroscopy to two-dimensional first MR images by introducing gradients into the magnetic field, allowing deriving spatial information about an object [4]. Sir Peter Mansfield then further processed the applications of gradients in the magnetic field. He also developed a way to mathematically analyze the MR signals which enabled fast generation of images based on the MR signal [5]. Following this, he developed the echo-planar-imaging technique (EPI), which allowed fast image acquisition and is still frequently used in today's research. Lauterbur and Mansfield received the Nobel Prize in Physiology or Medicine in 2003.

It was not until 1992, when functional MRI (fMRI) was developed [6, 7], a technique abundantly used nowadays both in research and medical diagnostics, allowing assessing the function of various regions of the brain.

Imaging Modalities

Today, MRI is an indispensable tool in diagnostics and biomedical research in both humans and animals. It is one of many non-invasive imaging modalities available, each of it with its advantages and disadvantages. The oldest biomedical imaging technique is X-ray imaging, which was further developed into computed-tomography (CT), the first modality to give high resolution and 3D images from inside a body. Due to its relatively low costs, high tissue contrast for fat, lean mass and bones, and high spatial resolution, it is one of the most popular imaging modalities used, despite its harmful ionizing radiation. Another imaging technique is positron emission tomography (PET), which detects radioactively labeled tracers that are incorporated into a biologically active molecule, diffuse through tissue or bind to a specific target. Despite the relatively poor spatial resolution, PET is a frequently used diagnostic tool, particularly in cancer diagnostics. The highly specific tracer-target interaction yields a high sensitivity. MRI was first known and used for its high soft tissue contrast. Due to the different properties of different tissues, the contrast can be adapted for best display of the target tissue. However, the technique has developed tremendously over the past 20 years, allowing not only to obtain anatomical and structural information of different parts of the body, but also providing information about (brain) function (fMRI), the vascular system (angiography), tissue perfusion (perfusion MRI), blood or tissue oxygenation (BOLD fMRI), diffusion tensor imaging (DTI) for measuring diffusion and depicting fiber tracts, and differences of tissue elasticity (MR elastography). Continuing research will contribute to further development of new techniques and refinement of existing techniques. In MRI, patients are not subjected to harmful radiation or substances; instead they are placed in a strong static magnetic field.

Basic Principles of MRI

The underlying physical property of the NMR and MRI technique is the nuclear magnetic resonance phenomenon. It describes the property of some nuclei, which, when placed in a magnetic field, may absorb energy from an applied electromagnetic pulse in the radiofrequency range and re-emit this energy at a specific resonance frequency in order to return back to the original energy state. This phenomenon is based on quantum physics principles, but the basics can also be explained by classical physics.

Every atomic nucleus is composed of small positively charged particles called protons and neutral particles called neutrons. Nuclei with odd proton and/or neutron numbers possess a property called 'nuclear spin' or simply 'spin', which can be imagined as a rotation around an axis with a certain frequency. The nuclear spin is associated with a magnetic moment, i.e. the nuclei behave like tiny magnets. The most abundant nuclear species possessing a spin is the hydrogen nucleus consisting of one proton only. When placed within a static magnetic field B_0, the spins align in the direction of the magnetic field. However, some will align with the field (parallel), while some align against the field (antiparallel), which corresponds to two different energy states. The magnetic moments of the protons in the different states will cancel each other out, nevertheless, a slight excess (approx. 10^{-6} at 1 T and 37 °C) will align with the B_0 field, leading to a net magnetization called longitudinal magnetization. The excess number of parallel protons increases proportional with increasing B_0.

All spins regardless of their energy state precess around the axis of the B_0 field with a certain frequency, which is proportional to B_0 and can be described by the Larmor equation:

$$\omega_{\emptyset} = \gamma \cdot B_0$$

ω_0 [Hz, MHz] is the Larmor or resonance frequency, B_0 [Tesla, T] the strength of the static magnetic field and γ the gyromagnetic ratio, a constant unique to every atom. For protons, the gyromagnetic ratio is 42.5 MHz/T.

Longitudinal magnetization cannot be measured by the receiver coils as it is aligned parallel to the B_0 field; to become measurable, the magnetization in z-direction needs to be forced

into the x-y-plane, where it precesses around the static field. This is accomplished by exciting the spins using a radiofrequency (RF) pulse at the resonance frequency. They absorb the energy and change to the higher energy level, corresponding to the antiparallel state, leading to a decrease of the net longitudinal magnetization due to a cancelling-out effect. In addition, the RF pulse synchronizes the spins in a way that they start to precess in phase around the static magnetic field, leading to a transverse magnetization vector oriented perpendicular to the B_0 field. The transverse magnetization induces an electrical current in a detector coil, resulting in the MR signal.

Once the RF transmitter is switched off, exponential recovery of longitudinal magnetization and exponential decay of transverse magnetization occur. These processes are commonly described as the following relaxation processes:

1) **T_1 (spin-lattice) relaxation**: T_1 refers to a time characteristic for the spins to realign with the z-axis, returning to the lower energy level (parallel state). As the spins do not realign simultaneously, longitudinal magnetization increases gradually. The energy released by this process is transferred to the surrounding tissue (lattice), reestablishing thermal equilibrium. The T_1 value is characteristic for different kinds of tissue, and depends on the B_0 field strength.

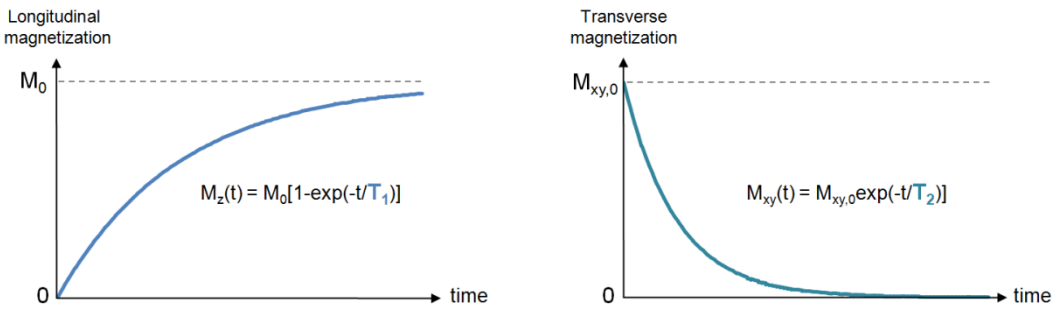

Figure 1-1: Relaxation rates of longitudinal magnetization ($1/T_1$) and transverse magnetization ($1/T_2$).

2) **T_2 (spin-spin) relaxation**: Interactions between neighboring spins and fluctuating changes in magnetic susceptibility lead to dephasing of the spins, inducing a decrease of transverse magnetization, resulting in an overall signal loss. The T_2 value is unique for every kind of tissue and determined predominantly by its chemical environment, while it is largely independent of the magnetic field strength. However, in reality, the transverse magnetization decays much faster than described by T_2. The faster decay is due to inhomogeneities of the main magnetic field, which may be produced by the measured tissue placed within the field. This relaxation rate, which is a more accurate measure of the signal decay, is named T_2*.

The spatial information of an object is obtained by applying gradient fields to the B_0 field. The frequency encoding gradient leads to small differences in the strength of the magnetic field as a function of the position, hence changing the precession frequencies of the spins at different locations. Depending on their position, they will therefore emit signals at different frequencies. A second gradient, called phase-encoding gradient, applied perpendicular to the frequency encoding gradient, brings the spins that precess with the same frequency, out of phase, the phase shift depending on their location in the second dimension. Multiple values of the phase encoding gradient are required to record an image. These doubly encoded signals are mathematically processed by Fourier transformation, which analyzes the signals with regard to frequency and phase, allowing the allocation of the signal intensity at specific locations in two dimensions, allowing for reconstruction of the image [8, 9].

Not only protons can be used for imaging, but any nucleus that possesses a spin and contains an odd number of protons and/or neutrons. However, protons (hydrogen nuclei) are most suitable for MRI since hydrogen is very abundant throughout the body, and it has one of the highest gyromagnetic ratios of all nuclei, i.e. yielding a high sensitivity per nucleus. Nevertheless, a lot of research is also carried out on non-proton NMR.

1.2 functional MRI

Functional MRI (fMRI) allows going beyond anatomical imaging by assessing physiological functions of the body, including e.g. dynamic cardiac imaging or perfusion imaging. In general, however, fMRI refers to measurements of local brain activation as a response to some kind of stimulus.

Physical and Physiological Background

Functional readouts are based on a process called neurovascular coupling, which describes the close coupling between neurons, astrocytes and the cerebrovascular system. Despite the relatively small size of the brain (2 %) compared to the rest of the body, it dissipates 20 % of total body oxygen and 25 % of total body glucose consumption. Neuronal activation, which comprises electrical signal transmission within the cell and chemical signal transmission between the cells, requires energy. As neurons are highly specialized cells, they cannot store glucose, therefore rely on external supply of glucose and oxygen.

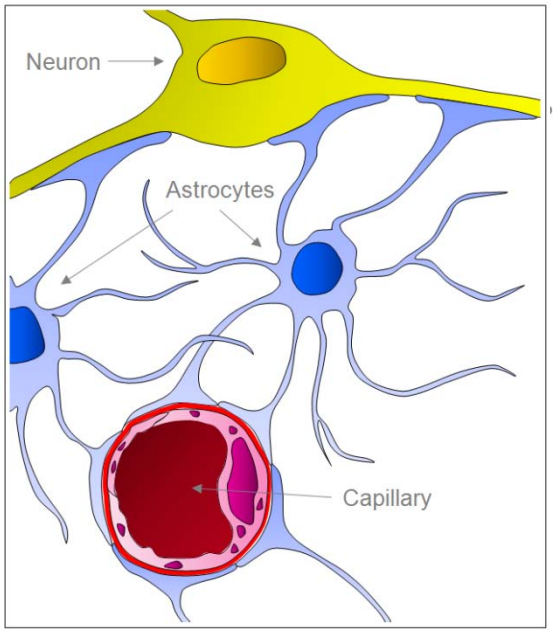

Figure 1-2: The neurovascular unit. Capillaries deliver oxygen and glucose to the neurons via the astrocytes. Changes in neuronal activity lead to increased cerebral blood flow and volume, which can be assessed by functional imaging. Adapted from [10].

This renders the central principle underlying the functional imaging techniques, which visualize local changes in brain activity by measuring changes in blood flow and energy metabolism (i.e. hemodynamic response) [11]. Therefore, these imaging techniques only provide an indirect readout of the local brain activity by measuring a linked physiological or metabolic process. The exact association between neuronal activation and changes in blood flow and energy metabolism are still not fully understood (for review and controversial points see: [12-15]).

Cerebral Blood Flow (CBF)

The basic functions of CBF regulation and thus neurovascular coupling was proposed by Roy and Sherrington in 1890, postulating a local increase in CBF as a response to neuronal activation [16]. CBF delivers glucose and oxygen used for local energy metabolism and transports CO_2 away from the cells. It is controlled by regulation of microcirculation and changes accordingly, in order to adapt to the varying demands of energy and oxygen by the neurons. CBF can be assessed by two different methods using fMRI: arterial spin labeling (ASL) and bolus tracking. Bolus tracking requires the intravenous administration of a contrast agent (CA), of which the first passage through the vascular system is analyzed to yield information about local blood flow values [17]. ASL does not require the application of an exogenous CA; instead the blood magnetization is changed at a specific point of an artery, inducing a change in signal intensity in the measurement located downstream of the labeling site, which is directly proportional to the blood flow. This procedure provides a repeatable, completely non-invasive technique for assessing CBF [18].

Cerebral Blood Volume (CBV)

Increases in CBV are also associated with neuronal activity and are usually assessed by injection of an exogenous CA, generally based on iron-oxide particles. Iron-oxide based CAs induce local inhomogeneities of the magnetic field, leading to a drop of signal in T_2-weighted images. After injection of the CA, it will recirculate in the vascular system; after a while, depending on the distribution volume and the clearance rate, its concentration will reach a

steady state, i.e. will change only very slowly over time. Hence, any change in signal intensity can be attributed to a change in the local blood volume, rather than to a change in CA concentration. At steady state, a baseline measurement is acquired before applying a stimulus which will lead to local changes in CBV. With increasing CBV, the amount of CA increases in this area, yielding a decrease in signal intensity. CBV measurements are popular to assess brain function in animals [19-25]. However, the method is not in clinical use due to the lack of approval of the CAs for this application by the regulatory authorities.

Blood Oxygenation Level Dependent (BOLD) Contrast

BOLD contrast, first described by Ogawa et al., is based on deoxygenated hemoglobin (dHb) as an endogenous CA [26]. In 1936, Pauling discovered the paramagnetic properties of dHb, in contrast to the diamagnetic properties of oxygenated hemoglobin (Hb)[27]. Paramagnetic substances such as dHb induce local field inhomogeneities, which lead to susceptibility differences between the dHb-containing compartments and the surrounding tissue. The inhomogeneities induce dephasing of the spins, shortening the T_2 relaxation time and leading to faster signal decay. Diamagnetic substances on the other hand (i.e. Hb), do not influence the signal decay. Upon neuronal activation, there is an increase of CBF, which exceeds the demands by the increased cerebral metabolic rate of oxygen ($CMRO_2$). This mismatch leads to an increase in blood oxygenation at the veins and capillaries. A decrease in the relative dHb concentration reduces field inhomogeneities and dephasing, leading to an increase of the MR signal intensity. BOLD fMRI sequences are T_2*-weighted, designed to pick up the BOLD signal increase as a response to neural activation.

Two years after Ogawa's discovery, the first functional studies were published, using dHb as an endogenous contrast agent [6, 7]. This introduced a new area of functional imaging, and today, BOLD fMRI is probably the most frequently used method for functional brain mapping in both humans and animals. BOLD fMRI is relatively easy to implement and does not depend on exogenous contrast agents. For more detailed information and reviews see [28-30].

1.3 fMRI in Small Animals

Sensitivity

The development of high-field MR systems has made this technique available for small animal research. Higher B_0 field strengths are one of several ways to increase the signal-to-noise ratio (SNR) needed in order to image small animals, usually one order of magnitude smaller than humans, with sufficiently high spatial and temporal resolution [31]. However, moving to higher field strengths increases T_1 relaxation times while T_2 and T_2^* relaxation times decrease, which may lead to longer acquisition times. In addition, susceptibility artifacts will appear more often and profoundly. Alternative methods to improve SNR such as increasing the voxel size or data averaging will impair spatial or temporal resolution.

A different strategy to increase the SNR is lowering the noise level instead of increasing the signal. Noise in fMRI can have three sources: i) physiological noise, which originates from the subject, ii) thermal noise coming from the receiver electronics, and iii) static sample noise. For human fMRI at field strengths of 3 T and higher, physiological noise is the largest contributor to the total noise [32-34]. However; in small animal fMRI, the sum of static and physiological noise is of comparable order as the noise from the receiver electronics. Therefore, a successful approach to increasing the SNR was the development of cryogenically cooled RF coils [35, 36]. All studies in this thesis were therefore conducted using a prototype 400 MHz cryogenic RF probe, operating at a temperature of 30 K, which today is commercially available (CryoProbe, Bruker Biospin AG, Fällanden, Switzerland).

Physiology and Anesthesia

Additional challenges when imaging small animals, such as mice and rats, is the maintenance of stable physiology and the choice and control of anesthesia, as animals are commonly anesthetized.

Stable physiology is of great importance as the detection of brain activation is based on a hemodynamic readout. In particular, the hemodynamic response is influenced by body temperature [37] and partial pressure of blood gases. Monitoring of body temperatures and

blood gas levels are therefore inevitable; blood gas levels also indicate how well ventilated the animal is. Endotracheal intubation and a well adjusted mechanical ventilation of the animal ensure stable arterial oxygen saturation and pCO_2 levels, an important prerequisite for animal fMRI. Application of a neuromuscular blocking agent and stereotactic fixation of the head prevent artifacts in MR images related to movement of the object and therefore help reducing physiological noise.

Anesthesia is a recurring issue in animal imaging, since any type of anesthesia will affect the neuronal or hemodynamic response to a stimulus. It is in the nature of anesthetics to render the animal unconscious and induce amnesia, muscle relaxation and analgesia [38]. It is therefore important to consider several points, before deciding on a particular anesthetic: 1) suitability for longitudinal studies; 2) receptor system(s) involved in anesthetic action; and influences on the 3) neuronal system, 4) neurovascular coupling, and 5) vascular system.

One of the most frequently used anesthetic in fMRI is α-chloralose, as it fully preserves neurovascular coupling and does only act slightly analgesic [39]. However, it is severely harmful to rodents and therefore not suitable for longitudinal studies, which somehow counteracts the idea of non-invasive imaging. Another anesthetic, which allows full recovery of the animal and which is becoming increasingly popular in fMRI studies, is isoflurane. It is an inhalation anesthetic with some analgesic effects and some influence on the neurovascular coupling; however, if kept at low levels and well controlled, it allows to accomplish robust and reproducible fMRI studies [19-21, 40-48]. For a detailed review on animal anesthesia used for fMRI consult [49].

1.4 Nociception and Pain

Pain comes from the Latin word *poena*, signifying penalty or punishment. It was probably the French philosopher and scientist René Descartes (1596-1650) who first described a concept of a pain pathway: *"If for example fire comes near the foot, the minute particles of this fire (…) have the power to set in motion the spot of the skin (…) and by this means pulling upon the delicate thread which is attached to the spot on the skin, they open up at the same instance the pore against which the delicate thread ends, just as by pulling at the end of a rope one makes to strike at the same instant a bell, which hangs at the other end."* (R. Descartes, Traité de l'Homme, 1662). Today, pain is defined as "… an unpleasant sensory and emotional experience associated with actual or potential tissue damage …" by the IASP (International Association for the Study of Pain). Nociception, on the other hand, refers to signals arriving at the central nervous system (CNS), resulting from nociceptor activation, providing information about potential or real tissue damage.

Figure 1-3: Illustration of the pain pathway in René Descartes' *Traite de l'homme*, 1662.

Pain does not equal pain; instead, several distinct types of pain exist. **Nociceptive pain** is an early-warning, physiological protective system, which is inevitable to detect damaging or noxious stimuli. This kind of pain is essential for survival and the lack of it is a serious problem. Rare genetic disorders leading to insensitivity to pain result in self-mutilation, amputations, joint deformities and early death [50, 51]. **Inflammatory pain** also serves to protect the body by increasing the sensitivity after tissue damage. Hypersensitivity protects the injured site by reducing the risk of further damage by preventing contact with, or movement of the injury. The third type of pain is not protective but maladaptive and is due to an abnormal function of the nervous system. **Pathological pain** can occur after lesions of

the nervous system (neuropathic pain), but also appears in patients without neural damage (dysfunctional pain). The underlying mechanisms of pathological pain are still not fully understood, but are most likely due to amplified sensory signaling in the CNS [52, 53]. Functional imaging may provide a tool to gain further insight to these mechanisms, as it already revealed structural changes in the brain associated with chronic pain [54].

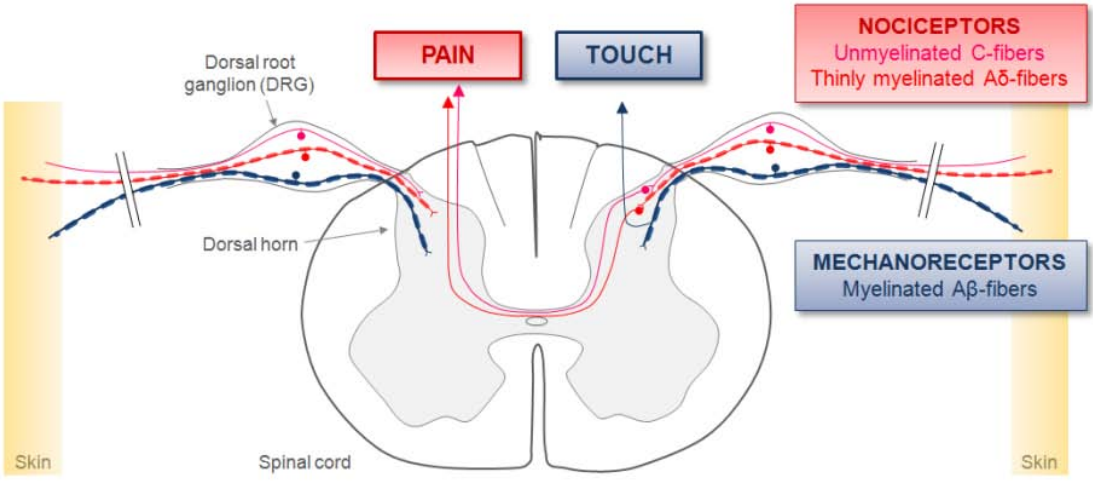

Figure 1-4: Primary sensory afferents transmit information from the peripheral tissues to the spinal cord. Their cell bodies are located in dorsal root ganglia (DRG). Large diameter, myelinated Aβ-fibers are involved in non-noxious sensation, transmitting information via the dorsal column pathway. The nociceptors, small diameter unmyelinated C-fibers or thinly myelinated Aδ-fibers, detect noxious stimuli, which are relayed to the brain via the spinothalamic tract.

The perception of nociceptive pain starts at specialized, primary afferent high-threshold neurons with free nerve endings, the nociceptors. Noxious information is transmitted by two types of small-diameter neurons, the thinly myelinated Aδ-fibers and to a greater part by the unmyelinated C-fibers. However, not all C- and Aδ-fibers are nociceptors, as some of them also transmit signals from innocuous mechanical, warm and cold stimuli. The cell bodies of all primary afferents are located in the dorsal root ganglion (DRG), from where one axon innervates peripheral tissue and reacts to peripheral stimuli, whereas another axon projects to

the dorsal horn of the spinal cord to relay information to the CNS. The basic function of nociceptors is to transmit information about damaging stimuli to higher-order neurons in the spinal cord. Many subclasses of nociceptors have been described, responding to cold, warm, noxious heat, mechanical stimulation or being multimodal [55-58].

Many receptors and ion channels responding to specific sensory stimuli have been identified in the past 30 years. Particularly the transient receptor potential (TRP) channel family plays an important role in nociception, particularly in the detection of heat and cold stimuli (for reviews: [59, 60]). The most prominent member of the TRP family is the polymodal vanilloid receptor 1 (TRPV1, VR1), also known as the capsaicin receptor. TRPV1 receptors are directly activated by capsaicin, the pungent ingredient of chili peppers, noxious heat, spider toxins and can be modulated by low pH [61, 62]. They are mainly associated with a subgroup of C-fibers that respond to noxious heat [63]. Besides TRPV1, there are numerous other receptors and ion channels involved in the perception of sensory stimuli; a summation of all inputs from the different types of primary sensory afferents generates the pain sensation.

Pain perception, however, is not an absolute value, but can be enhanced or diminished by many factors, such as attention, expectations, emotional state, anxiety, or associated past experiences and memories [64]. Neuroimaging techniques have revealed a so called 'pain matrix' of brain areas which are consistently, but not exclusively, activated upon noxious stimulation. These areas include the primary and secondary somatosensory cortices (S1, S2), anterior cingulated cortex (ACC), insular cortex (IC), prefrontal cortex (PFC), thalamus, periaqueductal gray (PAG), basal ganglia, cerebellum and the amygdala [65, 66], and these data acquired with functional imaging are consistent with anatomical studies [67, 68].

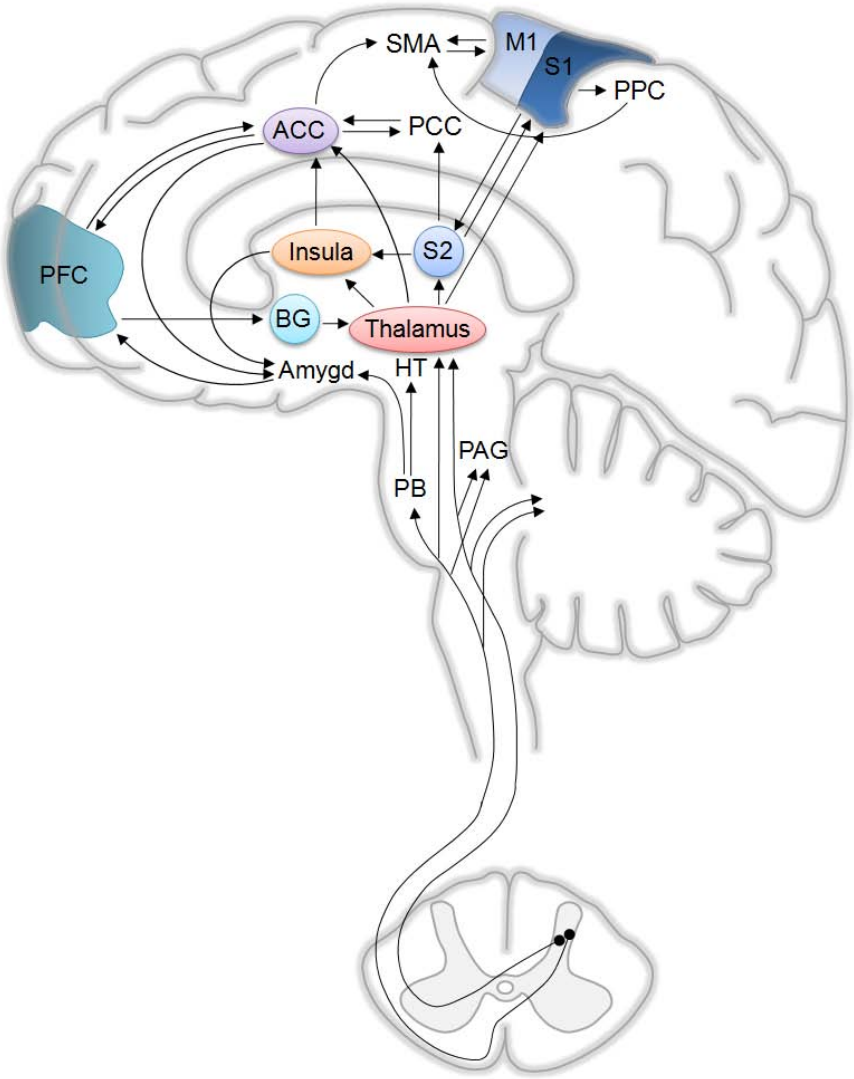

Figure 1-5: Schematic representation of the human brain, illustrating the ascending pain pathways and regions involved in pain processing ('pain matrix'). S1: primary somatosensory cortex; S2: secondary somatosensory cortex; M1: primary motor cortex; ACC: anterior cingulated cortex; PCC: posterior cingulated cortex; SMA: supplementary motor area; BG: basal ganglia; PFC: prefrontal cortex; HT: hypothalamus; PB: parabrachial nuclei; PAG: periaqueductal gray; PPC: posterior parietal cortex. Adapted from [67].

The pain matrix contains brain areas not only involved in nociception, but also in emotion and cognition, and they overlap with brain sites activated by placebo effects or opioids [69]. The perception of pain is mediated by interaction of all these regions, and modulated by a descending modulatory circuit, which receives input from different areas. The opioid-

sensitive descending modulation contributes to pain relief, as observed with the placebo effect, but has the ability to facilitate pain as well. Many centrally acting pain-relieving drugs activate or mimic the descending modulatory pathways, in order to diminish the pain experience (for review: [64]).

Many of these insights have been gained through neuroimaging studies which are becoming increasingly important in pain research (for review on neuroimaging of pain: [54]). Establishment of robust fMRI protocols to assess nociception in animals will allow getting further insight to different aspects of normal and pathological pain states; and is particularly interesting with regard to the many transgenic mouse models available.

Currently, rats are still the dominating species used for fMRI pain research, but with the availability of higher magnetic fields, mice are becoming increasingly popular. Nevertheless, only a few mouse studies have been published so far, most of them focusing on the methods used, and only to a lesser extent on biological applications and mechanisms [46, 70-72]. Rat fMRI, on the other hand has been used extensively to analyze many different aspects related to pain processing, including hyperalgesia [73], noxious and/or innocuous stimulation [25, 74-80], effects of stroke [21, 24], effects of different anesthetics [44, 81-84], nociceptive processing in the spinal cord [85-87], and functional connectivity and reorganization [47, 88, 89]. The application of these techniques to mice would be very promising in order to test different transgenic models of pathological pain.

1.5 Aim of the Thesis

The goals of the current work were the establishment and application of robust BOLD fMRI paradigms for mice. This comprised: 1) Developing and implementing robust BOLD fMRI protocols to assess brain responses to somatosensory and noxious stimulation. 2) Application of these protocols to different transgenic mouse models or to wild type mice subjected to pharmacological treatment.

Functional imaging has become an important tool in pain research to better understand the mechanisms underlying pathological pain. Non-invasive BOLD fMRI to measure nociception in rats has been well established in different labs [47, 48, 90, 91]. However, robust BOLD fMRI studies in mice are still sparse, but of great interest in view of the many transgenic mouse lines available.

Therefore, the first part of this thesis was dedicated to establish an electrical forepaw stimulation paradigm for mice at a 9.4 T scanner using the CryoProbe. This allowed for sufficiently high SNR, temporal and spatial resolution, to monitor BOLD signal changes of a few percent in small brain areas. An important aspect, beside the challenges of setting up a suitable fMRI protocol, was the tight control and maintenance of stable physiology of the mouse. This is critical for consistent BOLD signal readouts, since the technique relies on a well functioning hemodynamic system.

Two stimulation paradigms were developed to address questions related to somatosensory and nociceptive processing in mice. Repetitive stimulations of one paw, corresponding to a block design of stimulation and resting phases, were implemented to allow for statistical analyses based on voxel-by-voxel correlation. Prerequisites for the development of an applicable stimulation paradigm were robustness of the signal, high reproducibility, low inter-individual variability and a BOLD signal change which scaled with stimulus strength.

Electrical stimulation was performed at different amplitudes, ranging from innocuous to noxious, in order to obtain a 'dose-dependent' response. Once the paradigm was well established, we compared the performance of the 400 MHz CryoProbe to a room temperature (RT) coil of similar dimensions. This comparison has been performed earlier by evaluating phantom and anatomical data [36], while in this study we investigated the gain of sensitivity relevant for fMRI applications. In addition, we analyzed the effect of different temperatures of the ceramic shield of the coil, which is in direct contact with the mouse head, and its effect on BOLD signals and CBV.

The second part of this work was focused on application of the electrical stimulation paradigm to pharmacologically treated wild type mice and to different transgenic mice.

In order to establish a different stimulation paradigm, the last part of the thesis was dedicated to the development and implementation of a heat stimulation paradigm, using infrared laser diodes. Heat is a physiological stimulus which directly activates specific thermoreceptors on the primary afferents. It may therefore be more meaningful for certain applications than the electrical stimulation. The heat paradigm, with a temperature-controlling feedback-loop, was tested for two different temperatures. The specificity of the paradigm was tested using pharmacological interventions.

2. Assessment of Brain Responses to Innocuous and Noxious Electrical Forepaw Stimulation in Mice Using BOLD fMRI

2.1 Introduction

Processing of noxious stimuli involves different levels and structures of the neural system. In spite of substantial progress in understanding the molecular mechanisms underlying pain, many aspects are still poorly understood. Genetically engineered mouse lines displaying altered or pathological pain states may help to elucidate the physiological and molecular basis of normal and pathological pain processing [92-95]. Classically, sensory responsiveness in animals is characterized using behavior tests such as the hot plate, von Frey filaments or tail flick test [96]. These analyses, however, depend on the skills of the experimenter and require undisturbed motor function of the animal. Electrophysiological recordings of neuronal activity provide high spatial and temporal resolution. However, the method is invasive and does not allow recording signals over extended brain areas in a limited time period. An objective readout of neuronal signal processing that is non-invasive, independent of the observer performance and capable of covering the entire brain would be highly desirable. Functional magnetic resonance imaging (fMRI) has been widely used to assess changes in brain activity evoked by noxious stimuli. Noxious-evoked activation patterns revealed by fMRI correspond well with the structures of the pain processing pathway both in humans and animals [97-101]. There are two peripheral nerve types which process sensory input: low threshold fibers, mainly Aβ, primarily mediate touch, while high threshold fibers, mainly Aδ and C, conduct nociceptive signals [75]. The response to peripheral sensory or noxious stimulation in rats has been studied in depth [48, 90, 91]. In contrast, only few fMRI studies in mice using electrical stimulation paradigms have been reported to date [70-72, 102]. This is mainly due to experimental challenges related with the small size of mice, putting high demands on spatial resolution and thus sensitivity. Another challenge for robust fMRI

Published article: *"Assessment of Brain Responses to Innocuous and Noxious Electrical Forepaw Stimulation in Mice Using BOLD fMRI"*; Simone C. Bosshard, Christof Baltes, Matthias T. Wyss, Thomas Mueggler, Bruno Weber, Markus Rudin; PAIN, 151 (2010) 655–663.

measurements in mice is the maintenance of stable physiological conditions. While human fMRI experiments are carried out in awake subjects, the large majority of animal fMRI studies are performed in anesthetized animals. Therefore, anesthesia should neither interfere with brain activity nor act analgesic when investigating the response to noxious stimulation paradigms. Unfortunately, there is no such ideal anesthetic suitable for longitudinal studies e.g. for studying functional changes over time. In this work we used isoflurane, the advantages of which are ease of administration and controlled dosing. Despite these challenges, the development of robust mouse fMRI protocols is highly desirable for investigating mechanistic aspects of signal processing under normal and pathological conditions.

The aim of this study was to develop a reliable stimulation paradigm to analyze the somatosensory and nociceptive system in mice under isoflurane anesthesia. The high sensitivity of a cryogenic surface coil enabled detailed analysis of the BOLD response in activated brain regions elicited by electrical stimulation of the mouse forepaw as a function of time. BOLD signal intensities were found to correlate well with the amplitudes of the electrical stimulation applied. The quantitatively assessed dynamics of the temporal profile of the BOLD response yielded further insight into the hemodynamic response to electrical stimulation.

2.2 Materials and Methods

Animal Preparation

All experiments were performed in accordance with the Swiss law of animal protection. 15 female C57Bl/6 mice weighing 22 ± 3 g were anesthetized with Isoflurane (induction 2-3 %, maintenance 1.2 % in a 70 % air – 30 % oxygen mixture; Abbott, Cham, Switzerland), endotracheally intubated and mechanically ventilated throughout the entire experiment to ensure stable physiology (90 breaths/minute, respiration cycle: 25 % inhalation, 75 % exhalation; Maraltec, Alfos Electronics, Biel-Benken, Switzerland). Animals were paralyzed

by intravenous (i.v.) administration of a neuromuscular blocking agent (Pancuronium bromide, 1.0 – 1.5 mg/kg; Sigma-Aldrich, Steinheim, Germany), which avoided interference by spontaneous breathing and prevented movement artifacts during the fMRI experiments despite the low isoflurane levels. A rectal temperature probe (MLT415, AD Instruments, Spechbach, Germany) was inserted to keep the animal at 36.5 ± 0.5 °C. Body temperature was maintained using a warm-water circuit integrated into the animal support (Bruker BioSpin AG, Fällanden, Switzerland). A transcutaneous electrode (TCM4, Radiometer, Copenhagen, Denmark) was placed on the shaved upper hind limb of the mouse to measure blood gas levels (pCO_2). In some animals, heart rate and blood oxygenation were monitored using a MR-compatible infrared sensor (MouseOx® Pulse Oximeter, Starr Life Sciences, Oakmont, PA, USA). For accurate and reproducible positioning, the head of the animals was fixed with stereotactic ear bars and eye cream was applied to prevent the eyes from becoming dry. For the electrical stimulation a pair of needle electrodes (Genuine Grass instruments, West Warwick, USA) was inserted subcutaneously into the distal and proximal end of the palm of each forepaw with a distance of 2-3 mm between the two needles (Fig. 2-1). The identical set-up and parameters (1.5 mA) were used to stimulate the hind paw of four animals.

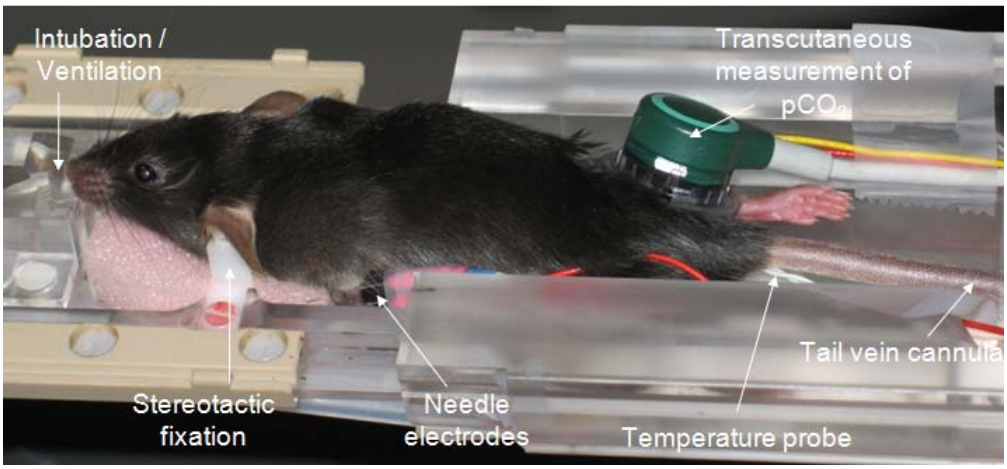

Figure 2-1: Mouse preparation and monitoring for fMRI experiments, using electrical forepaw stimulation.

The entire experiment lasted approximately 2 hours, of which 20 min were used for preparation of the mouse, and the remaining time was used for acquiring fMRI data. The mice were anesthetized throughout the duration of the experiment. Animals were used for more than one experiment.

MRI Equipment and Sequences

All MRI experiments were performed on a Bruker BioSpec 94/30 small animal MR system (Bruker BioSpin MRI, Ettlingen, Germany) operating at 400 MHz (9.4 Tesla). For signal transmission and reception a commercially available cryogenic quadrature RF surface probe (CryoProbe), consisting of a cylinder segment (180° coverage, radius = 10 mm) and operating at a temperature of 30 K was used (Bruker BioSpin AG, Fällanden, Switzerland) (for detailed information see [36]). The ceramic outer surface of the coil touching the mouse head was kept at 30 °C using a temperature-controlled heating device.

Anatomical reference images in coronal and sagittal directions (slice orientations are given using the nomenclature of the mouse brain atlas [103]) were acquired using a spin echo (Turbo-RARE) sequence with the following parameters: field-of-view (FOV) = 20 x 20 mm^2, matrix dimension (MD) = 200 x 200, slice thickness (STH) = 0.5 mm, interslice distance (ISD) = 1.0 mm, repetition delay T_R = 3500 ms, echo delay T_E = 13 ms, effective echo time $T_{E,eff}$ = 39 ms, RARE factor (number of echoes sampled for each excitation) = 32, and number of averages (NA) = 1. Subsequently, the slices for the fMRI experiment were planned on the anatomical reference image and BOLD fMRI data were acquired using a gradient-echo echo-planar imaging (GE-EPI) sequence with the following parameters: Five coronal slices covering a range of 2 to 5 mm anterior to the interaural line were recorded with FOV = 23.7 x 12.0 mm^2, MD = 90 x 60 (acquisition) and 128 x 64 (reconstruction) yielding an in-plane resolution of 200 x 200 μm^2, STH = 0.5 mm, ISD = 0.7 mm, T_R = 2500 ms, T_E = 8.5 ms, and NA = 3 resulting in an image acquisition time of 7.5 seconds. The individual sections comprised the forelimb and hind limb areas of the somatosensory and insular cortices, and the thalamus [103]. An fMRI experiment consisted of 112 repetitions and

lasted 14 min, except for the group of 2.0 mA, where the acquisition consisted of 96 repetitions and lasted 12 min.

Electrical Stimulation Paradigm

Electrical pulses of 0.5 ms duration at a frequency of 3 Hz were applied. Current amplitudes were 0.5 mA (n = 8 animals), 1.0 mA (n = 8), 1.5 mA (n = 7), and 2.0 mA (n = 8) [104]. The stimulus strength is determined by the local current density (electric current per unit area of cross section), which itself depends on the placement of the electrodes. Current thresholds for noxious stimulation were estimated from an experiment on the hairy skin of the wrist of a volunteer with analogous electrode placement as in mice (distance between electrodes). Stimulation amplitudes of 1.5 and 2.0 mA were experienced as being painful, while the amplitude of 0.5 mA was clearly innocuous. Although innervation of human and mouse skin may differ, a noxious threshold in the range of stimulation amplitude of 1.0 mA appears reasonable.

The stimulation paradigm consisted of a block design starting with a resting period of 120 seconds (baseline) followed by 60 seconds of stimulation. This series was repeated four times and fMRI data recording was continued for another 120 seconds after the last stimulation block. The duration between positioning of the mouse in the magnet bore and the beginning of the electrical stimulation and fMRI recording was kept constant at 40 minutes to ensure the same anesthesia conditions for all animals. This time was used for adjustment of MRI conditions as well as anatomical reference and high resolution scans. Stimulation started with the left paw in all animals. Following an 8 minute resting interval, the right paw was stimulated. These two stimulation cycles were followed by a control acquisition without electrical stimulation.

Data Analysis

Four regions of the brain were evaluated in detail, including the somatosensory cortex S1 contralateral and ipsilateral to the stimulated paw, the thalamus and a control region at the

ventral pallidum, a structure involved in neither the sensory nor the nociceptive pathway. In addition, we looked at the S2, insular and piriform cortex in the 1.5 mA group. Statistical t-maps were calculated using the general linear model (GLM) tool integrated in the Biomap software program (M. Rausch, Novartis, Switzerland). GLM assesses correlations on a pixel-by-pixel basis between the fMRI signal train and the stimulation paradigm. Activation was detected using a statistical threshold of p = 0.0001 for all experiments. With a minimal cluster size of 15 voxels, two coronal sections were analyzed, of which one slice covered the thalamus, the secondary somatosensory (S2) and insular cortex (IC) (2.8 mm anterior to the interaural line (IAL +2.8 mm)) and the other covered the forepaw areas of the primary somatosensory cortex (S1) (IAL +3.7 mm). The respective regions-of-interests (ROIs) derived from the GLM analysis, were used to extract BOLD signal changes as a function of time. In cases for which the correlation analysis revealed no activated voxels at the expected locations as well as for the unstimulated scans ROIs were transferred from the mouse brain atlas [103]. For group analysis, EPI images covering the S1 area (IAL +3.7 mm) and the thalamus (IAL +2.8 mm) were normalized to the coordinate system of the mouse brain atlas [103]. The fMRI coordinates were defined as followed: the origin of the right-hand coordinate system was chosen at the ventral end of the brain midline through the coronal sections. The second reference point was the dorsal end of the same midline, while the third point was placed on the edge of the right hemisphere at its widest point. The coordinate axes were defined along the midline (y-axis) and perpendicular to it (x-axis). The axes were then scaled to fit the dimensions of the mouse brain atlas, using an IDL-based software developed in-house [47].

For a detailed analysis of the fMRI time curve, the resulting BOLD profile was segregated into two components *S* ('slow') and *F* ('fast'). Component *S* was extracted by fitting the 8 data points before stimulation onset (light gray bars, shown in Fig. 2-4a, b) to a gamma-variate function: $y(t) = a \cdot t^r \cdot exp(-k \cdot t)$ with a (amplitude factor), r (power of growth curve), k (rate of exponential decay) being the parameters to be optimized, while t is measured with regard to the start of the first stimulation period ($t = 0$). The best fit curve (solid line, Fig. 2-3b) was then subtracted from the original data to yield component *F* of the fMRI signal (Fig. 2-4c). The maximal amplitudes of the fitted curve for component *S* and of

the extracted curve for the first stimulation period of component *F* (see Fig. 2-4) were analyzed as a function of the stimulation amplitude. The quantitative analysis was carried out for all ROIs.

We furthermore analyzed the rates of BOLD signal increase and decay for both the first stimulation cycle and the entire stimulation period. The data points of the signal decay at the end of the stimulation interval (indicated by the dotted line in Fig. 2-6a) were used to calculate a decay constant k_{off} assuming a single exponential decay function, $S(t) = S(t=0) \cdot exp(-k_{off} \cdot t)$, with $S(t)$ indicating the signal amplitude during the decay at time t and $S(t=0)$ the amplitude at the end of the stimulation period ($t = 0$). A minimum of four data points of the decay curve with an amplitude exceeding noise levels were required for each individual signal curve to allow for fitting. The BOLD signal decay rate constant was then correlated to the maximum BOLD response S_{max} of the single animals (Fig. 2-6c).

The constant k_{on} describing the initial build-up of the signal at the beginning of the stimulation to its maximum was calculated assuming the following relation: $(t) = S_{max} \cdot [1 - exp(-k_{on} \cdot t/S_{max})]$ for which the initial slope yields $(dS(t)/dt)_{t=0} = k_{on}$, i.e. the initial slope was assumed to be independent of the maximum BOLD signal.

Autoradiography and Intrinsic Optical Imaging

Autoradiography with [^{18}F]-2-fluoro-2-deoxyglucose (^{18}F-FDG) was performed on two female C57Bl/6 mice according to published protocols [105, 106]. The left forepaw was electrically stimulated at 1.5 mA using the parameters described above. A 5 minute stimulation period was followed by a one minute break. This was repeated for the entire time course of 45 minutes, before the animals were sacrificed and the brain extracted.

One mouse was used for intrinsic optical imaging. Reflectance from 570 nm light was measured through the exposed skull using a CCD camera. The left forepaw was stimulated with a 10 second pulse train of 0.5 ms pulses of 1.0 mA current amplitude at 3 Hz. These experiments were carried out under 1.5 % isoflurane anesthesia.

2. 3 Results

Animal Physiology and Anesthesia

Non-invasive monitoring of the mice showed stable physiology throughout the duration of the experiments. Blood gas levels of pCO_2 measured transcutaneously were in the range of 40 ± 10 mm Hg, which indicates a well adjusted ventilation of the animals [107]. Body temperature was kept stable at 36.5 ± 0.5 °C for the entire experiment. The monitored heart rate was stable around 500 beats per minute in all animals and no changes were detected during the stimulation. After completion of the fMRI investigation, the animals recovered fast and could be used for further experiments, an important prerequisite for longitudinal studies.

Signal and Image Quality

By exploiting the significant gain in sensitivity provided by the use of a cryogenic RF surface coil for signal detection [35, 36], BOLD fMRI data sets of high quality suitable for reproducible quantitative analysis have been obtained. Comparing the CryoProbe with a conventional room temperature coil of similar dimensions (for detailed information on the coils see [36]) using the GE-EPI sequence, a gain in image signal-to-noise ratio (SNR) of a factor of 3.1 ± 0.7 (mean ± standard deviation, unpublished data) was achieved. Using a coronal slice orientation proved advantageous as cross-sectional images recorded ≥ 3 mm anterior to the interaural line were largely devoid of geometrical distortions caused by local magnetic field inhomogeneities due to different magnetic susceptibilities of adjacent tissue compartments. In caudal brain structures, significant susceptibility artifacts have been observed due to the proximity of the air filled ear cavities. This also impaired the quality of images recorded in horizontal plane view, which would allow covering larger brain areas. Distortions caused by differences in susceptibility are experienced on an absolute scale, i.e. they affect more extended brain regions in mice than in rats due to the smaller dimensions of the mouse.

fMRI data showed good reproducibility (e.g. see error bars in Fig. 2-2g, h) and allowed for assessing differences in the BOLD response during stimulation at different amplitudes.

Spatial Distribution and Intensity of the BOLD Response

The spatial distribution of the activated areas after forepaw stimulation at 1.5 mA (threshold p=0.0001, cluster size: 15 voxels) for one representative animal is shown in Figure 2-2. The position of five coronal slices is indicated in the sagittal section shown in Figure 2-2a. Besides the forepaw S1 region activated areas are present in other S1 areas (Fig. 2-2c-f), the primary motor cortex (Fig. 2-2c-f), and several nuclei of the thalamus, including the ventral posterior nucleus which relays somatosensory information to the cortex (Fig. 2-2f) [103]. Figure 2-2i shows the distinction of the forepaw area (blue) and the hind paw area (red) after the respective stimulation as an activation map of two representative animals. As expected, hind paw somatosensory S1 areas were located median to the respective forepaw regions. The activated cluster at the brain midline reflects signal contributions from the sagittal sinus. No consistent deactivations were detected in any region of the brain.

Figure 2-3 shows statistical maps (threshold p=0.0001, cluster size: 15 voxels) depicted on the mouse brain atlas ([103], Fig. 2-3a-f: IAL +3.7 mm, Fig. 2-3g-l: IAL +2.8 mm) obtained from all animals at different stimulation amplitudes ((a, g) 0.5 mA, (b, h) 1.0 mA, (c, i) 1.5 mA, (d, j) 2.0 mA). The activated clusters of individual animals were overlaid, i.e. the intensity in the activation map corresponds to the number of animals displaying a significant BOLD signal (left and right forepaw for each animal). Activation in response to the forepaw stimulation appears in the somatosensory S1 and S2 cortices, in the thalamus and at higher amplitudes in the insular cortex (regions indicated in Fig. 2-3e, k). For all activated regions, the spatial extent of BOLD response exceeded the topological area defined on the basis of the mouse brain atlas [103]. This is attributed to the fact that fMRI assesses the hemodynamic response elicited by neural activity and not the neural activity per se.

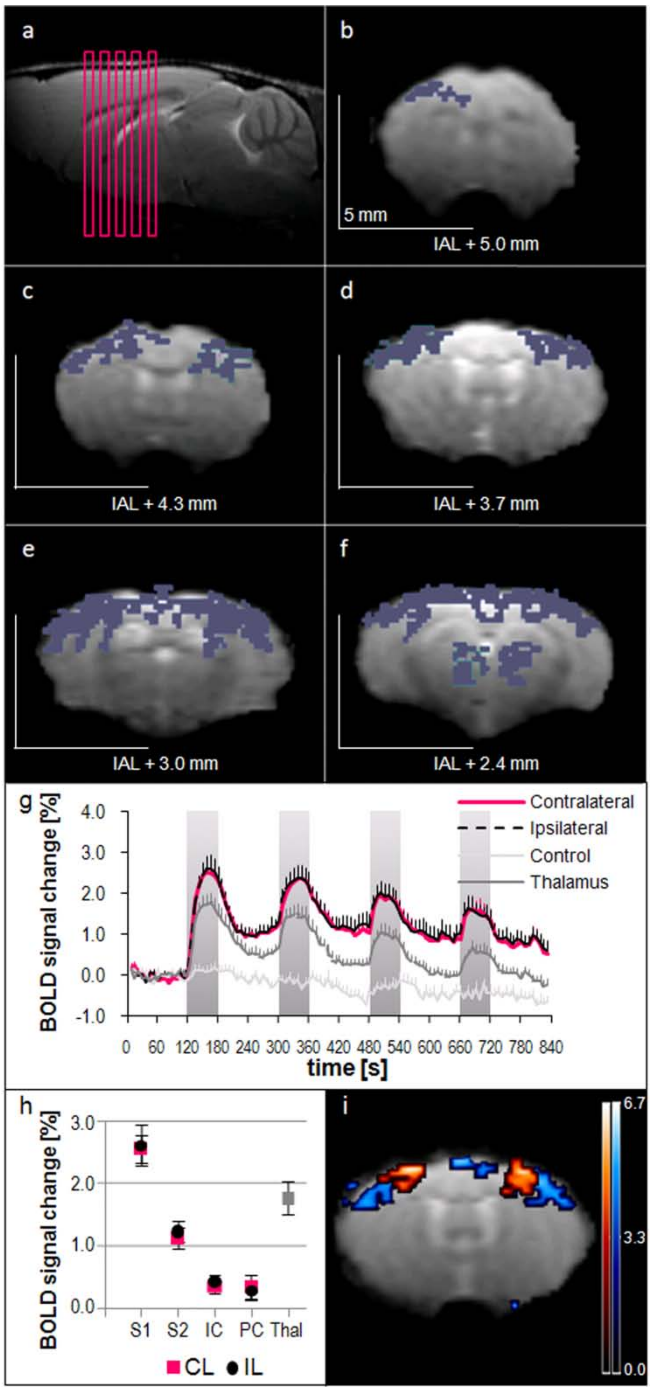

Figure 2-2: Spatial distribution of the BOLD activation. **(a)** Sagittal reference image indicating the positions of the coronal EPI slices covering a large section of the mouse forebrain. **(b)–(f)** Spatial distribution of the activated clusters (p = 0.0001) of one representative animal after unilateral forepaw stimulation. The left side of the image corresponds to the left hemisphere. Nominal distance to the interaural line (IAL) is given for each slice. Scale bar indicates 5 mm. Activated areas include the S1 forelimb area (c, d, e); motor cortex M1 (c, d, e); and several nuclei of the thalamus, including the ventral posterior nucleus which relays somatosensory information (f). Activated clusters are also observed at the sagittal sinus (e, f). **(g)** Time course of the BOLD signal after unilateral electrical stimulation of the forepaw at 1.5 mA for S1 contralateral to the stimulated paw (pink), S1 ipsilateral (dashed black), thalamus (gray), and the control region (light gray). Gray bars indicate the stimulation periods. The BOLD signals of the contralateral and ipsilateral S1 are almost identical. **(h)** Maximal signal amplitude of different regions (S1, S2, insular cortex (IC), piriform cortex (PC, control region)) ipsi- (black circles) and contralateral (pink squares) to the stimulated paw at 1.5 mA. All values are given as mean + SEM. **(i)** Activation map of two representative animals showing activation of the forepaw (blue) and hind paw (red) S1 area after stimulation of the respective paw at 1.5 mA, overlaid on an EPI image. Scale bars indicate t-values.

BOLD Signal Changes in Correlation to the Forepaw Stimulation Paradigm

The maximal BOLD signal intensity increased with increasing stimulation amplitude in all analyzed regions involved in sensory and nociceptive processing in a comparable manner as in the regions shown in Figures 2-4 and 2-5. Stimulation at the lowest amplitude of 0.5 mA led to a maximal BOLD signal of 0.93 ± 0.25 % (in % of baseline intensity) in the primary somatosensory cortex contralateral to the stimulated paw. For amplitudes of 1.0, 1.5, 2.0 mA, the maximal BOLD signal changes in this region amounted to 1.94 ± 0.20 %, 2.54 ± 0.22 %, and 3.52 ± 0.41 %, respectively (Fig. 2-4a). The maximum BOLD amplitude decreased for subsequent stimulation periods. Interestingly, the signal did not return to the initial baseline level within the two minutes resting interval following a stimulation episode, but stayed elevated until the start of the next stimulation block. The BOLD response to unilateral forepaw stimulation appeared consistently bilateral in all activated regions, including the S1 (Figs. 2-2, 2-3), thalamus, S2 and insular cortex (for 1.5 mA: Fig. 2-2h). The maximal BOLD signal amplitude in the regions of the S2 somatosensory and insular cortex was significantly lower as compared to the S1 area. This was observed at all stimulation amplitudes except at 0.5 mA, where the amplitudes for S1 and S2 area reached similar values (data not shown). There was no delay between ipsi- and contralateral responses within the time scale of the fMRI experiment (7.5 s temporal resolution).

The control region, which was located in the ventral pallidum, a structure not involved in sensory or nociceptive processing, showed no change in BOLD intensity for stimulation amplitudes ≤ 1.5 mA (Fig. 2-2g, 1.5 mA). At 2.0 mA a maximum signal increase of 0.81 ± 0.12 % was detected. This unspecific increase in the BOLD signal was observed in large parts of the brain. A second cortical control region, located in the piriform cortex, behaved comparable to the ventral pallidum (for 1.5 mA: Fig. 2-2h). No region-specific activation whatsoever, but only background noise was revealed by the analysis of the control fMRI data sets acquired without stimulation, indicating the stability of the fMRI set-up including the physiological preparation (data not shown).

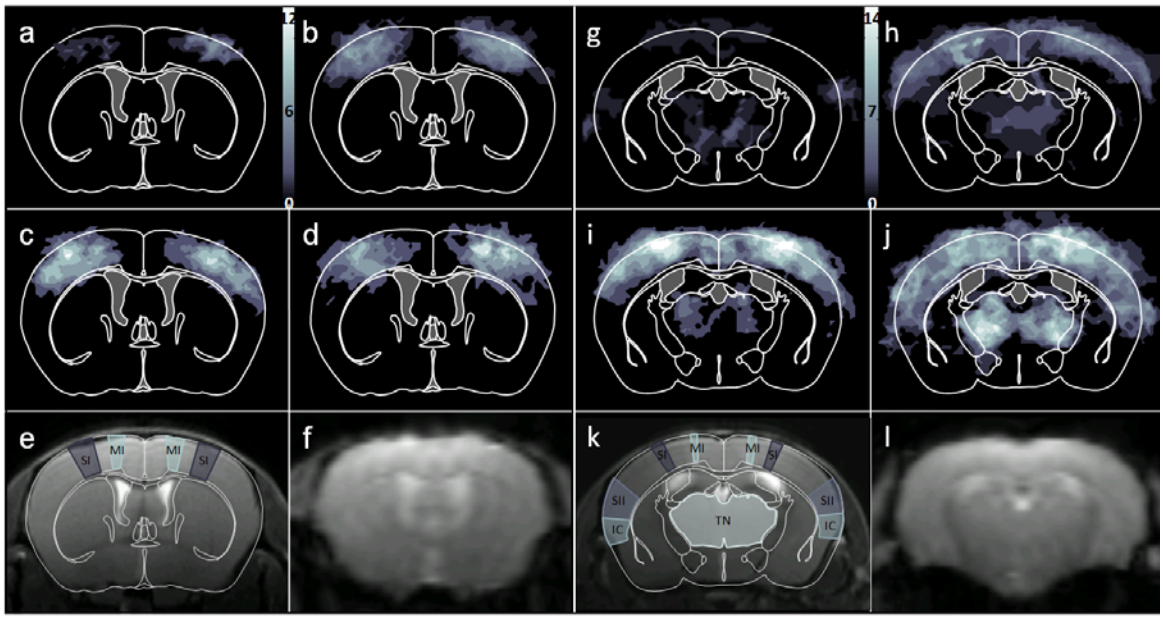

Figure 2-3: Activation maps of the cortex after left and right forepaw stimulation at **(a, g)** 0.5 mA, **(b, h)** 1.0 mA, **(c, i)** 1.5 mA, **(d, j)** 2.0 mA. Data show activated clusters derived from GLM analysis (p = 0.0001, cluster size: 15 voxels) for all animals overlaid on the mouse brain atlas at IAL +3.7 mm **(a-f)** and IAL +2.8 mm **(g-l)** [103]. **(e-k)** Mouse brain atlas with relevant regions (SI: primary somatosensory cortex, forepaw region; SII: secondary somatosensory cortex; IC: insular cortex; MI: primary motor cortex; TN: thalamic nuclei) overlaid on the anatomical image. **(f, l)** Representative EPI image revealing relatively little distortions. **(g-j)** Activation maps; intensity indicates the number of stimulation periods displaying significant BOLD activation at a given location (scale bar).

Amplitudes of the Two Signal Components *S* and *F* as a Function of the Stimulation Amplitude

The temporal profile of the BOLD response has been segregated into the two signal components *S* and *F* by fitting component *S* to a gamma-variate function and subtracting the best fit from the experimental data (Fig. 2-4b, c). Analysis of the maximal amplitude of both components for the two S1 regions and the thalamus was found to correlate with the stimulation amplitude. Linear regression analysis yielded correlation factors for component *S* (Fig. 2-6a) of R^2 = 0.98 for the contralateral, R^2 = 0.97 for the ipsilateral somatosensory cortex and R^2 = 0.81 for the thalamus. The values for component *F* (Fig. 2-6b) were R^2 = 0.97 for contralateral S1, R^2 = 0.98 for ipsilateral S1 and R^2 = 0.87 for thalamus.

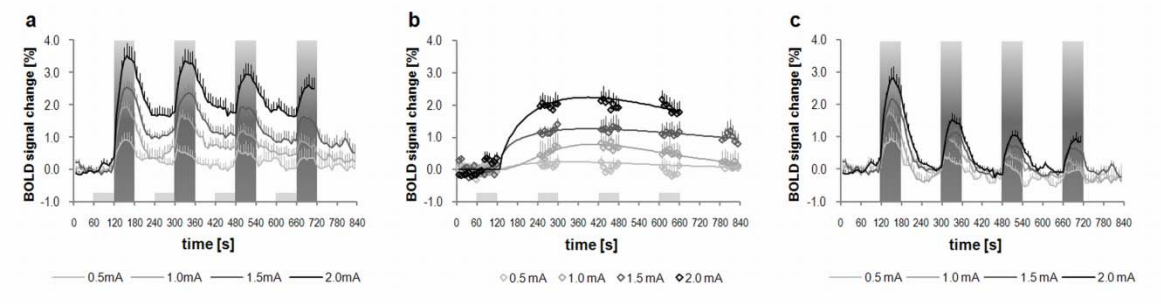

Figure 2-4: **(a)** Relative change of the BOLD signal intensity as a function of time during electrical forepaw stimulation for the different stimulation amplitudes. Dark grey bars indicate the stimulation periods, light gray boxes mark data points used for fitting the component *S* curve **(b)**. **(c)** Signal component *F* obtained by subtracting **(b)** from **(a)**. Values are given as mean + SEM.

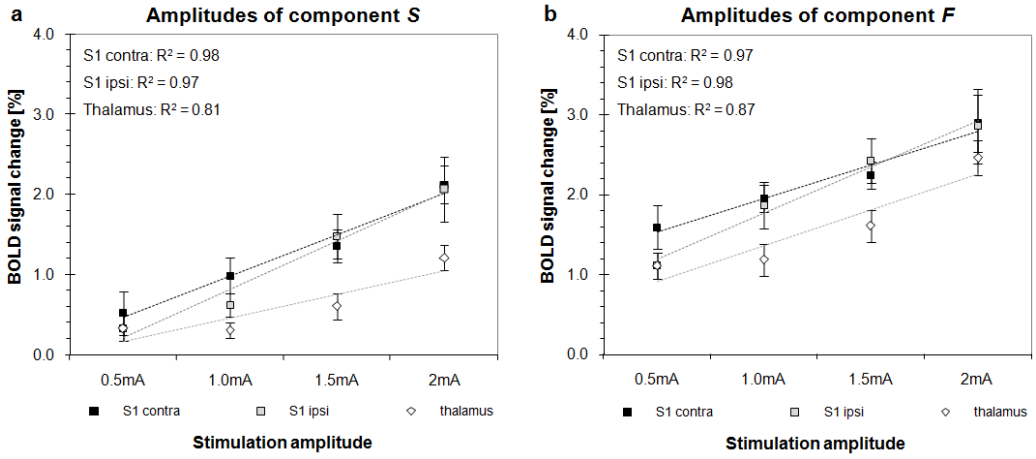

Figure 2-5: The amplitudes of the two components *S* **(a)** and *F* **(b)** as a function of the stimulation amplitude. **(a)** Linear regression analysis yielded correlation factors of R^2 = 0.98 for the contralateral and R^2 = 0.97 for the ipsilateral S1 somatosensory cortical area. The corresponding value for thalamus was R^2 = 0.81. **(b)** For the fast component the correlation factors were: R^2 = 0.97 for contralateral S1, R^2 = 0.98 for ipsilateral S1 and R^2 = 0.87 for thalamus. Values are given as mean ± SEM.

Analysis of the Signal Dynamics of Component *F*

Not only the amplitude but also the dynamic behavior of the BOLD response depended on the stimulation amplitude as demonstrated by the averaged temporal profile of component *F* of the first stimulation period of each animal (Fig. 2-6a). The maximum values for the S1 region contralateral to the stimulated paw were: 1.19 ± 0.48 %, 1.69 ± 0.21 %, 2.47 ± 0.18

%, and 2.81 ± 0.37 % for 0.5, 1.0, 1.5, and 2.0 mA, respectively. A striking feature of the observed BOLD response (Fig. 2-4c, 2-6a, b) is that the signal amplitude started to decay despite ongoing stimulation. The signal maximum was observed typically 30 seconds after stimulation onset, thereafter the amplitude decreased significantly by 5 % to 15 %. The fitted curves (Fig. 2-6a) were computed assuming single exponential signal build-up and decay with parameters described in the Materials and Method section. The exponentially decaying vasodilatory response of the neuronal signal is characterized by a time constant k_v = 0.02 s^{-1}.

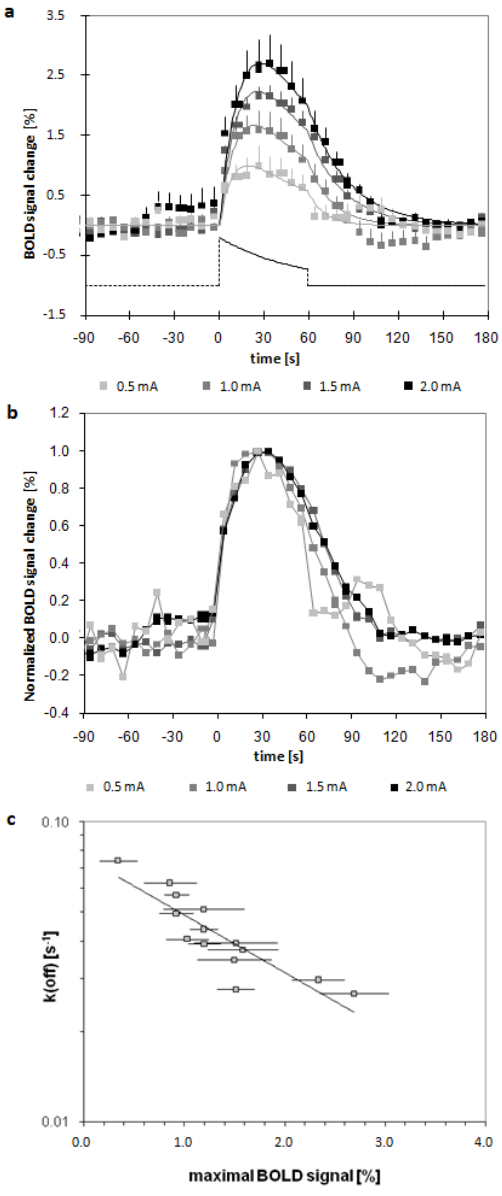

Figure 2-6: Analysis of component *F* of the fMRI response to electrical stimulation of the forepaw in the contralateral S1 cortical region. **(a)** Mean fMRI signal response for the first stimulation episode as a function of time and current amplitude. Solid lines indicate the BOLD response modeled as described in the text. The dashed line illustrates the vasodilatory stimulus, which displays a single exponential decay with a rate constant k_v = 0.02 s^{-1}. **(b)** The mean normalized fMRI response of the first stimulation period (normalized to 1) as a function of time and stimulation amplitude. The reduced rate of signal decay with increasing stimulus amplitude (and correspondingly higher maximum BOLD intensity) becomes apparent. For sake of clarity error bars have been omitted. **(c)** The decay rate constant of the BOLD signal of the single animals decrease with increasing maximal intensity of the BOLD signal. Linear regression yielded a correlation coefficient of R^2 = 0.76. Values are given as mean ± SEM.

For the build-up of the BOLD signal the same initial rate k_{on} = 0.002 s^{-1} was assumed, irrespective of the stimulation amplitude applied. In contrast, the value for the decay rate constant k_{off} was found to decrease with increasing stimulation amplitude. This is also apparent when normalizing individual BOLD signals to the respective maximum intensity value (Fig 5b). Single exponential fitting for the averaged curves yielded first-order rate constants of k_{off} values of 0.040 s^{-1} for 2.0 mA, 0.051 s^{-1} for 1.5 mA and 0.063 s^{-1} for 1.0 mA, displaying a linear dependence on the stimulation amplitude with a correlation factor of R^2 = 1.00 (data not shown). In the next step we tested whether the decay rate k_{off} depended on the maximal BOLD change. We therefore used the average BOLD signals of all stimulation cycles (four stimulation blocks per stimulation amplitude), which fulfilled the criteria with at least four data points exceeding the noise level used for the fitting procedure (Fig. 2-4c): a significant negative correlation has been found with R^2 = 0.76.

Autoradiography and Intrinsic Optical Measurements

The autoradiography data of the two animals (Fig. 2-7b) showed a clear bilateral increase in FDG uptake in the thalamus, consistent with the observed fMRI activation pattern (Fig. 2-7a). Cortical activation was found to be weak. Bilateral local increases in cortical blood volume indicative of neuronal activation were detected using intrinsic optical imaging (Fig. 2-7d), which is in line with our fMRI finding of bilateral cortical activation.

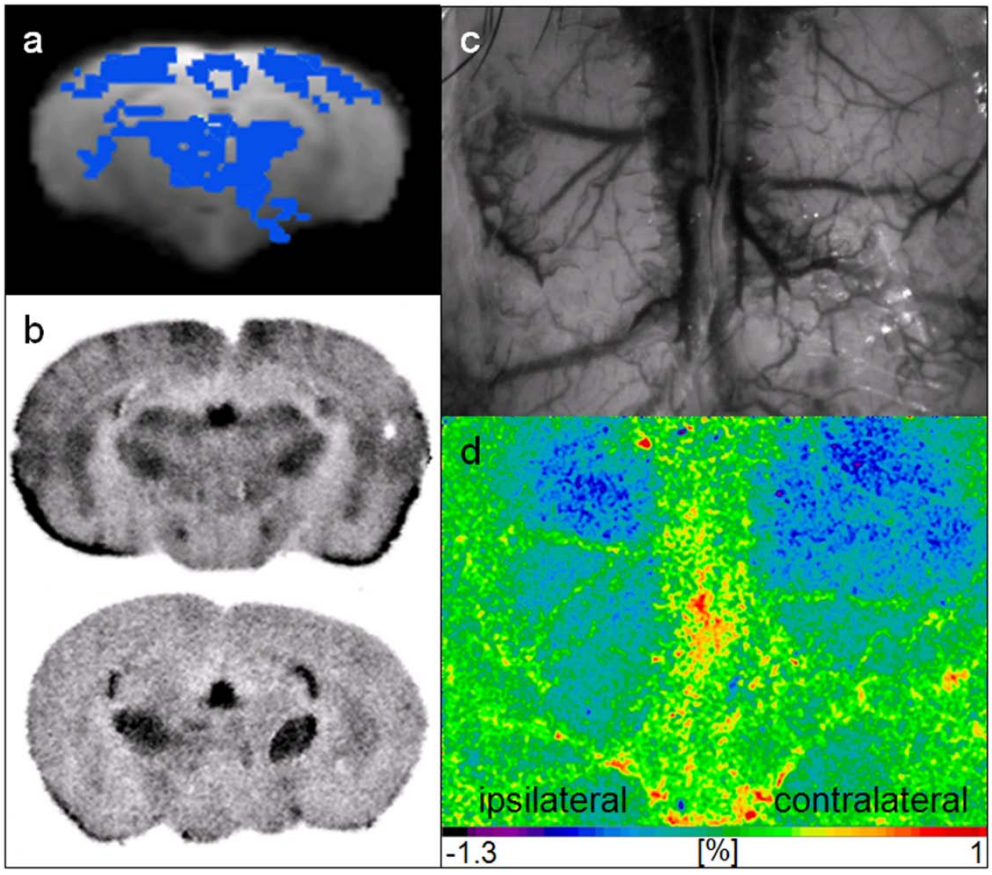

Figure 2-7: Autoradiography and intrinsic optical imaging. **(a)** fMRI activation map of a representative animal. **(b)** ^{18}F-FDG autoradiographies of two mice after unilateral forepaw stimulation show bilateral thalamic activation and some bilateral cortical activation (blue arrows). **(c)** Reflection of 570 nm light used for intrinsic optical imaging reveals the vascular anatomy at both sides of the sagittal sinus. **(d)** Activation map of intrinsic optical imaging shows bilateral activation of the somatosensory area. Regions with increased cerebral blood volume are recognized by a decrease in signal intensity (blue). Color bar indicates changes in signal intensity in [%].

2.4 Discussion

fMRI in rodents, predominantly in rats, has become an important tool in biomedical research e.g. to phenotype animal models of CNS disorders [19, 20, 40, 102]. In view of the many genetically engineered mouse lines the development of robust procedures for mouse fMRI protocols should be rewarding. By exploiting the significant gain in sensitivity provided by the use of a cryogenic RF surface coil for signal detection [35, 36], BOLD fMRI

data sets of high quality suitable for reproducible quantitative analyses have been obtained. The CryoProbe enabled fMRI at a spatial resolution of 200x200x500 μm^3, which is sufficient to resolve the major cerebral structures of the mouse brain and allows for detailed anatomical and functional studies.

The obtained fMRI data were highly reproducible with regard to both spatial extent and temporal profile. This allowed reliable detection of even small changes in the BOLD amplitude in response to stimulations at different current amplitudes. The BOLD intensity increased significantly at each stimulus onset, though there was a net decrease of BOLD amplitude for subsequent stimulation periods across the cycle consisting of four blocks. This was observed before [104, 108] and might be due to adaptation or habituation mechanisms, occurring either peripherally in the stimulated paw, or centrally in the brain. These mechanisms may also contribute to the signal decrease observed during ongoing stimulation (Fig. 2-4a, b).

Due to the lack of clear evidence whether stimulation was noxious or not, the parameters used were tested on a human subject under the presumption that the threshold to activate C- or Aδ-fibers is similar in humans and mice. However, as the innervation pattern differs, the human values cannot be translated directly to the mouse but should rather be used as an estimate of the noxious threshold. This stands in contrast to a study by Nair and Duong, which reports hind paw stimulation with amplitudes up to 7 mA to be somatosensory only [71]. To our experience, the stimulation used in that study was likely to be noxious, at least at higher amplitudes.

Data analysis revealed a robust activation of the S1 cortical forelimb area. However, the signal was not confined to the S1 region contralateral to the stimulated paw, but was also observed on the ipsilateral side with essentially the same amplitude and spatial extent. This stands in contrast to the majority of fMRI studies in healthy rats which report strictly unilateral responses during unilateral electrical stimulation [25, 77, 109, 110] including our own study using isoflurane anesthesia [47]. We performed additional experiments to modulate the laterality of the fMRI response: varying anesthesia depths, male instead of

female mice, or preparing only one paw with electrodes to prevent possible crosstalk between the leads carrying the needle electrodes. None of these interventions affected the bilateral symmetry of the activation pattern observed (data not shown). In addition, electrical forepaw stimulation at 1.5 mA in another strain (HsdWin:NMRI) showed the same bilateral activation pattern (data not shown). Bilateral activation of the areas responsible for pain processing has also been observed in humans [111-115]. These bilateral signals may be conveyed by fibers of the corpus callosum [116] or by commissural neurons of the spinal cord [117]. The occurrence of bilateral activation has also been reported previously for rat studies [118]. However, due to our relatively slow temporal resolution of 7.5 s, we were not able to resolve a possible delay between the onset of activation in the two hemispheres. Even increasing the temporal resolution to 1 s was not sufficient to reveal a potential delay of the ipsilateral versus the contralateral activation (data not shown).

Although carried out with a small number of animals, autoradiography and intrinsic optical imaging experiments support our fMRI findings. Autoradiography revealed a distinct bilateral activation of the thalamus, most pronounced in the ventral posterior nuclei, structures known to relay nociceptive information. One mouse also showed bilateral cortical activation in the regions of S2, insula and motor cortex. The intrinsic optical measurement showed a clear bilateral activation of similar amplitudes in both hemispheres. These experiments, which were performed independently from our fMRI set-up, are in line with the results obtained with BOLD fMRI.

Besides the S1 region, bilateral activation was observed in the thalamus, the motor, S2 and insular cortex. These regions are known to be part of the nociceptive network. Motor cortex activation might originate from antidromic stimulation of the efferent motor fibers as seen in a study by Cho and colleagues [76]. These activated areas are in accordance with those reported for similar studies in rats [109].

Anesthesia is a recurring issue in animal imaging, in particular when investigating nociception. Isoflurane is an attractive anesthetic as it is easy to administer and control; however, there are also drawbacks. Isoflurane is a potent vasodilator causing a global increase

of cerebral blood flow (CBF) in a dose-dependent manner [119]. The basal energy level as derived from the cerebral metabolic rate of glucose consumption (CMR_{glc}) is lower than in the awake state. A reduction by approximately 40 % was reported for an isoflurane concentration of 1.4 % [43]. In comparison, α-chloralose was found to reduce baseline CMR_{glc} by approximately 60 % [118]. The higher energy consumption, the high CBF and concomitantly the dilated vessels in isoflurane anesthetized animals during baseline conditions reduce the dynamic range of the hemodynamic response as compared to α-chloralose anesthesia [120, 121]. The vasodilatory effects however are dose dependent and can therefore be significantly reduced by using relatively low isoflurane levels (at around 1 %). At this low level we assume reduced antinociceptive efficacy of isoflurane. Deady et al. showed that the hypnotic effects of isoflurane occurred at lower concentrations than the antinociceptive effects [122]. Also, low concentrations of isoflurane appear to exhibit minimal neuro-suppressive effects, as the flow-metabolism coupling was shown to remain preserved [123]. The robust BOLD response reported in this study as well as data from other studies performed under isoflurane anesthesia prove it to be a useful anesthetic for fMRI studies in rodents [19-21, 40, 45, 71].

A recent study [70] performed on mice using electrical forepaw stimulation claims the α_2-adrenergic receptor agonist medetomidine to be better for long time studies than other anesthetics. However, the occurrence of BOLD activation in less than 60 % of all scans performed (our study: > 95 %) and the noisy temporal BOLD profiles do not clearly show the superiority of medetomidine anesthesia.

When analyzing the temporal BOLD profile, it became obvious that it consists of two components, of which one is in phase with the stimulation (component *F*), while the other one is much slower, starting with the onset of the first stimulation (component *S*). The two components might be explained in terms of the underlying physiological processes: Component *F* being in phase with the stimulation episodes, is probably associated with the peripheral neuronal input of the A- and C-fibers, while the underlying signal described by component *S* might reflect a slow vascular response.

The BOLD signal amplitude of both components depended linearly on the stimulation amplitude. A similar linear dependence has been demonstrated using cerebral blood volume (CBV) [102] and CBF [104] measurements in mice and rats, respectively. Torebjörk et al. also showed that nociceptor responses and individual pain ratings in humans both linearly correlated with the applied heat stimulation [124].

By averaging and normalizing the BOLD signal curves of all animals, it became apparent that the rate of the signal decay following a stimulation episode decreased with increasing stimulation amplitudes. Stimulation at high amplitudes led to a larger BOLD response and thus to a higher content of oxyhemoglobin (and correspondingly a lower concentration of deoxyhemoglobin) in the vessels, as compared to stimulations at lower amplitudes. This is in line with the hemodynamic model described by Friston and colleagues [125], which combines the balloon model with a linear dynamic model of changes in CBF as caused by neuronal activity. The balloon model describes the link between CBF and the BOLD signal and is able to predict nonlinear effects of the BOLD signal, which contrast the linear relationship of CBF and synaptic activity. The central concept of the model is to treat the venous compartment as an expandable balloon, which is inflated by an increase in CBF, leading to a dilution of the deoxygenated blood and an increased expelling rate of the blood [126]. The model predicts the recovery rate following a stimulation episode to be proportional to the amount of deoxyhemoglobin in the vessel [125-127], which is in line with our experimental results (Fig. 2-6). In contrast, the initial rate of the build-up of the BOLD response was found independent on the current amplitude within error limits.

A further aspect that becomes apparent from the temporal profile of the BOLD response is that the BOLD amplitude decays during stimulation despite ongoing peripheral input. This can be explained by a decaying vasodilatory signal, which is also subject to feedback regulation by CBF, in response to a prolonged neuronal stimulus [77, 113]. The neuronal input is described as an initial peak followed by a decay to a lower level [125, 126].

We could demonstrate that reproducible mouse BOLD fMRI data can be obtained following sensory stimulation. The high quality of the data and the use of isoflurane make longitudinal fMRI studies in mice feasible.

3. Increased BOLD Sensitivity in the Mouse Somatosensory Cortex during Electrical Forepaw Stimulation Using a Cryogenic RF Probe

3.1 Introduction

Functional MRI (fMRI) of small rodents puts high demands on the signal-to-noise (SNR) ratio of the MR acquisitions: i) changes in the BOLD (blood oxygen level dependent [26]) signal intensity during the resting state or in response to a stimulus do not exceed a few percent of the baseline signal intensity; ii) quantitative analysis of the BOLD time course requires a high temporal resolution as the hemodynamic response function is characterized by time constants of the order of seconds [128, 129]; and iii) the small dimensions of the rodent brain imply that high spatial resolutions (200-500 μm) are required in order to resolve functional brain structures. Substantial efforts have been made to improve the SNR for small animal MRI, e.g. to increase the signal by using higher main magnetic field strengths B_0 [31]. However, with higher magnetic field strengths, the T_2 and T_2^* relaxation times are inherently decreased, and T_1 increases. Thus, MRI sequence parameters have to be adjusted (e.g. use of longer repetition delays, resulting in longer acquisition times) in order to extract maximum benefit from the increased polarization. Furthermore, the higher susceptibility differences at tissue interfaces (e.g. soft tissue-bone, soft tissue-air) intrinsically associated with higher magnetic fields will aggravate the severity of image artifacts. Alternatively, the signal can be improved by data averaging or by increasing the dimensions of the volume element (voxel) being sampled, which would compromise either temporal or spatial resolution.

An attractive strategy to improve SNR is to decrease the noise level in the data. In fMRI experiments three noise contributions must be considered: (i) the (thermal) noise of the receiver electronics, (ii) 'static' sample noise and, (iii) when analyzing serial MRI data

Published Article *"Increased BOLD Sensitivity in the Mouse Somatosensory Cortex during Electrical Forepaw Stimulation Using a Cryogenic RF Probe";* Christof Baltes*, Simone C. Bosshard*, Thomas Mueggler, David Ratering, Markus Rudin; NMR in Biomedicine 2010. *contributed equally

acquisitions, such as fMRI, noise originating from fluctuations in the physiological state of the animal caused, for example, by changes in metabolic rate, blood flow, blood volume, de/oxyhemoglobin concentrations, cardiac and respiratory motion. In humans, the effect of physiological noise on BOLD fMRI has been investigated in detail for various imaging parameters (spatial resolution, echo time, etc.) [32, 33] and for increasing field strengths (1.5, 3, and 7 T) [34]. Recently, Kalthoff et al. [89] have investigated the effect of physiological noise on BOLD fMRI in the resting state in rats at 11.7 T. The first measure for the minimization of physiological noise in fMRI studies in small rodents is the stable preparation of the animal with respect to motion and hemodynamic conditions [48]. Stereotactic fixation or neuromuscular blocking agents are used to prevent motion artifacts. Furthermore, physiological parameters such as heart rate, blood gas levels and body temperature, must be monitored and maintained within physiological limits.

For the small sampling volumes typical in rodent MRI the noise contributions of the biological sample and of the receiver electronics are of comparable order. Cooling of the radiofrequency (RF) coils and preamplifier has been shown to lead to an increase in SNR [130, 131]. In recent studies, SNR gains of a factor of 1.8 at 4.7 T [35] and a factor of 2.5 at 9.4 T [36] have been reported for structural *in vivo* MRI of the mouse brain using cryogenic coils operating at 30 K.

The aim of this work is to investigate to what extent physiological noise associated with BOLD fMRI studies affects the gains in SNR that have been reported for structural *in vivo* MRI when using detection at low temperature. For this purpose fMRI experiments in mice using an electrical forepaw stimulation paradigm were performed employing either a 400 MHz cryogenic surface coil (dimensions: 27x20 mm^2) operating in quadrature transceive mode, or a room temperature (RT) receive-only coil of comparable dimensions (28x17 mm^2). The fMRI data series was evaluated with respect to both the SNR within individual images and the temporal SNR (tSNR) between the images of the time series. The tSNR serves as quality measure for the analysis of an fMRI time series taking signal fluctuations between images into account, which originate from small temporal changes in the animal's

physiology. Furthermore, as the cryogenic probe is equipped with a temperature-controlled thermal shield to insulate the mouse head from the cryogenic transceiver coil, the effect of the thermal shield temperature on the fMRI contrast-to-noise ratio (CNR) was evaluated.

3.2 Materials and Methods

Theory

In MRI the SNR has been demonstrated to be linearly proportional to the main magnetic field strength B_0 [132] and can be described as:

$$SNR \approx \frac{\Delta V \cdot M_0 \cdot \sqrt{N_{PE} \cdot N_A}}{\sigma} \qquad [1]$$

with the equilibrium magnetization given by:

$$M_0 \approx \frac{\gamma^2 \cdot \hbar^2}{4 \cdot k \cdot T} B_0$$

where γ is the gyromagnetic ratio, $\hbar = h/2\pi$ is Planck's constant an k is Boltzmann's constant. M_0 is proportional to the main magnetic field strength B_0 and inversely proportional to the absolute temperature T. In equation [1], ΔV represents the voxel dimensions, and N_{PE} and N_A are the number of phase encoding steps and the number of averages, respectively. Noise contributions σ are attributed to different sources: the thermal noise of the receiver chain σ_C and the sample noise σ_S (consisting of static noise of the subject $\sigma_{S,S}$, and physiological noise $\sigma_{S,P}$ of the subject) [32, 33]. Assuming the noise contributions to be uncorrelated and of Gaussian type, we obtain

$$\sigma = \sqrt{\sigma_C^2 + \sigma_S^2} \qquad [2]$$

with $\sigma_S = \sqrt{\sigma_{S,S}^2 + \sigma_{S,P}^2}$.

Although, in structural human MRI, thermal noise of the receiver chain is negligible compared with the subject noise, σ_C and σ_S are of comparable order in small-animal MRI. Accordingly, reducing the noise contribution of the receiver chain by cooling RF coil and preamplifier results in an increased SNR. However, during serial MRI acquisitions, such as fMRI studies, the physiological noise $\sigma_{S,P}$ constitutes a non-negligible contribution to the total noise, which depends on the signal levels. According to Krueger et al. [32, 33] the tSNR, taking into account the physiological noise, can be defined as

$$tSNR = \frac{SNR_0}{\sqrt{1+\lambda^2 \cdot SNR_0^2}} \quad , \qquad [3]$$

where SNR_0 is the single image SNR and λ represents a physical measure of the SNR degradation caused by physiological fluctuations over time.

Typically, in BOLD fMRI studying the response to stimulatory input (e.g. sensory stimulation) two states are compared: the resting period and the activation period during stimulation. Accordingly, the (maximum) signal difference (ΔS) between the resting and activated state can be considered as a measure for the BOLD sensitivity (CNR) of the MR sequence. Assuming that the noise variance remains unchanged during activation, the CNR becomes

$$CNR = \frac{\Delta S}{\sigma} \quad . \qquad [4]$$

MR Instrumentation

Imaging experiments were carried out on a preclinical small-animal MR system (BioSpec 94/30, Bruker BioSpin MRI, Ettlingen, Germany) operating at 400 MHz and equipped with a gradient coil system capable of generating a maximum strength of 400 mT/m with a minimum rise time of 80 μs. Two RF coil set-ups were compared with respect to their sensitivity to detect BOLD signal changes in fMRI during sensory forepaw stimulation in mice. One coil set-up operating at RT (293 K) consisted of two coils driven in cross-coil

mode: a linearly polarized bird-cage resonator (inner diameter: 72 mm) for transmission and a curved rectangular quadrature receive-only surface coil [side-by-side overlapping coils; total size: 28 x 17 mm^2 (arc length x length), outer dimension of one coil element: 20 x 17 mm^2] (Bruker BioSpin MRI). The second coil set-up was a transceive cryogenic quadrature RF surface probe (CryoProbe, total size: 27 x 20 mm^2; outer dimension of one coil element: 16 x 20 mm^2) operating at 30 K with an integrated cooled preamplifier (operating at 77 K). Although constant cooling of the CryoProbe was ensured using a closed-loop system connected to a remote cryocooler, the flexible design allowed for a fast and easy exchange of the cryogenic coil. The outer surface of the CryoProbe touching the animal's head consisted of a cylinder segment (180° coverage; radius: 10 mm) and was equipped with a temperature sensor and a resistive heater controlled by a proportional, integrative and derivative (PID) unit. The temperature of the thermal shield could be freely adjusted over a wide range (20-38 °C) and was kept constant by the temperature-controlled heating system. This ensured a defined thermal environment for the animal and a complete thermal insulation from the cold RF coil. The distance between the cold RF coil to the outer surface of the coil assembly was about 1 mm. Both, the cryogenic RF probe and the appropriate cooling unit, were provided by Bruker BioSpin AG, Fällanden, Switzerland.

Animal Preparation

All in vivo experiments were carried out in strict adherence with the Swiss law for animal protection. Female C57Bl/6J mice were anesthetized using 1.5 % Isoflurane (Abbott, Cham, Switzerland) in an oxygen-air (20 % : 80 %) mixture. Animals were intubated using fine tubing made of polythene (inner/outer diameter: 0.4 / 0.8 mm; length: 25 mm) and artificially ventilated (Maraltec, Alfos Electronics, Biel-Benken, Switzerland) using the following settings: 90 breaths per min; inhalation / exhalation period: 25 % / 75 %. Furthermore, the neuromuscular blocking agent pancuronium bromide was administered at a dose of 1-1.5 mg/kg (Sigma-Aldrich, Steinheim, Germany) to paralyze the animals. Animals were placed in a prone position and ear bars secured reproducible positioning on the same animal support for both RT cross-coil and CryoProbe measurements. Physiological

parameters were monitored by a rectal temperature probe and a transcutaneous electrode (TCM4, Radiometer, Copenhagen, Denmark) on the upper part of the hind limb, measuring blood gas levels (pCO_2). pCO_2 levels remained stable throughout the experiment within physiological values of 35-50 mmHg, indicating a well adjusted ventilation [107]. The body temperature of the animals was kept at 36.0 ± 0.5 °C for all experiments, while the CryoProbe assembly temperature was varied between 20 °C and 38 °C. Five animals were measured in experiments investigating the accuracy of the fast B1 calibration method. In fMRI experiments 25 animals were examined in total: 16 using the CryoProbe (three at 20 °C, three at 27 °C, seven at 30 °C, and three at 38 °C) and nine using the RT probe. Furthermore, the temperature on the scalp was measured in two animals as a function of the CryoProbe shield temperature (20, 27, 30, and 38 °C) and compared with that measured for the RT probe. Cerebral blood volume (CBV) measurements were performed in 13 animals: nine using the CryoProbe and four using the RT coil set-up.

RF Pulse Angle Adjustment

For surface coils, such as the CryoProbe, maps of the RF pulse angle distribution commonly are acquired to allow for an accurate pulse angle adjustment. However, conventional pulse angle mapping methods such as the double angle method (DAM) [133] are hampered by their long acquisition time, whereas, in contrast, short periods between the induction of anesthesia and actual fMRI acquisition are desired in fMRI experiments. For this reason, the Bruker standard adjustment method, using slice selective excitation (thickness: 1.5 mm) in coronal view, was chosen to allow for fast pulse angle adjustments within a few seconds. In the initial experiments this standard adjustment method was compared with DAM using the following acquisition parameters: field of view (FOV): 25.6x25.6 mm^2; slice thickness (STH): 0.5 mm; acquisition matrix (MTX): 128x128; spatial resolution (RES): 200x200 μm^2; pulse angle α = 60° and 120°; echo time (T_E)/effective echo time ($T_{E,eff}$)/repetition time (T_R): 30.0/30.0/7000 ms; number of averages (N_A) = 1; scan time: 2x 14 min 56 s.

Functional MRI

Anatomical reference images in axial and sagittal view were acquired using a rapid acquisition with relaxation enhancement sequence (RARE [134]) for positioning of the fMRI slices. The imaging parameters were as follows: FOV: 20x20 mm^2; STH: 0.5 mm; MD: 200x200; RES: 100x100 μm^2; interslice distance (ISD): 1.0 mm, α = 90°; T_E / $T_{E,eff}$ / T_R: 13 / 39 / 3500 ms; RARE factor: 32; and N_A = 1. Magnetic field homogeneity was improved prior to the fMRI acquisition by voxel-based shimming in the frontal cortex covering all fMRI slices using the FASTMAP technique [135]. BOLD fMRI experiments were performed using a gradient-echo, echo-planar sequence (GE-EPI) with the following parameters: five slices of 0.5 mm thickness, FOV: 22.7x12.0 mm^2; ISD: 0.7 mm; MD: 90x60 (acquisition) and 128x64 (reconstruction); RES: 253x200 μm^2; α = 90°; T_E / T_R: 8.6 / 2500 ms; N_A = 3; temporal resolution: 7.5 s; 112 repetitions; total scan time: 14 min. The stimulation paradigm consisted of sequential bilateral forepaw stimulation with subcutaneous needle electrodes following a block design (amplitude: 1.5 mA, frequency: 3 Hz, pulse duration 0.5 ms). One stimulation cycle consisted of a 120-s 'off' period used as baseline and of four repetitions of 60-s 'on' periods separated by 120-s 'off' periods. Consecutive stimulation cycles were separated by a resting period of 8 min. In addition, a GE-EPI acquisition with identical parameter settings was acquired without electrical stimulation.

To investigate the effect of the CryoProbe thermal shield temperature on the BOLD sensitivity, fMRI protocols were repeated in different scan sessions adjusting for various thermal shield temperatures.

As a measure of baseline perfusion the relative CBV (rCBV) was assessed using a spin-echo (RARE) sequence with the following parameters: five slices of 0.5mm thickness, FOV: 23.7x12.0 mm^2; ISD; 0.7 mm; MD: 90x56 (acquisition) and 128x60 (reconstruction); RES: 264x214 μm^2; α = 90°; T_E / $T_{E,eff}$ / T_R: 10 / 40 / 3000 ms; RARE factor: 8; N_A = 1; temporal resolution: 21 s. Identical positions of CBV and BOLD fMRI images were adjusted. The native signal intensity (S_{Pre}) was estimated prior to the injection of the contrast agent (CA). Subsequently, the iron-oxide based CA Endorem (Guerbet, France) was administered via the

tail vein at a dose of 33 mg/kg body weight. After an initial wait time of 10 min, allowing CA to reach a steady-state, a series of 120 images was acquired over 42 min. Initially the CryoProbe thermal shield temperature (T_{shield}) was adjusted to 30 °C. After acquiring the baseline signal for 10 min, the thermal shield temperature was changed to T_{shield} = 20, 27 or 38 °C. To maintain the animal's body temperature at 36.0 ± 0.5 °C the temperature of the warm water bath was adapted accordingly. Subsequently, a transition period of 15 min was taken into account, allowing the animal to reach constant thermal conditions. For the measurements using the RT coil set-up, the identical protocols, procedures and waiting times were used, except that, for the post CA scan, a series of only 43 images were acquired over 15 min 3 sec, as conventional RT coils do not provide the option to change the coil assembly temperature, and thus no thermal adaptation of the coil assembly was possible. The animal's body temperature was kept constant at 36.0 ± 0.5 °C using the identical warm water bath set-up as employed for the CryoProbe measurements.

Temperature Dependence

Additional measurements of the temperature on the scalp of the animal were carried out using a digital thermometer (Conrad Electronic, Wollerau, Switzerland). These measurements served as an estimate for the effective thermal environment experienced by the animal when using a conventional RT coil set-up or the CryoProbe at different thermal shield temperatures. Following the preparation of the animal, as described above, the scalp temperature was measured after an initial stabilization period of 15 min for the RT coil and the CryoProbe at 30 °C. When using the CryoProbe, the second measurement of the scalp temperature was taken 10 min after adjusting the CryoProbe thermal shield temperature to 20, 27, or 38 °C.

Data Analysis

SNRs were analyzed in both structural spin-echo (RARE) and functional gradient-echo (GE-EPI) images. For this purpose operator-interactive selection of regions of interest (ROIs) at

the left and right somatosensory cortex (S1) areas was performed. Noise levels were estimated from the same scans for ROIs selected outside of the subject.

tSNR was estimated from unstimulated scans acquired in each animal using the first 40 repetitions (representing, in a fMRI scan using electrical forepaw stimulation, one baseline and one stimulation and recovery cycle) as the temporal mean of the S1 signal divided by the standard deviation (SD) of the temporal signal course. Prior to analysis, unstimulated scans were linearly corrected for slow signal drifts.

BOLD sensitivity was estimated as the difference between baseline and the maximum BOLD signal change of the first stimulation period divided by the SD of the signal in an unstimulated scan (Fig. 3-4a, eq.[4]). The maximum BOLD signal changes were tested for statistical outliers (data were rejected when exceeding the range: mean ± 2SD) resulting in the exclusion of two of 43 scans in total. Statistical analysis of variance (ANOVA) with subsequent *post hoc* comparison of means (Bonferroni) was performed in Origin (Version 8.0725, OriginLab, Northampton, MA, USA) using a significance level of 0.05. rCBV values were estimated according to [19, 136]:

$$rCBV \propto -\frac{100}{T_E} \ln\left(\frac{\overline{S_{post}}}{\overline{S_{pre}}}\right), \qquad [5]$$

where $\bar{S}_{pre}$ and $\bar{S}_{post}$ represent the average signal intensity prior to CA administration and the average steady-state signal after CA administration, respectively. An arbitrary factor of 100 was used for precision and scaling purposes during visualization. Slow signal drifts caused by the washout of the CA were corrected for by fitting a linear function to the initial phase after CA administration. Assuming a constant washout of CA during the duration of the experiment, the fitted linear function was subtracted from the signal time curve prior to rCBV calculation. For the CryoProbe measurements, a second CBV value was estimated by calculating $\bar{S}_{post}$ as average signal intensity after a stabilization period of 15 min following the change of the CryoProbe thermal shield temperature.

3.3 Results

In initial experiments the accuracy of the pulse angle adjustment based on the fast Bruker method and on DAM was compared. Figure 3-1 shows a representative pulse angle map in axial view at the level of the S1 areas. The comparison reveals that the Bruker adjustment method leads only to a slightly lower pulse angle compared with DAM (Bruker adjustment / DAM = 91 ± 2 %).

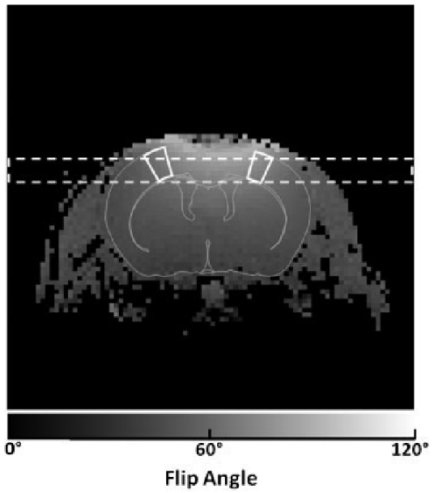

Figure 3-1: Radiofrequency (RF) pulse angle map in axial view at the level of the somatosensory cortex (S1) area (full line) acquired using the double-angle method (target pulse angle, 608). The broken line illustrates the positioning of the coronal slice used for fast pulse angle adjustment by the Bruker standard procedure.

Anatomical images in coronal view recorded at position 3.7 mm anterior to the interaural line (IAL +3.7 mm) covered the somatosensory cortices (Fig. 3-2a, 3-2b). The corresponding fMRI images acquired using a GE-EPI sequence displayed good image quality with little spatial distortion, which allowed for an unambiguous identification of the somatosensory cortices directly on the GE-EPI images (Fig. 3-2d, 3-2e). Structural RARE images were analyzed with respect to single image SNR_0 (Fig. 3-2c) using ROIs in the somatosensory cortex and a region comprising noise (Fig. 3-2a,b), yielding values of 73 ± 7 and 207 ± 11 (mean ± SD)for RT coil and CryoProbe, respectively. This resulted in a SNR_0 gain of 2.84 ± 0.31 provided by the CryoProbe. Correspondingly, when using a GE-EPI sequence, a SNR_0

gain of 3.10 ± 0.66 was obtained (x-axis, Fig. 3-2f). In order to investigate the influence of physiological noise on the fMRI data, the relationship between tSNR and SNR_0 was analyzed (Fig. 3-2f). Although, for the RT coil, tSNR (308 ± 93) and SNR_0 (289 ± 50) were equal within error limits, tSNR (546 ± 243) is significantly reduced (paired sample t-test: $p < 0.001$) compared to SNR_0 (897 ± 109) for the CryoProbe, which resulted in a tSNR gain by the CryoProbe of 1.77 ± 0.96. Linear least-squares fitting of these data according to equation 3 yielded a λ value of 0.00144 ($R^2 = 0.94$).

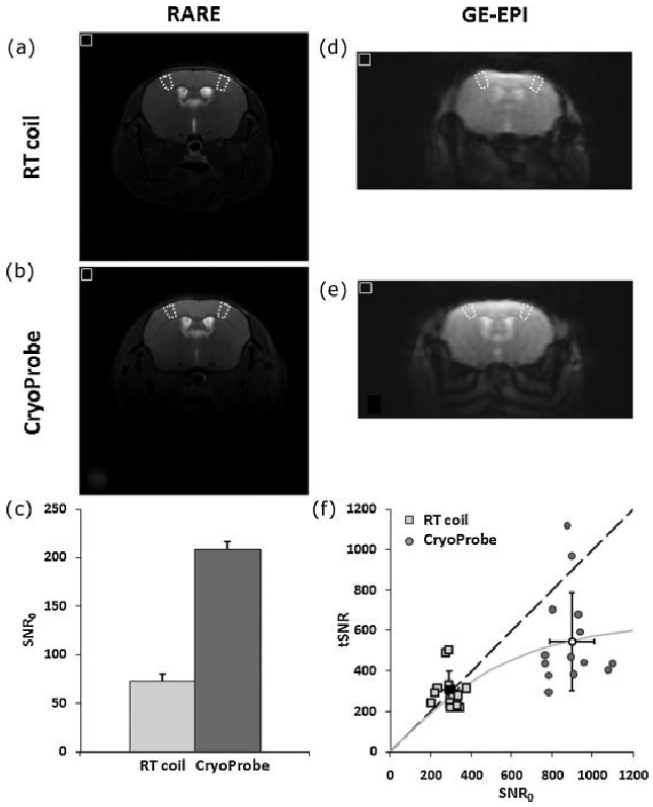

Figure 3-2: Anatomical spin-echo (rapid acquisition with relaxation enhancement, RARE) images of the mouse brain acquired using room temperature (RT) coil **(a)** and CryoProbe **(b)**. The broken boxes indicate the left and right primary somatosensory cortices (S1), and the filled squares were selected for raw image noise estimation. **(c)** Comparison of image signal-to-noise ratio (SNR_0) at the location of the S1 area in structural RARE images using region of interest (ROI) selections as indicated in (a) and (b). Functional MR images were acquired using a gradient-echo echo planar imaging (GE-EPI) sequence with both RT coil **(d)** and CryoProbe **(e)**. **(f)** Temporal SNR (tSNR, see section on 'Data analysis') plotted vs. SNR_0 at the location of the S1 area for RT and CryoProbe functional MRI (fMRI) data acquired without electrical stimulation. The broken line represents the line of identity, and the gray line indicates the result of linear least-squares fitting according to eqn. [3] ($\lambda = 0.00144$, $R^2 = 0.94$).

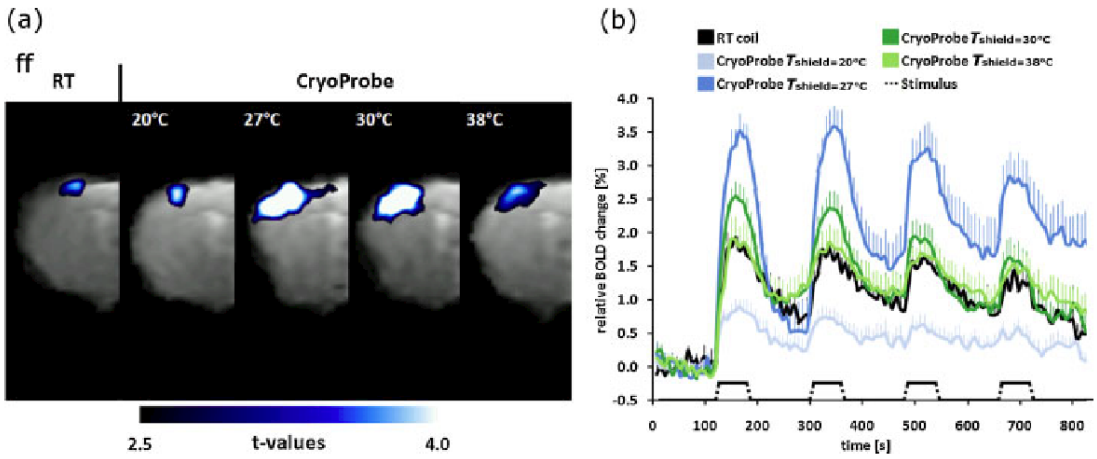

Figure 3-3: (a) Functional activation maps of representative animals during electrical stimulation of the right forepaw acquired using the room temperature (RT) probe and the CryoProbe at T_{shield} = 20, 27, 30 and 38 °C. **(b)** Relative blood oxygen level-dependent (BOLD) signal time curves acquired using the RT coil and the CryoProbe with increasing thermal shield temperatures. Error bars indicate the standard error of the mean (SEM) for the RT coil (13 scans) and the CryoProbe at T_{shield} = 20, 27, 30 and 38 °C (6, 6, 13 and 5 scans, respectively). Dotted lines mark periods of stimulation.

Figure 3-3a shows the activation in the S1 area contralateral to the stimulation side for representative animals measured using the conventional RT coil and the CryoProbe at increasing thermal shield temperatures, which were found to influence the BOLD signal amplitude. Figure 3-3b displays BOLD signal changes for thermal shield temperatures T_{shield} of 20, 27, 30 and 38 °C in comparison with the signal profile acquired using the RT coil, for which the temperature could not be adjusted. During all experiments the animal's body temperature was monitored via a rectal probe and kept constant at 36.0 ± 0.5 °C using a warm water circuit. Although a signal increase during the stimulation periods of 60 s was detected irrespective of the shield temperature, the maximum BOLD signal amplitudes of the first stimulation period varied significantly. This effect was investigated in detail by estimating BOLD sensitivity from stimulated and unstimulated scans (Fig. 3-4a): Standard deviations (σ) of the baseline signal were calculated for each of the unstimulated scans, while the maximum BOLD signal changes (ΔS) were derived from the profiles of the stimulated scans, respectively. For all T_{shield} values, reduced noise levels (SD of the unstimulated scan)

were found when compared to the RT coil [ANOVA: $F(4, 42) = 10.46$, $p < 0.001$]. *Post hoc* comparison of means revealed significant differences between the RT coil and the CryoProbe for thermal shield temperatures T_{shield} of 20, 27, 30, and 38 °C (Fig. 3-4b). The differences in σ between RT coil (0.37 ± 0.08 %) and CryoProbe for T_{shield} = 20 °C (0.23 ± 0.07 %), T_{shield} = 27 °C (0.25 ± 0.05 %), T_{shield} = 30 °C (0.22 ± 0.07 %), and T_{shield} = 38 °C (0.23 ± 0.02 %) were significant, resulting in a decrease of the temporal noise level of the RF electronics by factors of 1.63±0.59 (T_{shield} = 20 °C), 1.49 ± 0.44 (T_{shield} = 27 °C), 1.65 ± 0.61 (T_{shield} = 30 °C), and 1.59±0.35 (T_{shield} = 38 °C). There was no effect of the thermal shield temperature on the σ value of the baseline signal.

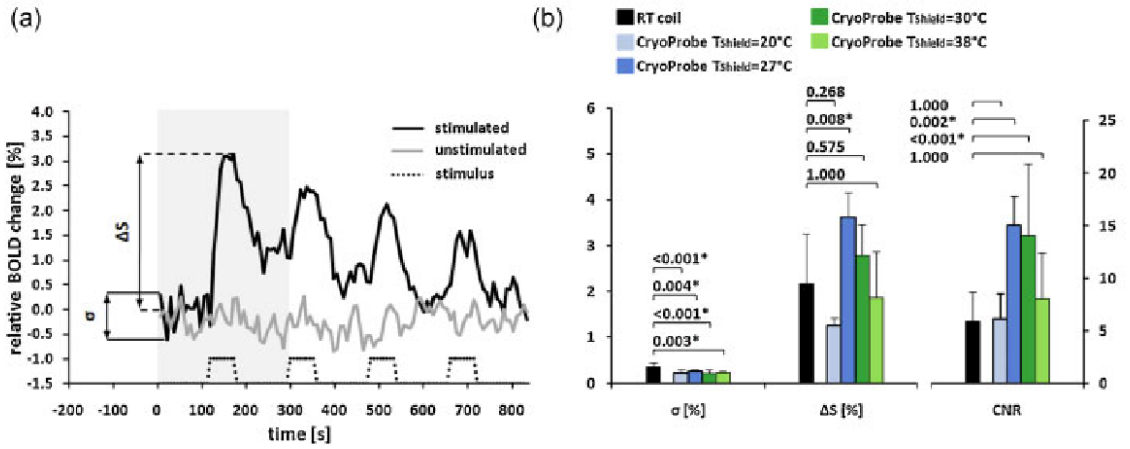

Figure 3-4: Analysis of blood oxygen level-dependent (BOLD) sensitivity (contrast-to-noise ratio, CNR). **(a)** For each animal, CNR values were calculated as the maximum BOLD signal change (DS) of the first stimulation period divided by the standard deviation (s) of the first 40 repetitions (gray area) of the unstimulated scan acquired in the same animal. Stimulation periods are indicated by the dotted line. **(b)** Comparison of noise level, maximum BOLD signal change and BOLD sensitivity between the room temperature (RT) coil and the CryoProbe for increasing thermal shield temperatures. Error bars indicate standard deviations over different functional MRI (fMRI) scans. Asterisks indicate statistically significant differences of the CryoProbe values at the respective thermal shield temperatures in comparison with the RT coil ($p<0.05$). Comparisons of means between CryoProbe values for different thermal shield temperatures are listed in the 'Results' section.

The BOLD signal amplitude varied strongly for different T_{shield} values. Statistical analysis of the means revealed a main effect of temperature [ANOVA $F(4, 42) = 8.04$, $p < 0.001$]. No

significant differences were found for ΔS between RT coil set-up (2.17 ± 1.08 %) and CryoProbe at T_{shield} = 20 °C (1.25 ± 0.17 %, p = 0.268), T_{shield} = 30 °C (2.79 ± 0.66 %, p = 0.575) and T_{shield} = 38 °C (1.86 ± 1.00 %, p = 1.000), but ΔS was significantly higher for T_{shield} = 27 °C (3.62 ± 0.54 %, p = 0.008). Accordingly, a significant effect of temperature was found for CNR [ANOVA F(4, 42) = 8.75, p < 0.001].

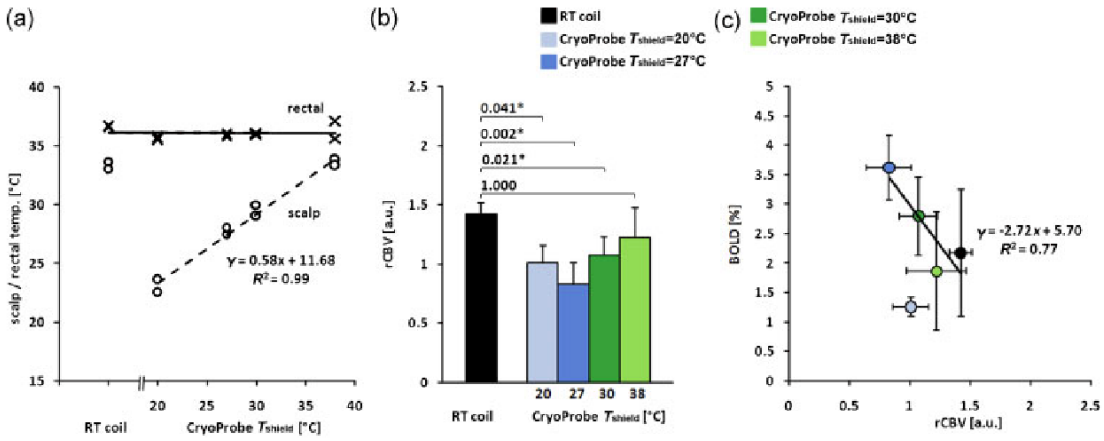

Figure 3-5: (a) Body and scalp temperatures, measured in two animals each, when positioned under the conventional room temperature (RT) coil and the CryoProbe at increasing thermal shield temperatures. The broken line represents the linear regression between the CryoProbe thermal shield and scalp temperatures. **(b)** Relative cerebral blood volumes (rCBV) determined in the somatosensory cortex (S1) using either the RT coil or the CryoProbe at different thermal shield temperatures. **(c)** Relationship between maximum blood oxygen level-dependent (BOLD) signal change and rCBV. The full line represents linear regression, excluding the values obtained for T_{shield} = 20 °C. Values are given as the mean ± standard deviation.

The dependence of the BOLD signal changes on the CryoProbe thermal shield temperature was investigated more thoroughly by (i) measuring the temperature on the scalp (Fig. 3-5a), and (ii) measuring rCBV in S1 area to assess baseline perfusion (Fig. 3-5b and 3-5c). Although a constant body temperature was maintained for the experiments (36.1 ± 0.5 °C) irrespective of T_{shield}, the scalp temperature depended on CryoProbe thermal shield temperature (Fig. 3-5a). Linear regression analysis revealed a linear relationship between T_{shield} and scalp temperature (R^2 = 0.99). Scalp temperatures comparable to the RT values (33.4 °C)

were found for a CryoProbe thermal shield temperature of T_{shield} = 38 °C (33.6 °C). Further experiments estimating the CBV (eq.[5]) as measure for the baseline perfusion revealed comparable values for the RT coil (1.42 ± 0.09) and the CryoProbe at T_{shield} = 38 °C (1.22 ± 0.25), and significantly reduced values at T_{shield} = 20 °C (1.01 ± 0.14), T_{shield} = 27 °C (0.83 ± 0.18), and T_{shield} = 30 °C (1.07 ± 0.16). A significant effect of temperature was found for the CBV [ANOVA $F(4, 22) = 6.57$, $p < 0.002$]. The relationship between maximum BOLD signal change (ΔS) and baseline perfusion (CBV) is depicted in Figure 3-5c. A linear relationship (R^2 = 0.77) was found between CBV and ΔS when excluding measurement values obtained with the CryoProbe at T_{shield} = 20 °C. Thus, changing T_{shield} affects CBV values with a corresponding impact on the BOLD response.

3.4 Discussion

The application of cryogenically cooled RF probes has recently been reported to increase SNR in structural *in vivo* MRI of small animals [35, 36]. However, it has not yet been investigated how the SNR gain provided by the cryogenic RF coil translates into sensitivity improvements during fMRI studies based on BOLD contrast. The BOLD amplitude elicited by sensory input is of the order of a few percent of the baseline signal, and hence fMRI in small animals such as mice, remains a challenge, which is commonly accounted for by using high magnetic field strength [132] and/or by optimizing sequence parameters [35, 48, 130]. The aim of this work was to investigate how increased SNR provided by the CryoProbe [34, 89] translates into enhanced BOLD sensitivity by comparing fMRI data acquired using either CryoProbe or RT coil set-up at the same field strength.

Analysis of T_2-weighted structural images of the mouse brain revealed a SNR gain of a factor of 2.8 ± 0.3 for a ROI located within the somatosensory area S1 when using the CryoProbe compared with the RT coil set-up. This value exceeds those reported earlier for structural mouse brain imaging using identical RF coils as in the present work [36]. The higher value can be explained by the superficial location of the ROIs in the S1 area. The slightly larger

dimensions of the individual coil elements (arc length) of the RT probe when compared to the CryoProbe translate into higher SNR gains for ROIs close to the surface coils [36].

In fMRI using GE-EPI sequences, a gain of SNR_0 of a factor of 3.1 ± 0.7 was found, whereas tSNR was degraded by physiological noise resulting in a tSNR gain of 1.8 ± 1.0. However, this SNR decrease was less pronounced when compared with values reported in literature [89]. Yet, direct comparisons of the absolute SNR with literature remain difficult because of different imaging parameters, such as voxel dimensions, sequence timing (T_E/T_R) and different main magnetic field strengths. Increased scattering of tSNR values was observed for the CryoProbe relative to the RT coil set-up, revealing the increased sensitivity of the CryoProbe to contributions from static and physiological subject noise, as predicted by theory (eq. [2]). The variance of the baseline signal was found to be consistently reduced when using the CryoProbe as compared to the RT probe irrespective of the thermal shield temperature of the CryoProbe. The standard deviation of the baseline signal recorded with the CryoProbe was 63 ± 3 % (range 59-67 %) of the corresponding RT values, indicating a gain in sensitivity by a factor of 1.60 ± 0.07. When investigating activation patterns over the entire brain, the effective gains in SNR_0 and tSNR are expected to decrease for deeper brain structures due to the surface coil design of the CryoProbe. For the investigation of localized activation this effect might be partly compensated for by optimizing pulse angles for the area of interest.

The maximum BOLD amplitude varied as a function of the CryoProbe thermal shield temperature (Fig. 3-4b), albeit not significant for all comparisons. We attribute these differences to the effects of hypo- or hyperthermia on baseline brain metabolic activity and hemodynamics. CBV increases significantly as a function of T_{shield} in the temperature range 27 °C < T_{shield} < 38 °C. At T_{shield} = 38 °C, thermal conditions (Fig. 3-5a) and CBV values (Fig. 3-5b) were found comparable to those measured with the RT coil. The baseline CBV values affect the BOLD response: high baseline CBV will reduce the capacity of cerebral vessels to further dilate on demand. In the range of mild hypothermia (27 °C < T_{shield} < 38 °C) an inverse proportional relation (slope = -2.7 %) was found between the BOLD amplitude and

baseline CBV. However, when further lowering the temperature to T_{shield} = 20 °C (severe hypothermia) a strong deviation from this linear relation was observed. Strong hypothermia is known to induce a massive reduction of the cerebral metabolic rate and probably affects cerebrovascular autoregulatory mechanisms. It has been shown that the relative cerebral blood flow is significantly reduced under hypothermic conditions [137]. Under these conditions, the system appears to be incapable of adequately responding to the increased metabolic and hemodynamic demands associated with excitatory input.

The temperature dependence of the maximum BOLD signal change emphasizes the importance of defined thermal conditions for fMRI studies, as stated previously in earlier reports [48]. Although usually only the body temperature of the animal is kept in a narrow range, in this work, the local thermal environment of the mouse head can be additionally controlled by the CryoProbe thermal shield, an option which is not available for conventional RT coils. The CryoProbe shield temperature is a further optimization parameter to enhance BOLD sensitivity, though care must be taken to stay within physiological limits.

In conclusion, the consistently lower noise level of the cryogenic surface RF probe leads to an increased image SNR (SNR_0) and increased temporal SNR (tSNR) compared with a conventional RT coil set-up at the same spatial resolution and main magnetic field strength. As expected, tSNR was found to be smaller than SNR_0, reflecting the impact of physiological noise contributions. Furthermore, the comparison of the CryoProbe and the RT coil performance with respect to fMRI revealed an increased BOLD sensitivity. Two factors contribute to the increase in SNR: the reduction of temporal fluctuations because of cryogenic cooling of the RF probe (factor 1.59 ± 0.25 on average over all investigated T_{shield}) and the increased BOLD response as a result of optimized thermal conditions controlled by the CryoProbe thermal shield (1.67 ± 0.86 for T_{shield} = 27 °C). The gain in sensitivity leads to increased statistical significance of BOLD-fMRI data, which may be exploited to improve temporal or spatial resolution or to study weak BOLD responses. This is of particular interest

for fMRI studies in mice, which are becoming increasingly important in view of the large number of genetically engineered models of human cerebral pathologies.

4. Cannabinoid Signaling Involved in Hyperalgesia Caused by Local Anesthetic Lidocaine at Low Doses

4.1 Introduction

Sensory and nociceptive processing involves a complex network of neural structures, with the first mediator being the nociceptor, a high threshold sensory neuron connecting peripheral tissues with the CNS [52]. Substantial progress has been made in understanding the molecular mechanisms of normal or pathological pain states, much of it with the help of genetically engineered mice displaying altered sensitivity to noxious input [92-95].

Lidocaine, a widely used local anesthetic, blocks voltage-gated sodium channels, thereby preventing the propagation of action potentials [138]. In clinics, formulations of 1-5 % (approx. 35-180 mM) lidocaine are commonly used for inducing regional anesthesia in order to suppress pain [139]. In addition, lidocaine has been reported to affect potassium channels [140, 141], and Leffler et al. showed the ability of lidocaine to directly activate and sensitize the transient receptor potential channel TRPV1 [142]. The capsaicin receptor TRPV1 is located on C-fibers and activated by a variety of chemical or physical stimuli [61].

The purpose of this study was to investigate effects of lidocaine on modulating sensory processing in response to noxious stimuli using functional magnetic resonance imaging (fMRI) by assessing local changes in cerebral blood oxygenation levels (BOLD [26]) [46]. FMRI has been previously used for studying pain processing in humans and rodents, mostly in rats [91, 97-101] and recently also in mice [46]. Mice are attractive models as genetically engineered mouse lines may yield information on molecular mechanisms involved. We made the unexpected observation that pretreatment with lidocaine at concentrations 100x lower than those used therapeutically, prompted a robust hyperalgesic effect as reflected both by increased BOLD-fMRI responses and behavioral readouts. A recent report suggested a critical involvement of type 1 cannabinoid (CB_1) receptors in central C-fiber activity-dependent

Article submitted: *"Cannabinoid signaling involved in hyperalgesia caused by local anesthetic lidocaine at low doses"*; Simone C. Bosshard, Christof Baltes, Hanns Ulrich Zeilhofer, Markus Rudin

hyperalgesia: the authors provided evidence that activation of CB_1 receptors by spinal endocannabinoids produced in response to strong noxious stimulation led to a reduction in the synaptic inhibition in the dorsal horn and thereby to a sensitization of the nociceptive sensory neurons [143]. We therefore hypothesized that the hyperalgesia observed following administration of lidocaine at low doses might be centrally mediated by activation of CB_1 receptors located in the dorsal horn of the spinal cord. To test this hypothesis, we used transgenic mice globally lacking the CB_1 receptor ($CB_1^{-/-}$) [144]. These animals did not display any lidocaine-induced hyperalgesia. These observations were endorsed by an experiment with pharmacological inhibition of CB_1 receptors: systemic administration of the specific CB_1 receptor blocker rimonabant (SR 141716) to wild type mice completely abolished the lidocaine-induced hyperalgesia. Together, these results indicate that central CB_1 receptors play a relevant role in mediating the increased sensitization following administration of the local anesthetic lidocaine at low doses.

4.2 Material and Methods

Animals and Stimulation Paradigm

All experiments were performed in accordance to the Swiss law of animal protection. 60 female C57Bl/6J mice and 8 female global $CB_1^{-/-}$, weighing 22 ± 3 g, were used for the experiments. The mice were anesthetized with isoflurane (induction 2-3 %, maintenance 1.2 % in a 70 % air – 30 % oxygen mixture; Abbott, Cham, Switzerland), endotracheally intubated, mechanically ventilated and paralyzed (for more details refer to [46]. The tail vein was cannulated for drug administration, and body temperature was maintained at 36.5 ± 0.5 °C using a warm-water circuit integrated into the animal support (Bruker BioSpin AG, Fällanden, Switzerland). Heart rate and blood oxygenation were monitored using a MR-compatible infrared sensor (MouseOx® Pulse Oximeter, Starr Life Sciences, Oakmont, PA, USA). For electrical stimulation a pair of needle electrodes (Genuine Grass instruments, West Warwick, USA) was inserted subcutaneously into the distal and proximal end of the palm of each forepaw, with a distance of 2-3 mm between the two needles. Electrical

stimulation was carried out using the following parameters (for details see [46]): current amplitude 1.5 mA, frequency 3 Hz, pulse duration 0.5 ms, stimulation period 60 s (180 pulses), and resting period 120 s.

Experimental Groups

The study design consisted of three sets of experiments: (1) Effects of lidocaine in wild type mice: 10 µl of lidocaine hydrochloride dissolved in 0.9 % NaCl was injected into the left forepaw 40 min prior to electrical stimulation. The following concentrations were used: 0.15 mM (n=9), 0.3 mM (n=7), 0.45 mM (n=7), 0.6 mM (n=7), 70 mM (n=6). Saline solution (0.9 % NaCl) served as a control and was injected into the right forepaw prior to electrical stimulation in all animals. The dynamic von Frey filament test was used to confirm the fMRI data (n=6). Baseline measurements of the forepaw withdrawal threshold were recorded in 6 awake, freely moving mice prior to the injection of 0.3 mM lidocaine under short isoflurane anesthesia. The forepaw withdrawal threshold was continuously measured during 60 minutes following the lidocaine injection. (2) Effects of lidocaine in $CB_1^{-/-}$ mice: electrical stimulation (n=8) as described above was carried out first to rule out any differences between the $CB_1^{-/-}$ and the wild type animals without administration of lidocaine. In a second experiment 10 µl of 0.3 mM lidocaine and 10 µl of 0.9 % NaCl were injected into the left forepaw and right forepaw, respectively, prior to electrical stimulation. (3) Pharmacological inhibition of CB_1 using rimonabant: The CB_1 antagonist/inverse agonist rimonabant (SR 141716, Anawa trading SA, Wangen, Switzerland) [145] was dissolved in a mixture of ethanol, Cremaphor (Sigma-Aldrich, Steinheim, Germany), and 0.9 % NaCl (1:1:18) and administered intravenously (10 mg/kg) prior to electrical stimulation only (n=4) or electrical stimulation after lidocaine injection (0.3 mM, n=5). For control experiments only the vehicle was injected prior to electrical stimulation after lidocaine injection (0.3 mM, n=5).

MRI Equipment and Sequences

All MRI experiments were performed on a Bruker BioSpec 94/30 small animal MR system (Bruker BioSpin MRI, Ettlingen, Germany) operating at 400 MHz (9.4 Tesla). For signal

transmission and reception a commercially available cryogenic quadrature RF surface probe (CryoProbe), consisting of a cylinder segment (180° coverage, radius = 10 mm) and operating at a temperature of 30 K was used (Bruker BioSpin AG, Fällanden, Switzerland) (for detailed information see [36]). Anatomical reference images in coronal and sagittal directions (slice orientations are given using the nomenclature of the mouse brain atlas [103]) were acquired using a spin echo (Turbo-RARE) sequence with the following parameters: field-of-view (FOV) = 20 x 20 mm^2, matrix dimension (MD) = 200 x 200, slice thickness (STH) = 0.5 mm, interslice distance (ISD) = 0.7 mm, repetition delay T_R = 3500 ms, echo delay T_E = 13 ms, effective echo time $T_{E,eff}$ = 39 ms, RARE factor (number of echoes sampled for each excitation) = 32, and number of averages (NA) = 1. The slices for the fMRI experiment were planned on the anatomical reference image and BOLD fMRI data were acquired using a gradient-echo echo planar imaging (GE-EPI) sequence with the following parameters: Five coronal slices covering a range of 2 to 5 mm anterior to the interaural line (IAL +2-5 mm) were recorded with FOV = 23.7 x 12.0 mm^2, MD = 90 x 60 (acquisition) and 128 x 64 (reconstruction) yielding an in-plane resolution of 200 x 200 μm^2, STH = 0.5 mm, ISD = 0.7 mm, T_R = 2500 ms, T_E = 8.5 ms, and NA = 3 resulting in an image acquisition time of 7.5 seconds. One fMRI experiment consisted of 112 or 152 repetitions and lasted 14 or 19 min.

Data Analysis and Statistics

The general linear model (GLM) tool integrated in the Biomap software program (M. Rausch, Novartis, Switzerland) was used to calculate statistical t-maps. GLM assesses correlations on a pixel-by-pixel basis between the fMRI signal and the stimulation pattern. The statistical threshold to detect activation was set to p=0.0001 for all experiments. Two coronal sections (IAL +2.8 mm and IAL +3.7 mm) covering the primary and secondary somatosensory cortices, the thalamus and the insula, were analyzed using a minimal cluster size of 15 voxels. The respective regions-of-interests (ROIs) derived from the GLM analyses were used to extract BOLD signal changes as a function of time. In cases for which the correlation analysis revealed no activated voxels, ROIs were transferred from the mouse brain

atlas [103]. EPI images covering the S1 area (IAL +3.7 mm) were used for group analysis as described in [46]. Comparative statistics was performed taking the maximal BOLD value of the first stimulation period of each animal. Values were not normally distributed and therefore tested at the $\alpha = 0.05$ level using the non-parametric Kruskal-Wallis test followed by the *post hoc* Fisher test (comparison between different groups). All values are presented as mean ± SEM.

Behavioral Test: Von Frey Filaments

The behavioral testing was made in 6 wild type mice, which were kept in the test cages for one hour prior to testing to allow accommodation. For baseline recording, each mouse was tested on each forepaw to obtain at least 5 data points measuring paw withdrawal thresholds to stimulation with electronically controlled von Frey filaments. Another baseline of 3 measurements per paw per mouse was recorded before injection of 10 µL 0.3 mM lidocaine into both forepaws. This was done under short isoflurane anesthesia (2 %, 1-2 min), after which the animals were put back to the test boxes. Only 4 animals received lidocaine injections, the other two received sham injections to serve as controls. The observer was blind to the treatment of the mice. Measurements were taken during 60 min after lidocaine injection in all animals. Values were averaged for intervals of 10 min and are presented as mean ± SEM.

4.3 Results

Pretreatment with Low Doses of Lidocaine Causes Hyperalgesia

Electrical stimulation of the forepaw using a current amplitude of 1.5 mA was shown to activate brain areas attributed to the pain matrix [46]. Consistent BOLD responses (in > 95 % of all animals studied) have been observed in the areas of the primary and secondary somatosensory cortices (S1 and S2), the thalamus and the insular cortex as revealed by general linear model (GLM) analysis (Fig 1a). The temporal changes of the BOLD amplitude

in the regions involved corresponded well with the four stimulation periods (Fig. 4-1b for S1 area contralateral to the stimulated paw). Non-invasive physiological monitoring of the mice showed stable parameters throughout the entire experiment: no changes in body temperature (36.5 ± 0.5 °C), arterial O_2 saturation (> 98 %), or heart rate (approx. 500 beats per minute) could be detected during the stimulation periods.

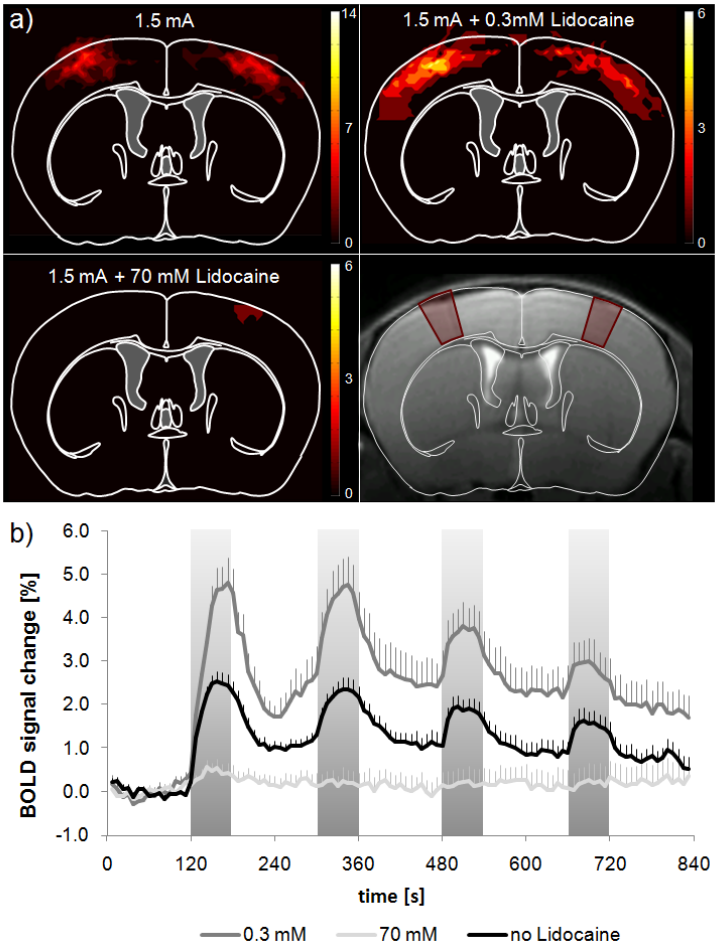

Figure 4-1: (a) Activation maps of the cortex after left and right electrical forepaw stimulation of 1.5 mA. Data show activated regions derived from GLM analysis (p = 0.000001, cluster size 15 voxels) for all animals overlaid on the mouse brain atlas at IAL +3.7 mm. The intensity indicates the number of animals showing significant BOLD activation at the given threshold. Scale bar is adjusted to the total number of scans performed. Bottom left: Mouse brain atlas overlaid on the anatomical MR image. Red indicates the forepaw region of the S1 somatosensory cortex. **(b)** Temporal profile of the relative change of the BOLD signal intensity as observed in the contralateral S1 area during electrical forepaw stimulation. Traces show electrical stimulation only (black), after injection of 0.3 mM lidocaine (dark gray) and after injection of 70 mM lidocaine (light gray). Grey bars indicate stimulation periods. All values are indicated as mean ± SEM.

Local administration of low concentrations of lidocaine into the mouse forepaw 40 min prior to the fMRI study led to a significant increase of the maximum BOLD signal change as compared with the untreated forepaw stimulated at the same current amplitude.

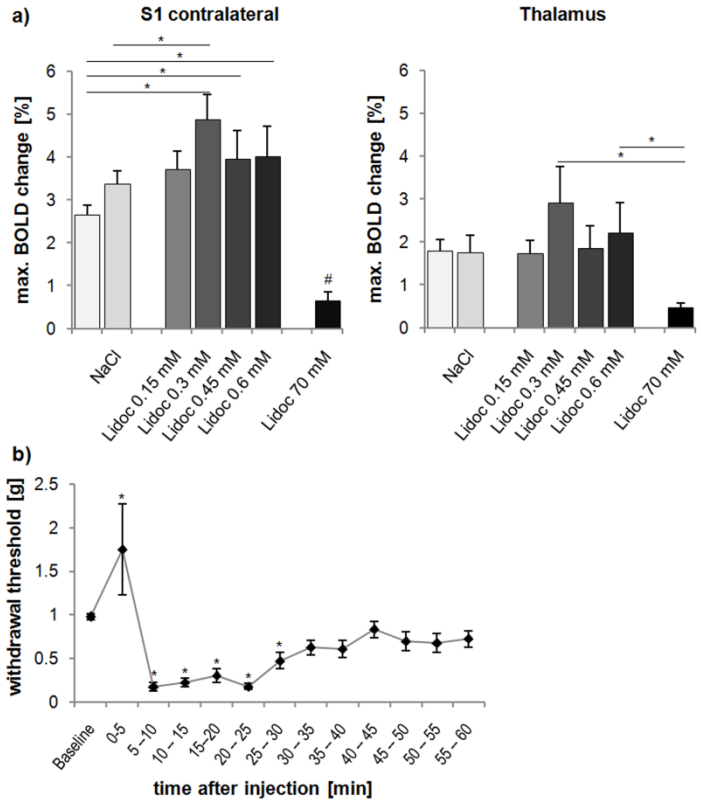

Figure 4-2: (a) Maximum BOLD signal changes in the S1 contralateral to the stimulated paw and in the thalamus in naïve WT animals and animals pretreated with lidocaine or NaCl. All values are indicated as mean ± SEM. (*p < 0.05, #p < 0.05 compared to all other groups). **(b)** Withdrawal threshold of the forepaws measured with dynamic von Frey filaments after injection of 0.3 mM lidocaine. An increased sensitivity was observed up to 30 min after lidocaine injection. All values are indicated as mean ± SEM. (*p < 0.05).

The maximal BOLD signal change (in % of baseline values) in the S1 region contralateral to the stimulated paw in naïve animals was 2.65 ± 0.2 % (Fig. 4-1b, Fig. 4-2a). This differed significantly from the maximal BOLD values of 4.89 ± 0.6 % (p = 0.0003), 3.96 ± 0.6 % (p = 0.03), and 4.01 ± 0.7 % (p = 0.02) for 0.3, 0.45, and 0.6 mM (10 µl) lidocaine, respectively, except for the lowest concentration used (0.15 mM), for which a value of 3.71 ± 0.4 % (p = 0.06) has been obtained. The BOLD response was dose-dependent with a maximum effect at 0.3 mM lidocaine (Fig. 4-2a). Clinically relevant doses (70 mM, 2 %) of

lidocaine almost completely abolished the BOLD signal (0.67 ± 0.2 %; Fig. 4-1b, Fig. 4-2a)). Activation maps for the 70 mM lidocaine group derived from GLM analysis (using $p = 10^{-6}$ as threshold) showed weak activation in the S1 area with clearly decreased intensity and extent as compared with the untreated and low dose lidocaine-treated groups (Fig. 4-1a). Injection of the vehicle (0.9 % NaCl) led to a maximal BOLD signal change of 3.37 ± 0.3 %, which was not significantly different from the untreated animals ($p = 0.16$), but significantly smaller than the response following administration of 0.3 mM lidocaine ($p=0.02$; Fig. 4-2a). The dependence on the lidocaine dose and the lack of response to the vehicle administration indicate that the increased sensitivity is caused by the local anesthetic administered at low concentrations. To further validate these unexpected fMRI findings we assessed the sensitivity of the mice in response to mechanical stimulation of the injected paw with von Frey filaments. The forepaw baseline withdrawal threshold of 1.0 ± 0.04 g was reduced significantly to 0.18 ± 0.05 g ($p = 0.0002$) 10 min and to 0.5 ± 0.09 g ($p = 0.00007$) 30 min after injection of 0.3 mM lidocaine. The hyperalgesic effect lasted for 30 min in the awake and moving animals before values slowly returned to baseline levels (Fig. 4-2b).

Lidocaine-Induced Hyperalgesia Requires the Type 1 Cannabinoid Receptor (CB_1)

In global CB_1 knock-out mice ($CB_1^{-/-}$) electrical stimulation of the forepaw at 1.5 mA yielded a maximal BOLD signal change of 2.28 ± 0.2 % in the S1 contralateral to the stimulated

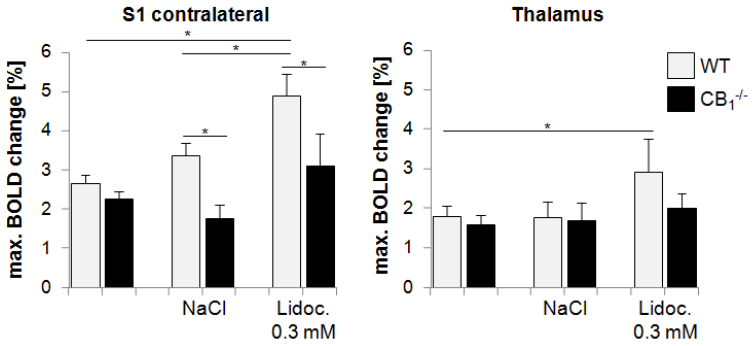

Figure 4-3: Maximum BOLD signal changes in the S1 contralateral to the stimulated paw and in the thalamus comparing WT (gray bars) and $CB_1^{-/-}$ (black bars) with or without lidocaine pretreatment. All values are indicated as mean ± SEM. (*$p < 0.05$)

paw, indicating no difference of sensitivity as compared with the WT animals (p = 0.39). However, following pretreatment of the forepaws with 0.3 mM lidocaine (10 µL), $CB_1^{-/-}$ did not show the hyperalgesic response observed in WT animals. The maximal BOLD values were 3.11 ± 0.8 % in $CB_1^{-/-}$ versus 4.89 ± 0.6 % in WT, respectively, which was statistically significantly different (p = 0.006). In contrast there was no difference in BOLD signal amplitudes in $CB_1^{-/-}$ mice with and without lidocaine treatment (p = 0.15). Also, injection of 10 µl NaCl into the forepaw of the $CB_1^{-/-}$ mice did not affect the maximal BOLD signal change (1.76 ± 0.4 %, p = 0.40) (Fig. 4-3).

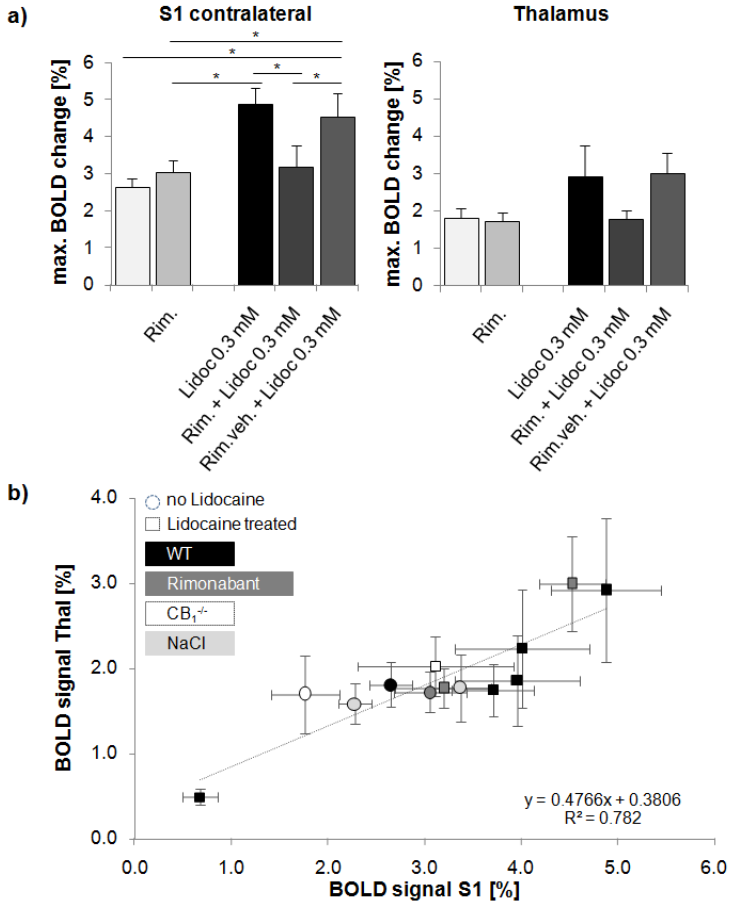

Figure 4-4: (a) Maximum BOLD signal changes in the S1 contralateral to the stimulated paw and in the thalamus of WT animals (naïve or pretreated with lidocaine and/or the CB_1-blocker rimonabant). **(b)** Correlation of the maximum BOLD signal changes in the thalamus and the S1 contralateral to the stimulated paw. (Squares: Lidocaine treatment, black: WT, white: $CB_1^{-/-}$, dark gray: Rimonabant (vehicle), light gray: NaCl). All values are indicated as mean ± SEM. (*p < 0.05)

The involvement of the CB_1 receptor in eliciting the hyperalgesic response to lidocaine was confirmed by pharmacological inhibition of CB_1 receptors using the selective antagonist/inverse agonist rimonabant. In the absence of lidocaine, rimonabant did not affect the BOLD signal change (3.06 ± 0.4 % versus 2.65 ± 0.2 % without rimonabant, p = 0.39) in response to electrical stimulation. Systemic administration of rimonabant following pretreatment with 0.3 mM lidocaine completely abolished the hyperalgesic effects of lidocaine (3.20 ± 0.5 % compared to 4.88 ± 0.6 % with and without rimonabant, p = 0.01). In contrast, administration of the rimonabant vehicle did not affect the hyperalgesic reaction to low dose lidocaine and led to a maximal BOLD signal change of 4.53 ± 0.3 %, which is comparable to the values observed following application of lidocaine alone (4.88 ± 0.6 %, p = 0.55), but is significantly different from the application of rimonabant combined with lidocaine (p = 0.04) (Fig. 4-4a).

For all experiments, the BOLD signal changes in the thalamus showed trends that are in line with the changes observed in the S1 region contralateral to the stimulated paw. This is reflected by the good correlation (R^2 = 0.8) of the BOLD responses of the two regions (Fig. 4-4b).

4.4 Discussion

Functional MRI in small animals has become an important tool in biomedical research, as it provides global insight of brain activation while being non-invasive allowing the coverage of large brain volumes. Studies in humans and animals showed noxious-evoked activation patterns to correspond with the structures of the pain matrix [46, 97-101]; hence, fMRI allows studying aspects of pain processing non-invasively. However, due to the hemodynamic origin of the signal, the activated areas are usually not tightly confined to the functional brain entities but include territories covered by irrigating and draining vessels. Correspondingly, the activated areas in mouse brain identified by fMRI correlation analysis extend beyond the functional maps of the brain atlas (Fig. 4-1a) [103].

Lidocaine is a widely used local anesthetic and antiarrhythmic agent, which acts through inhibition of the voltage-gated Na^+ channels. Voltage-gated Na^+ channels play a crucial role in the generation and propagation of action potentials. Blocking Na^+ channels by lidocaine has been investigated in neurons and in the heart by various methods [146-148].

Unexpectedly, administration of lidocaine at low dose caused significant and reproducible hyperalgesia, a rather surprising observation for a compound clinically used for analgesia. While the BOLD response to paw stimulation following pretreatment with lidocaine at a dose of 2 % (70 mM) lidocaine, which is commonly used for local anesthesia, was almost completely suppressed, concentrations of lidocaine in the range 0.15 to 0.6 mM elicited a significant increase in local brain activity as reflected both by an increased amplitude and extent of the BOLD signal. Experiments using the behavioral von Frey filament test revealed that these observations were not an artifact of the fMRI experiment but rather reflected hyperalgesia. This sensitization following lidocaine injection could be reproduced in all animals studied. The effect did not last quite as long as in the fMRI experiments, which is most likely due to the fact that the mice in the behavioral test were awake and moving, while the animals in the fMRI experiments were anesthetized for the entire duration of the experiment. The underlying mechanisms acting in the sensory afferents are not entirely understood. Experiments with injection of NaCl indicate a slight, though not significant, increase of the BOLD response, which largely excludes the increased amount of liquid and electrolytes in the paw, which might alter the electrical conductivity, to be the cause for the hyperalgesic response observed.

Several mechanisms might account for the initial nociceptive input, which triggers the secondary hyperalgesic effect observed in the fMRI experiments following administration of lidocaine at a low dose. It has been shown that lidocaine activates and sensitizes the TRPV1 receptors and thereby directly activates C-fibers, at concentrations exceeding 1 mM [142]. However, as the concentrations used in this study are up to 10-fold smaller, activation of C-fiber signaling through lidocaine binding to TRPV1 channels appears unlikely. Another possibility might be the blocking of K^+ channels, which already occurs at much smaller

lidocaine concentrations than required for the blocking of Na^+ channels, and therefore might lead to a change in the excitability of these neurons and to an enhanced sensitivity to noxious input. This would be in line with reports on the enhancement of delayed-rectifier K^+ currents at <0.1 mM lidocaine and a partial channel block at concentrations >0.1 mM [141].

Independent of these potential peripheral mechanisms leading to a sensitization, central mechanisms have to be considered as well. Based on a recent report [143], we hypothesized that injection of lidocaine might lead to an activity-dependent endocannabinoid-mediated secondary hyperalgesia. Pernia-Andrade et al. demonstrated the activation of CB_1 receptors of the dorsal horn in the spinal cord during strong nociceptive (C-fiber) input [143]. This would then cause a disinhibition of the pain-specific neurons in the dorsal horn, which are rendered sensitive to input even from non-nociceptive A-fibers, thereby resulting in hyperalgesia in the area surrounding the original nociceptive input. The observation that in $CB_1^{-/-}$ mice the BOLD response to electrical stimulation was not affected by administration of 0.3 mM lidocaine (the concentration that elicited the largest effect in WT animals) and that the lidocaine induced hyperalgesic affect could be completely inhibited by administration of CB_1-blocker rimonabant, clearly prove an involvement of the endocannabinoid system in the development of hyperalgesia due to injection of low concentrations of lidocaine prior to electrical stimulation. Additional studies are warranted to elucidate molecular mechanisms underlying this phenomenon.

Another report by Fioravanti et al. [149] may also be of interest in this context linking the CB_1 receptors to the TRPV1 channel on nociceptors. It has been shown that in cells coexpressing CB_1 and TRPV1, CB_1 activation either inhibits or stimulates TRPV1 depending on the activation of the cAMP cascade [150]. Fioravanti et al. have shown that the TRPV1 channel remains in a sensitized state induced by tonic activity of the CB_1 receptor [149], which would be in line with enhanced sensitivity to sensory input. This mechanism should also be considered when trying to resolve the processes underlying the sensitization induced by lidocaine as observed in this study.

Of course one has to consider that fMRI studies are typically carried out in anesthetized animals, a recurring issue, in particular when investigating nociception. Ideally, anesthesia should neither interfere with brain activity nor act analgesic. However, many anesthetics suitable for longitudinal studies have an analgesic component and some even affect the neurovascular coupling. We used isoflurane in this study as it allows easy administration and controlled dosing. In previous studies, we [46] and others [71, 73, 151] have shown that robust and reproducible fMRI signals can be obtained in response to sensory and noxious stimuli. In the latter case significant activation has been observed in brain areas involved in pain processing, indicating the feasibility of such studies using this anesthesia protocol.

Aside from the mechanistic implications, the findings of our study might also be of clinical relevance. In spite of the higher concentrations of lidocaine applied clinically, there will be regions in the boundary area of the infiltrated tissue, in which concentrations are as low as the ones used in this study. Similarly, in the course of drug wash-out and degradation low concentrations will inevitably occur. The observation that such low concentrations can cause a sensitization could partially account for postsurgical hyperalgesia.

5. Reduced BOLD Response in Mice Lacking Nociceptor Specific Sodium Channels ($Na_V1.7$)

5.1 Introduction

Voltage-gated sodium channels are integral membrane proteins found in neurons and most other electrically excitable cells. They are responsible for the rising phase of the action potential, and contain nine structurally related α-subunits that form sodium selective aqueous pores in the cell membrane [152, 153]. Pharmacologically, the sodium channel subtypes can be distinguished by their sensitivity to tetrodotoxin (TTX), a neurotoxin isolated from the puffer fish and other members of the order of *Tetraodontiformes.* The larger group comprises the so called TTX-sensitive channels which are blocked by nanomolar concentrations of TTX, while the TTX-resistant channels cannot be blocked by micromolar concentrations of TTX [154]. The role of sodium channels in pain pathways has become increasingly important due to alterations of the proteins that occur in pain states [155-157].

The TTX-sensitive sodium channel $Na_V1.7$, which is located at the terminal of small-diameter sensory neurons, plays an important role in pain mechanisms. Studies with nociceptor specific knock-out mice ($Na_V1.7R^{-/-}$) revealed a reduction in mechanosensation, a strong deficit in the development of inflammatory pain, and hyposensitivity to noxious thermal stimulation as measured with the Hargreave's apparatus [94].

After the development of a robust stimulation paradigm to study pain processing in mice using BOLD fMRI [46], we tested for its specificity by applying the paradigm to $Na_V1.7R^{-/-}$ * mice.

5.2 Methods

Three groups of animals were examined for this study: (i) the wild type (WT) group consisted of 8 female C57Bl/6 mice of 3-6 months of age. (ii) The $Na_V1.7R^{-/-}$ group consisted of 6 animals, 4 males and 2 females, aged 2-8 months. (iii) The WT littermates of

* The $Na_V1.7R^{-/-}$ mice were kindly provided by Prof. Dr. John Wood, University College London, UK.

the $Na_V1.7R^{-/-}$ mice consisted of 2 females and 3 males, aged 2-8 months. The $Na_V1.7R^{-/-}$ and their WT littermates were kindly provided by Dr. John N. Wood, University College London, United Kingdom.

Preparation of the animals included intubation and mechanical ventilation, stereotactic fixation of the head, and monitoring of body temperature and blood gas levels. The experiments were performed under isoflurane anesthesia. The stimulation consisted of sequential bilateral forepaw stimulation using a stimulation amplitude of 1.5 mA. A detailed description of preparation, stimulation, MR parameters, and data analysis is available in Chapter 2.2 and [46].

5.3 Results

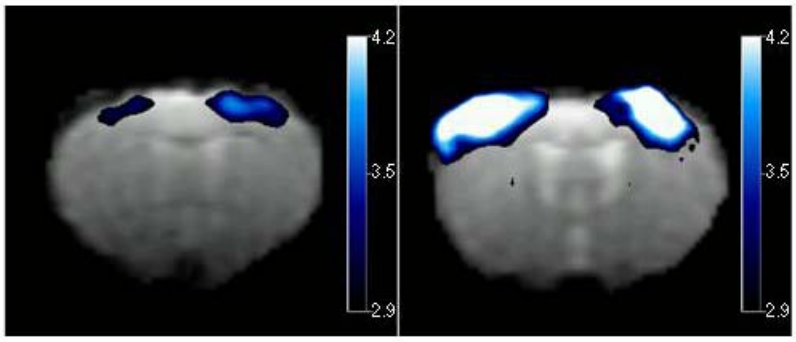

Figure 5-1: Statistical t-maps (2D low pass filtered) obtained with GLM analysis of two representative animals: **(a)** $Na_V1.7R^{-/-}$; **(b)** WT. Statistical maps are overlaid on the EPI image, showing activation after stimulation of the left forepaw. T-values are indicated at the scale bar.

Electrical forepaw stimulation led to a statistically significant BOLD signal change in all experimental groups. Distinct activation was detected in the somatosensory cortex ipsi- and contralateral (Fig. 4-1) to the stimulated paw and in the thalamus. While the temporal profiles of the WT and WT littermates are virtually identical, the $Na_V1.7R^{-/-}$ mice display a significantly reduced BOLD response (Fig. 4-2). The maximal BOLD signal changes of the somatosensory cortex contralateral to the stimulated paw were 1.3 ± 0.4 % ($Na_V1.7R^{-/-}$), 2.54 ± 0.2 % (WT) and 2.03 ± 0.3 % (WT littermates).

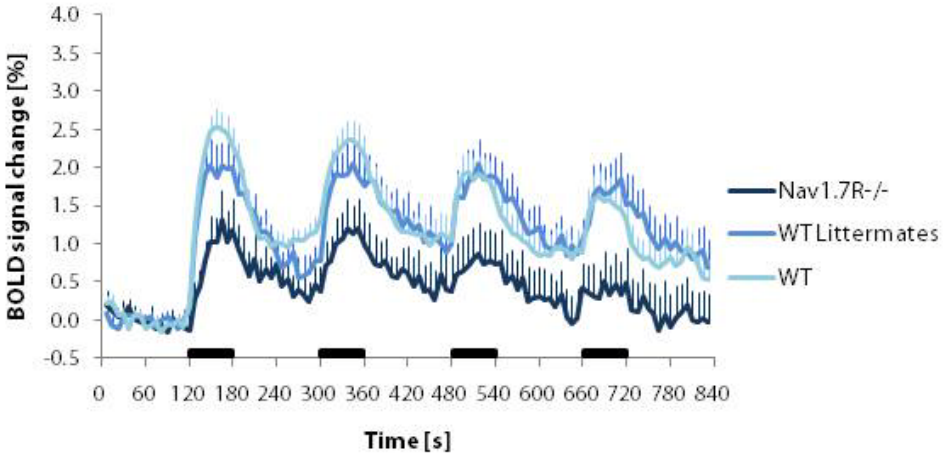

Figure 5-2: Relative change of BOLD signal in contralateral somatosensory S1 area during electrical forepaw stimulation at 1.5 mA for the $Na_v1.7R^{-/-}$ (dark blue, n=6), WT littermates (blue, n=5) and the WT animals (light blue, n=8). Black bars indicate stimulation periods. All values are presented as mean+SEM.

The values of the integrated BOLD profiles of the contralateral somatosensory cortex (120 s – 180 s) yielded 111.2 ± 28 %s, 224.1 ± 43 %s, and 232.2 ± 21 %s for the $Na_V1.7R^{-/-}$, WT littermates and WT mice, respectively (Fig. 4-3). The values for the $Na_V1.7R^{-/-}$ were significantly different compared to the WT littermates (p = 0.04) and the WT mice (p = 0.01).

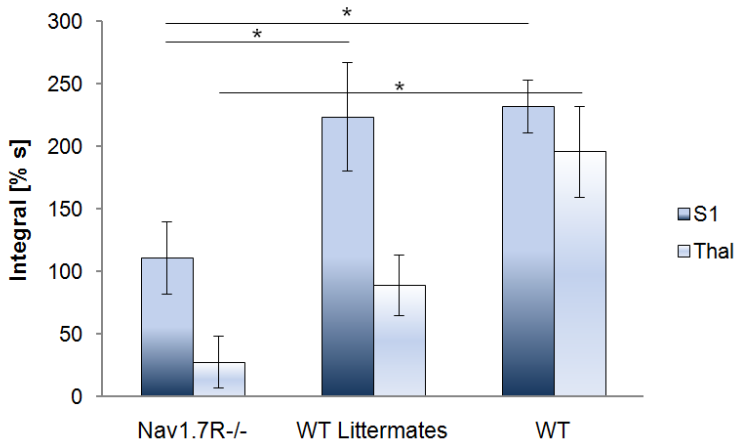

Figure 5-3: Areas under the curve of the S1 area contralateral to the stimulated paw and the thalamus, integrated during the four stimulation periods. All values are presented as mean ± SEM. Asterisks indicate a significant difference at the 0.05 level.

For the thalamus, the situation is less clear: The maximal BOLD amplitudes are 1.76 ± 0.26 % for the WT animals, 0.74 ± 0.22 % and 0.76 ± 0.33 % for the WT littermates and the $Na_V1.7R^{-/-}$, respectively. The integral values for the $Na_V1.7R^{-/-}$ (27.8 ± 20 %s) are significantly smaller than those of the WT animals (196.1 ± 36 %s, p = 0.0006). However, the values of the WT littermates were also quite low (89.2 ± 24 %s), but not significantly different compared to either of the other groups.

5.4 Discussion

Electrical stimulation of the forepaws using a current amplitude of 1.5 mA led to robust and reproducible BOLD signal changes in brain areas associated with nociception (somatosensory cortices, thalamus). As expected, the cortical and thalamic BOLD response was significantly reduced in $Na_V1.7R^{-/-}$ mice. This is in line with behavioral data reported for these mice, which show a dramatic reduction in mechanosensation [94]. However, electrical stimulation of the forepaw might not be the ideal paradigm to test for nociception and its pathologies due to different reasons: 1) it is difficult to determine whether the stimulation using certain parameters is noxious or still innocuous, since the intensity depends on the current density in the tissue. Due to the experiments described in chapter 2.2 we believe that the stimulation used in this study is noxious and therefore recruits predominantly Aδ- and C-fibers. 2) It is not possible to discriminate whether the detected fMRI signal in the brain is only related to the noxious stimulation or due to direct electrical activation of the primary afferents, which include Aβ-, Aδ- and C-fibers. Direct electrical activation of the afferents might explain why we still detect a BOLD signal change of more than 1 % in the $Na_V1.7R^{-/-}$ mice, despite the lack of the $Na_V1.7$ sodium channels which should inhibit signal transmission on nociceptors. Therefore, it will be of interest to test these mice with the strictly noxious thermal stimulation paradigm described in chapter 6.

The results obtained of the thalamus are not in good agreement with the cortex data. The BOLD signal of the $Na_V1.7R^{-/-}$ is still markedly reduced as compared to the WT animals. However, the BOLD signal of the WT littermates is also reduced in comparison to the WT

animals, with a maximum amplitude in the range of the $Na_V1.7R^{-/-}$ mice. The reason for the decreased thalamus activation needs to be determined in further studies.

6. TRPV1-Mediated Entry of the Quaternary Lidocaine Derivative QX–314 Leads to Inhibition of Nociceptive Input as Measured by BOLD fMRI in Mice Using Thermal Stimulation

6.1 Introduction

Functional magnetic resonance imaging (fMRI) in animals enables non-invasive studies of brain function, e.g. involving the sensory system. Electrical stimulation is a commonly used stimulation paradigm for such studies [70-72, 91, 102] and has recently been applied to analyze sensory and nociceptive processing in mice [46]. However, there are several drawbacks to this type of stimulation besides the fact that it is not physiological: 1) the needle electrodes need to be inserted subcutaneously into the skin, which induces a stimulus even in the absence of an electric current. 2) The stimulus strength is determined by the local current density, which depends on the (relative) placement of the electrodes. 3) The electrical current may activate the neurons directly instead of only inducing a peripheral stimulus, which then leads to the activation of neurons. In view of these drawbacks, we aimed at establishing a physiological stimulation paradigm with better controllable parameters suitable for fMRI studies. We adopted noxious stimulation by local heating of the forepaws using an infrared laser source operating at 975 nm. Our data show that this protocol leads to reproducible changes in the blood oxygen level dependent (BOLD) signal intensity in the various brain areas associated with the pain processing as a function of temperature.

Pain sensation caused by heat is mediated by receptors of the transient receptor potential (TRP) family, the most important being the vanilloid receptor TRPV1, which is activated by temperatures of 42 °C and above [61] and located on C-fiber afferents [158]. Other members of the TRP family respond to similar (TRPV3, activation threshold: 33-39 °C, into noxious

Article in preparation: "*TRPV1-Mediated Entry of the Quaternary Lidocaine Derivative QX–314 Leads to Inhibition of Nociceptive Input as Measured by BOLD fMRI in Mice Using Thermal Stimulation*"; Simone C. Bosshard, Florian Stuker, Constantin von Deuster, Markus Rudin.

range,) or higher (TRPV2, activation: 52 °C) temperatures [159, 160]. TRPV2 channels were reported to activate thinly myelinated Aδ-fibers [161, 162], whereas TRPV3 channels are only located in keratinocytes in mice [160], but not in dorsal root ganglia (DRGs).

To demonstrate the specificity of the paradigm for assessing nociceptive signaling we applied the quaternary lidocaine derivative QX-314 (lidocaine N-ethyl chloride) to the forepaws. QX-314 is a permanently positively charged molecule which, due to its charge, cannot cross cell membranes. The compound has no effect on sodium channels when applied extracellularly, however, intracellularly applied, it was found to block sodium channels, leading to local anesthesia [163-166]. Binshtok and colleagues established a method to selectively block nociceptive signaling by activating TRPV1 channels; Also known as capsaicin receptor, TRPV1 is located on C-fiber nociceptors and activated by a wide range of physical and chemical stimuli, among them capsaicin [61]. Binding of capsaicin activates and opens the TRPV1 channel, allowing the QX-314 molecule to enter the cell and block the sodium channels from the inside, inhibiting the propagation of action potentials [167].

Indeed, in this fMRI study we showed that application of QX-314 in combination with capsaicin led to an abolishment of the BOLD signal in response to the thermal stimulation, while administration of either compound alone did not affect the signal amplitude.

6.2 Methods

Animal Preparation

All experiments were performed in accordance with the Swiss law of animal protection. 20 female C57Bl/6 mice weighing 22 ± 3 g were anesthetized with isoflurane (induction 2-3 %, maintenance 1.2 % in a 70 % air – 30 % oxygen mixture; Abbott, Cham, Switzerland), endotracheally intubated and mechanically ventilated throughout the entire experiment. Further preparation included stereotactic fixation of the head, monitoring of body temperature, heart rate and arterial oxygen saturation; and administration of a neuromuscular

blocking agent. Most animals were used for more than one experiment. For more detailed information on animal preparation please refer to Chapter 2.2 and [46].

Non-invasive monitoring of the mice showed stable physiology throughout the experiments. Body temperature was kept stable at 36.5 ± 0.5 °C for the entire experiment. Heart rate was stable around 500 beats per minute in all animals and did not change during stimulation. Arterial oxygen saturation was > 97 %, indicating a well adjusted ventilation of the animals. After completion of the fMRI experiments, the animals recovered fast and could be used for further experiments.

Experimental Groups

For the implementation and optimization of thermal stimulation paradigm three conditions have been evaluated: (Group 1) Stimulation at 45 °C using a 2 mm diameter laser spot ($n_{animals}$ = 10, n_{scans} = 19). (Group 2) Stimulation at 46 °C using a 2 mm diameter laser spot ($n_{animals}$ = 6, n_{scans} = 11). (Group 3) Stimulation at 45 °C using a laser spot of 1 mm in diameter ($n_{animals}$ = 6, n_{scans} = 12).

Using the paradigm yielding the maximal BOLD signal with no obvious side effects due to heat stimulation (corresponding to 45 °C using a 2 mm diameter laser spot), the specificity of the protocol was evaluated using pharmacological modulation of the thermal stimulation. Again three groups of animals have been used: (Group 4) Animals receiving an injection of 10 µl of a solution containing 67 mM QX-314 and 1.6 mM capsaicin locally into the left and right forepaw 80 and 100 min before thermal stimulation, respectively ($n_{animals}$ = 7, n_{scans} = 14). The mixture was prepared from stock solutions of 5 µl QX-314 (134 mM, lidocaine N-ethyl chloride, Sigma-Aldrich, Steinheim, Germany) dissolved in 0.9 % NaCl and 5 µl capsaicin (3.3 mM, Sigma-Aldrich, Steinheim, Germany) dissolved in ethanol and diluted with 0.9 % NaCl.

Two control groups have been used: (Group 5) Animals receiving 10 µl of 67 mM QX-314 in 0.9 % NaCl into the left and right forepaw 80 and 100 minutes prior to thermal stimulation, respectively ($n_{animals}$ = 3, n_{scans} = 6), and (Group 6) mice receiving10 µl solution

containing 1.6 mM capsaicin dissolved in ethanol and 0.9 % NaCl into the left and right forepaw 80 and 100 minutes before stimulation ($n_{animals}$ = 3, n_{scans} = 6).

Thermal Stimulation

Thermal stimulation was performed using a custom built stimulation device consisting of the following parts: two 9 W infrared laser diodes operating at 975 nm (BMU8_975_01_R, Oclaro, San Jose, CA, USA) were connected to 5 m glass fibers (Thorlabs Inc., München, Germany) which entered the Faraday cage of the scanner. The power output of the laser was regulated by a custom built driver (Meerstetter Engineering GmbH, Rubigen, Switzerland). Two types of cubes made from black plexiglas with a small hole drilled in the center (1 or 2 mm) were mounted on the SMA connector at end of the glass fibers, allowing choosing between two different diameters of the laser spot (1 or 2 mm) (Fig. 6-1b). In addition, a temperature probe was placed next to the bore to record the temperature of the paw (Fig. 6-1b). The temperature probe was connected to an electrical thermometer (P600, Dostman Electronic, Wertheim-Reicholzheim, Germany). The homebuilt proportional-integral-derivative (PID) controller was used as a feedback control, regulating the laser driver in order to maintain the measured temperature at the paw at the set target temperature. The stimulation paradigm was controlled from the physiological monitoring device (Powerlab, ADInstruments, Spechbach, Germany), sending a trigger pulse to the PID controller (Fig. 6-1a).

The stimulation paradigm consisted of a block design starting with a resting period of 120 s (baseline) followed by 60 s of stimulation. This series was repeated four times and fMRI data acquisition was continued for another seven minutes after the last stimulation block. A stimulation experiment was considered successful if the target temperature at the paw was maintained for at least 30 s with an accuracy of ± 0.5 °C. Stimulation started with the left paw in all animals. Following a resting period of 8 minutes, the right paw was stimulated.

The feedback controlled temperature regulation of the laser worked reliable for both spot diameters. On average 20-25 s were used to reach the target temperature, which was

maintained for the remainder of the stimulation period with ± 0.5 °C deviation at the most (Fig. 6-1c). Only 2 out of 64 scans had to be discarded because the target temperature was not reached within 30 s.

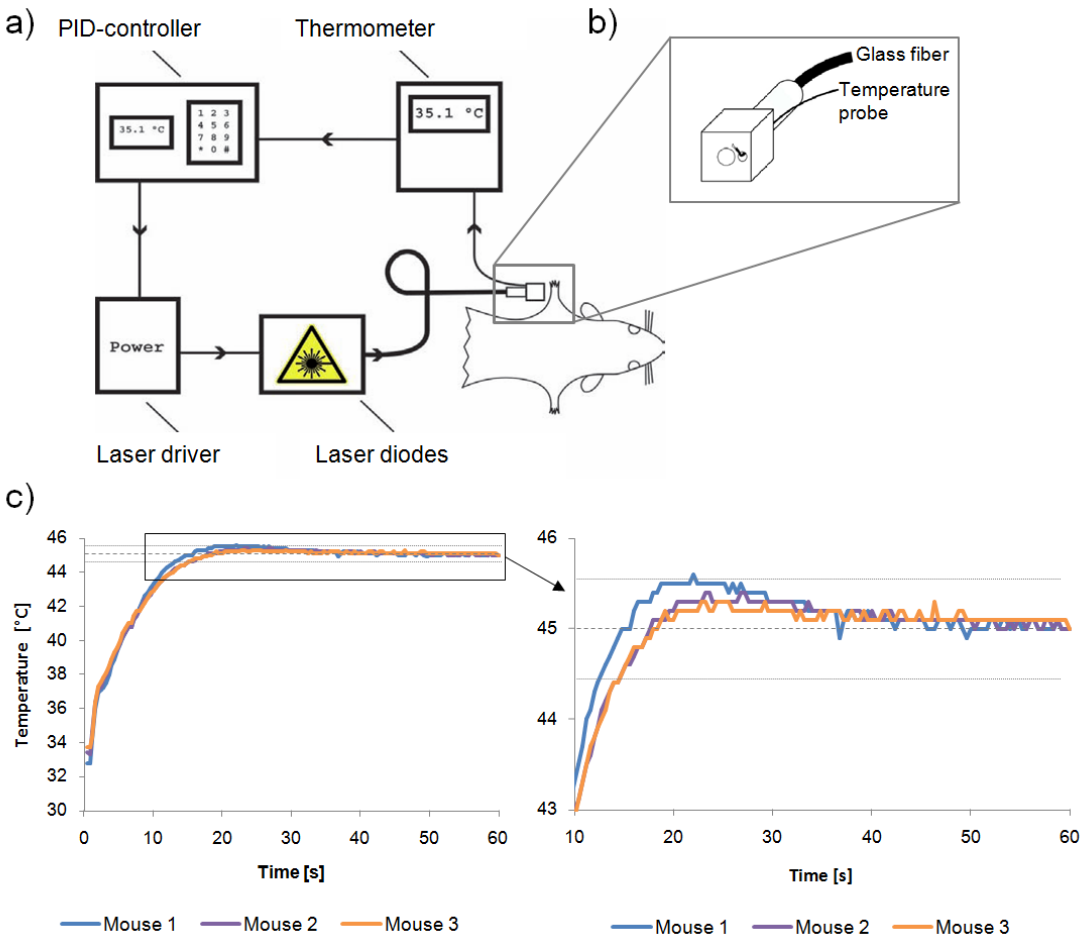

Figure 6-1: **(a)** Set-up of the laser stimulation with temperature-feedback-loop. **(b)** Close-up of the plexiglas cube and temperature control placed at the paw; the hole allowed using two spot diameters (1 and 2 mm). **(c)** Temperatures during stimulation, recorded at the mouse forepaw for three different scans. Target temperature of 45 ± 0.5 °C was reached for at least 30 s.

MRI Equipment and Sequences

All experiments were carried out on a Bruker BioSpec 94/30 small animal MR system (Bruker BioSpin MRI, Ettlingen, Germany) operating at 400 MHz (9.4 Tesla). For signal transmission and reception a commercially available cryogenic quadrature RF surface probe

(CryoProbe) operating at 30 K was used (Bruker BioSpin AG, Fällanden, Switzerland) (for detailed information see [36]). The ceramic outer surface of the coil touching the mouse head was kept at 30 °C using a temperature-controlled heating device.

Anatomical reference images in coronal and sagittal directions (slice orientations are given using the nomenclature of the mouse brain atlas [103]) were acquired using a spin-echo (Turbo-RARE) sequence (for detailed parameters see Chapter 2.2 and [46]). Subsequently, the slices for the fMRI experiment were planned on the anatomical reference images and BOLD fMRI data were acquired using a gradient-echo echo planar imaging (GE-EPI) sequence with the following parameters: Five coronal slices covering a range of 2 to 5 mm anterior to the interaural line were recorded with a field-of-view FOV = 23.7 x 12.0 mm2, matrix dimension MD = 90 x 60 (acquisition) and 128 x 64 (reconstruction), yielding an in-plane resolution of 200 x 200 µm2, slice thickness STH = 0.5 mm, interslice distance ISD = 0.7 mm. For the optimization experiments (1) and (2), values for repetition time TR = 2500 ms, echo time TE = 8.5 ms, number of averages NA = 3, and number of repetitions NR = 152 have been used, resulting in an image acquisition time of 7.5 seconds. For all remaining experiments, the parameters were as follows: TR = 1000 ms, TE = 8.5 ms, NA = 1 and NR = 1140, resulting in a temporal resolution of 1 second. All fMRI acquisitions lasted 19 min.

Data Analysis and Statistics

Data analysis was performed using the Biomap software program (M. Rausch, Novartis Institute for Biomedical Research, Switzerland). Statistical t-maps were calculated using the general linear model (GLM) tool, which assesses correlations on a pixel-by-pixel basis between the fMRI signal train and the stimulation paradigm. Activation was detected using a statistical threshold of p = 0.0001 for all experiments. With a minimal cluster size of 15 voxels, two coronal sections were analyzed, of which one slice covered the thalamus, the secondary somatosensory (S2) and insular cortex (IC) (2.8 mm anterior to the interaural line (IAL + 2.8 mm)), and the other covered the forepaw areas of the primary somatosensory cortex (S1) (IAL + 3.7 mm). The respective regions-of-interest (ROIs) derived from the GLM analyses were used to extract the BOLD signal changes as a function of time. In cases

for which the correlation analysis revealed no activated voxels at the expected locations, ROIs were transferred from the mouse brain atlas [103]. In addition to these regions, a control region located at the ventral pallidum and not involved in nociceptive processing was evaluated. GLM-derived activation patterns (EPI images covering the S1 area (IAL +3.7 mm)) were used for group analysis as described in [46].

Comparative statistics was performed taking the maximal BOLD value of the first stimulation period of each animal. Values were not normally distributed and therefore tested at the $\alpha = 0.05$ level using the non-parametric Kruskal-Wallis test followed by the *post hoc* Bonferroni test (comparison between different groups). All values are presented as mean ± SEM.

6.3 Results

BOLD Signal Changes Correlate with the Thermal Stimulation Paradigm

Thermal stimulation of the forepaws led to consistent BOLD responses in the S1 and S2 somatosensory cortices and the thalamus. The signal changes correlated well with the stimulation pattern and intensity. The image and signal quality was high even when increasing the temporal resolution to 1 second.

The maximal BOLD signal change at 45 °C was 2.8 ± 0.5 % in the S1 area contralateral to the stimulated paw and 1.8 ± 0.4 % in the thalamus. At 46 °C, the maximal BOLD signal changes in the contralateral S1 area were 4.4 ± 0.9 % and 4.1 ± 0.6 % for the laser spots of 2 mm and 1 mm in diameter, respectively. The maximal BOLD signal changes in the thalamus were 3.3 ± 1.0 % (2 mm diameter) and 3.1 ± 0.6 % (1 mm diameter). The BOLD amplitude was influenced by the stimulation temperature, but not by the diameter of the laser spot (Fig. 6-2b).

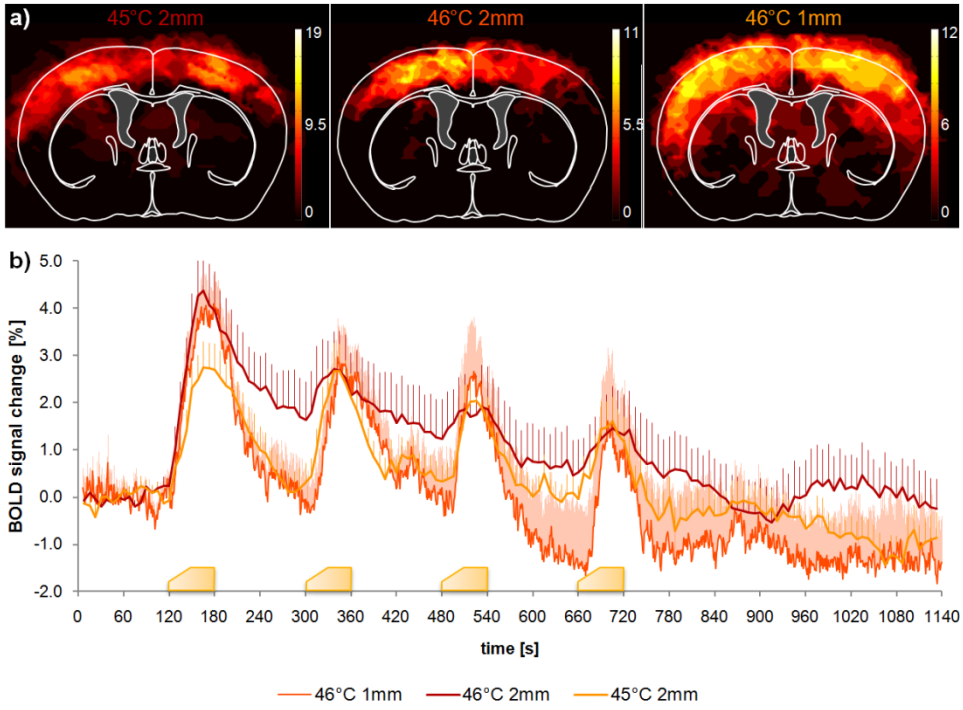

Figure 6-2: (a) Activation maps after left and right thermal forepaw stimulation of 45 and 46 °C. **(b)** Temporal BOLD profile of the somatosensory cortex (S1) contralateral to the stimulated paw. Stimulation parameters were: 46 °C, 1mm spot size (dark orange), 46 °C, 2mm spot size (red), and 45 °C, 2mm spot size (light orange). Yellow blocks indicate stimulation periods. All values are given as mean + SEM.

Nociceptive Block Induced by QX-314 and Capsaicin

Combined application of the lidocaine derivative QX-314 and capsaicin led to a decreased BOLD activation detected in the brain (S1: 0.6 ± 0.3 %, p = 0.01; thalamus: 0.5 ± 0.2 %, p = 0.1) indicative of a specific inhibition of neuronal signal transmission via C-fibers. This inhibitory effect was not observed in the control experiments, where either compound was applied separately. Administration of QX-314 alone led to a maximal BOLD signal change of 4.9 ± 0.7 % in the S1, which was not significantly different from the untreated animals (p = 0.14) but significantly different from the combination treatment capsaicin plus QX-314 (p = 0.0002). Similar results have been found for the thalamic activation: the BOLD intensity of 4.0 ± 0.5 % was not different compared with untreated mice but significantly different (p=0.0001) from values obtained with the combination treatment. Application of capsaicin

alone led to maximal BOLD signal changes of 5.1 ± 0.8 % and 4.0 ± 0.7 % in the S1 and thalamus, which were both significantly larger than the corresponding values measured after combined treatment (p = 0.0002 and p = 0.0009, respectively). However, compared with the untreated animals, only the thalamus showed a significant increase (p = 0.02), while the S1 area was not different (p = 0.08, p = 0.02; Fig. 6-3a).

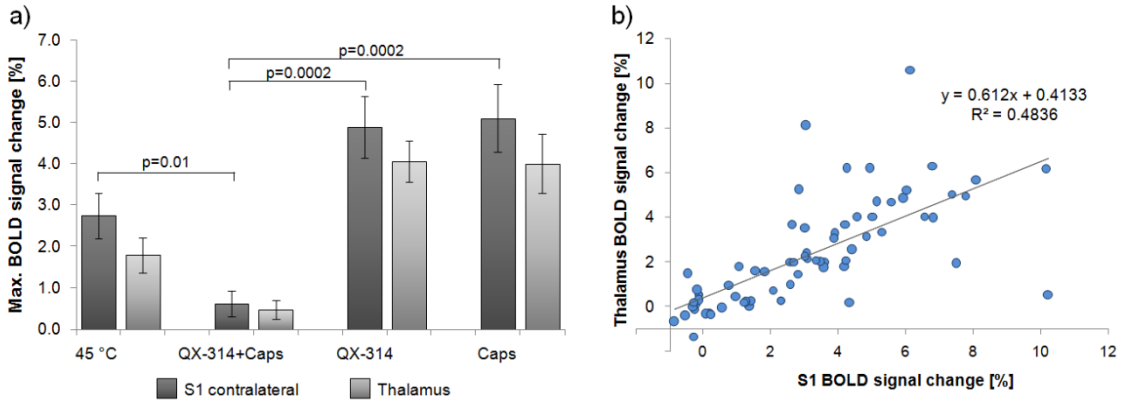

Figure 6-3: (a) Maximum BOLD signal changes of the S1 contralateral to the stimulated paw, and the thalamus. Pretreatment with QX-314 and capsaicin abolished the BOLD signal, while treatment with either substance alone did not decrease the BOLD signal change. All values are given as mean ± SEM. **(b)** Linear regression analysis of the BOLD signal changes in the thalamus and the S1yielded a correlation factor of R^2 = 0.4836.

When pooling all experimental results for untreated and treated animals, a relatively good correlation was found between the elicited BOLD signals of the S1 area and the thalamus. (R^2=0.48, Fig 6-3b).

The group analysis (Fig. 6-4) of all animals reflects the BOLD signal changes after thermal stimulation and treatment with QX-314 and/or capsaicin. The activity maps show the main activation appearing in the S1 area after stimulation of both paws at 45 °C (Fig. 6-4c). Pretreatment with QX-314 combined with capsaicin only led to some cortical activation in two of 14 scans (Fig. 6-4d). Pretreatment of either compound alone did not diminish the activation, but rather increased the activated areas in the brain (Fig. 6-4 e: QX-314, Fig. 6-4 f: capsaicin).

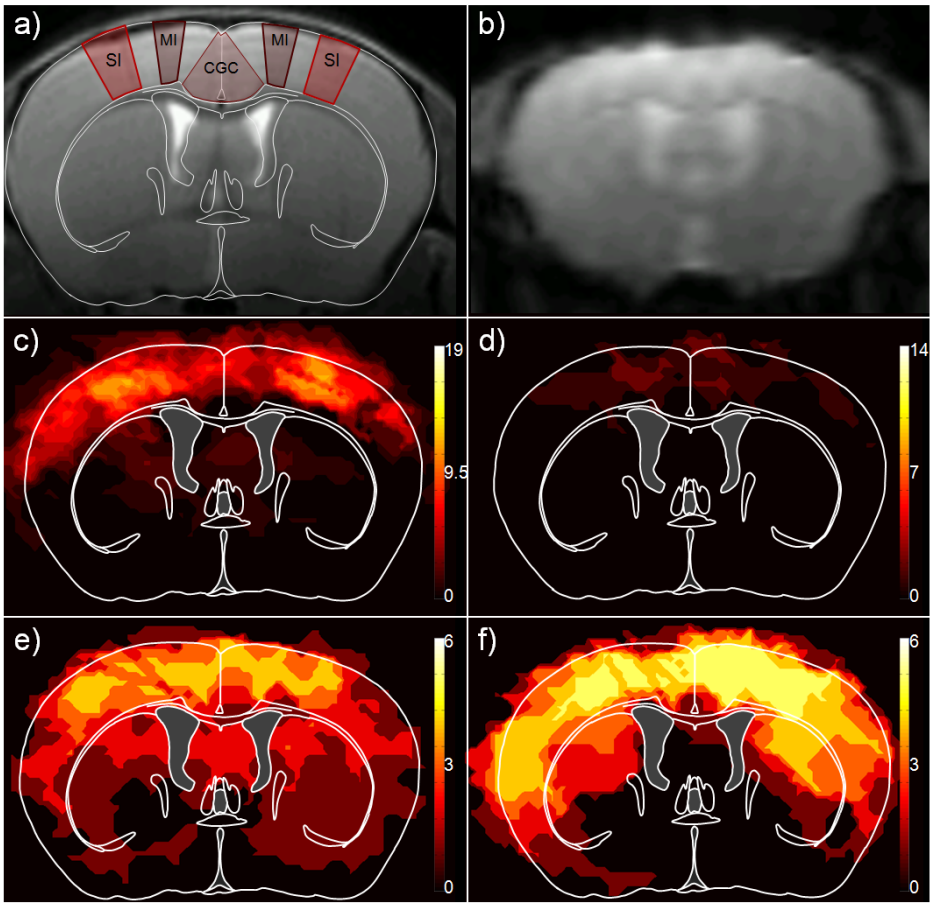

Figure 6-4: **(a)** Mouse brain atlas (IAL +3.7 mm) with relevant regions (SI: primary somatosensory cortex, forepaw region; MI: primary motor cortex; CGC: cingulated cortex) overlaid on the anatomical MR-image. **(b)** Representative EPI image. **(c-f)** Activation maps after left and right thermal forepaw stimulation of 45 °C **(c)**; **(d)** after pretreatment with QX-314 and capsaicin; **(e)** after pretreatment with QX-314; and **(f)** after pretreatment with capsaicin. Data show activated regions derived from GLM analysis (p = 0.001, cluster size 15 voxels) for all animals overlaid on the mouse brain atlas. The intensity indicates the number of animals showing significant BOLD activation at the given threshold. Scale bars are adjusted to the total number of scans performed for each experiment.

6.4 Discussion

fMRI has become an important and widely used tool in animal research, as it allows non-invasive monitoring of brain functions in large brain volumes. Multiple studies in humans and in rodents have shown a good correspondence of the noxious-evoked activation patterns detected by fMRI and the network of the pain matrix [46, 97-101]. However, one has to

keep in mind that due to the hemodynamic nature of the signal, the activated areas may not be tightly confined to the functional brain structures but include areas covered by draining vessels. Therefore, the brain areas designated as being active from fMRI data extend beyond the structures as defined in the mouse brain atlas derived on the basis of electrophysiological results [103].

In imaging in general and in fMRI in particular, there is a trade-off between sensitivity (i.e. signal-to-noise ratio, SNR), temporal resolution and spatial resolution. In this study we have optimized a protocol [46] to improve temporal resolution from 7.5 s to 1 s, while maintaining spatial resolution and only minimally compromising SNR in order to be sensitive enough to detect signal changes of only a few percents. Increasing the temporal resolution to 1 s is essential for better characterizing of the hemodynamic response and signal dynamics as a response to the stimulus.

In contrast to electrical stimulation, thermal stimulation constitutes a physiological stimulus, which directly activates the nociceptive system. Temperature exceeding a threshold value is a noxious stimulus, which can be well controlled by adjusting several parameters such as the target temperature, spot diameter and stimulation duration. By choosing target temperatures of 45 or 46 °C, we predominantly induce TRPV1-mediated activation of the neural system. TRPV1 receptors are activated at temperatures of 42 °C and above, and the signal is transmitted via the unmyelinated C-fiber afferents [158]. Activation of the Aδ-afferents would occur by activation of the TRPV2 receptors, which have an activation threshold of 52 °C [159], a temperature not reached with our stimulation paradigm. Temperatures should be kept below 50 °C to avoid any skin damage on the paw. In view of our relatively long stimulation period, skin damage might occur already at lower temperatures. Therefore all experiments were carried out at a temperature of 45 °C, a temperature leading to a robust BOLD signal change of 2.8 ± 0.5 % in the S1 area, which was considered sufficient for studying the pharmacological modulation of the response. Using these stimulation parameters, the animals were not injured and could be used for more than one experiment, an important prerequisite for longitudinal studies.

The temporal profile of the BOLD signal changes correlated well with the stimulation periods. The rise of the BOLD signal was slightly delayed with regard to the stimulus onset, which was due to the nature of the stimulus. The baseline temperature of the paw was usually around 31 °C and on average it took 20-25 seconds to reach the target temperature of 45 or 46 °C at the paw. Since heat starts to be noxious at 42-43 °C, this was only reached a few seconds after stimulus onset, leading to brain activation as detected by BOLD measurements.

The BOLD signal amplitude was influenced only by the target temperature, but not by the spot diameter. However, the signal shape appeared to be influenced by the spot diameter used. For the experiments performed with the 2 mm spot it seems that the signal decayed slower and did not return to baseline levels, indicating the presence of an underlying slower component as described earlier [46]. The temporal BOLD profile of the experiment carried out using the 1 mm spot shows faster signal decay in the initial phase after the stimulation, and the signal returns to baseline levels. All three profiles show fast signal decays during the first 20-30 s after stimulation, followed by a slower decay or stable signal, which might be due to hemodynamic effects. Another feature of the BOLD signal is the decrease in signal amplitude despite ongoing stimulation. This may be due to adaptation as has been shown for dorsal root ganglia cells, which show a slow decrease in activity over 2-3 s to continuous stimulation [161]. Another explanation may be the decaying vasodilatory signal which is subject to feedback regulation by CBF in response to a prolonged neuronal stimulus [77, 113] and which has also been observed in experiments using electrical stimulation paradigms [46].

To verify the specificity of the BOLD signal readout, we pharmacologically modulated the nociceptive signal transmission. Binshtok et al. demonstrated in a recent study that the cationic lidocaine analogue QX-314 was able to enter neurons through opened TRPV1 channels. Inside the cells, QX-314 blocks the sodium channels, thereby preventing the propagation of action potentials and inducing local anesthesia [167]. The opening of the TRPV1 channels can be achieved by applying capsaicin, a highly potent agonist. Since TRPV1 channels are only found on C-fiber afferents in the peripheral nervous system [158],

entering of QX-314 will cause a C-fiber specific nociceptive block. In contrast, neutral local anesthetics such as lidocaine can penetrate all fiber types and upon binding to sodium channels will lead to a transient sensory and motor inhibition [138, 139]. Since thermal stimulation predominantly activates C-fibers, we expected a significant decrease of the BOLD signal after application of QX-314 in combination with capsaicin. Indeed, the BOLD signal was almost totally abolished supporting the hypothesis that it reflects nociceptive processing in mice.

The anesthetic properties of QX-314 are somewhat controversial. While several studies reported the compound not being able of passing the cell membrane and thus no anesthetic efficacy [163, 164, 167, 168], other studies claimed to have found an anesthetic effect of QX-314 comparable to that of lidocaine, but with a slower onset [169, 170]. They attribute the possible cell entry of the compound to the tonic activity of the TRPV1 channels [171], since application of the TRPV1 antagonist capsazepine prevents sensory blockade induced by QX-314 [169]. Our data demonstrating inhibition of nociceptive transmission by QX-314 only in the presence of capsaicin, but not when administered a single compound, are rather in line with the hypothesis of the compound not penetrating neurons.

The application of either substance separately did not lead to a decrease of the BOLD signal. In contrast, there was a trend towards an increase in the maximal signal amplitude. After capsaicin application this may be due to a sensitization effect since both capsaicin and noxious heat act on the same receptors. It has been shown that direct activation of the TRPV1 receptor may sensitize it to other stimuli [172]. The same may apply for the positively charged molecule QX-314, as a study by Ahern et al. has shown that cations directly gate and sensitize TRPV1 channels [173]. A transient reduction of thermal response latency in rats after injection of either 67 mM QX-314 or capsaicin (1.6 mM) has also been reported [167].

This study describes a robust and physiological stimulation paradigm to study noxious processing in mice non-invasively using BOLD fMRI. Reproducible activation has been observed in brain areas attributed to the pain matrix (S1 and S2, thalamus). The abolishment

of the signal after inhibition of nociceptive signaling demonstrates the specificity of the stimulation protocol and validates the BOLD readout as a response to noxious thermal stimulation. The method is non-invasive and therefore provides a tool for longitudinal studies of pain processing in normal and genetically engineered mice e.g. to investigate mechanism involved in hyperalgesia.

7. Conclusions and Outlook

7.1 fMRI and Pain

Pain is much more than just a transient unpleasant feeling after injury; it is a highly complex sensation involving somatosensory, emotional and psychological aspects. Acute nociceptive and inflammatory pain serves to guard the body from potentially damaging stimuli or to protect an injured site. The underlying mechanisms are quite well understood and pain is manageable by different types of analgesics. Chronic pain on the other hand is a serious health problem, which is a major cause of suffering and disability in our society. It does not serve a supportive function in the body, as it does not assist tissue repair or healing, but instead is caused by a malfunctioning somatosensory and nociceptive system. Neuropathic pain results from lesions to the peripheral or central nervous system, which induce alterations of nociceptive signal processing. This can lead to an enhancement of the response to a noxious stimulus (hyperalgesia), or to a pain sensation elicited by a normally innocuous stimulus (allodynia). Dysfunctional pain occurs in absence of any identifiable noxious stimuli, neural lesions or inflammation. Chronic pain can cause more disability and suffering than the original injury by which it was elicited. Long lasting changes of the nervous system, where complex interactions between ascending and descending branches of the somatosensory and pain conducting system take place, can lead to pain syndromes which persist long beyond the point of normal healing [174, 175]. Mechanisms underlying chronic pain, such as structural reorganization, central sensitization, disinhibition or neuro-immune reactions have been identified in recent years [176]. However, many still unresolved mechanisms together with complexly linked genetic, cellular and molecular components complicate the diagnosis and treatment of chronic pain. Much research is therefore conducted in this area, in order to develop treatment strategies for chronic pain patients.

Functional imaging in humans and small animals is a promising tool to gain further insights into the mechanisms and pathologies of chronic pain. fMRI and PET studies of the human

brain and spinal cord have led to new knowledge of functional connectivity in pain pathways and of functional and structural changes occurring in chronic pain patients [177]. Application of whole brain imaging to small animals allows the translation from animal models to humans. However, in order to be able to explore the mechanisms underlying chronic pain, strategies to assess acute pain processing need to be implemented first, particularly when imaging animals, which are not able to articulate their sensations. In addition, one has to keep in mind that subjective and emotional symptoms associated with pain are too complex to be evaluated with animal models. Nevertheless, animal imaging is a tool of great potential in pain research, particularly in view of the increasing possibilities and techniques available to create genetically modified mouse models.

Conventionally, sensory function in animals is assessed by behavioral tests that often measure reflex responses or innate behavior elicited by a stimulus. These tests have several drawbacks: they rely on intact motor function, the experimenter may be biased and the outcome measures reflex responses which are processed in spinal or supraspinal circuits, but do not involve cortical processing [178]. Functional imaging provides a method to objectively assess nociception which is used in animals and human studies and therefore allows performing comparable tests, at least to a certain extent. fMRI techniques are suitable to image the entire brain, including cortical and subcortical areas crucial for pain processing, resulting in a more thorough assessment of nociceptive processing as compared to the conventional behavioral tests. The use of a comparable method is an important prerequisite for translational research; nevertheless, there are still some restrictions to rodent fMRI which are mainly due to the small dimensions of the animals.

Rat BOLD fMRI has been established for several years, leading to distinct activation patterns in the brain and spinal cord upon somatosensory or noxious stimulation. The activated brain areas are in good agreement with the areas belonging to the pain matrix, which was determined by functional imaging in humans [65, 66]. In contrast, mouse BOLD fMRI studies are still sparse despite the availability of numerous transgenic mouse models for pain research. The small dimensions of the mouse require high spatial resolution to display the

small brain areas. The main limiting factor is therefore the signal-to-noise (SNR) ratio for a given acquisition time. Increasing SNR can be achieved in several ways, one of them being the use of higher B_0 fields. In addition to a strong magnetic field (9.4 T) a cryogenically cooled radiofrequency coil (CryoProbe) was used for all experiments of this thesis. Cooling the receiver electronics significantly reduces the noise in small animal imaging, leading to an increase of SNR. The application of the CryoProbe allowed for high spatial resolution in combination with relatively high temporal resolution, high SNR and comparably short acquisition times. Using this set-up, we were able to not only detect BOLD signal responses to peripheral stimulation, which are in the in the order of a few percent, but in addition we could modulate the stimulation and detect minute differences between BOLD responses to different peripheral inputs. EPI images, which are prone to distortion due to susceptibility artifacts, were acquired in a quality allowing precisely allocating the activated regions to a mouse brain template. The direct comparison to a room temperature coil of similar dimensions revealed a significant gain of SNR and a reduction of the variance of baseline signal. The gain in sensitivity allowed establishing a robust and sensitive BOLD readout at high spatial and temporal resolution in mice.

7.2 Stimulation Paradigms

An important aspect of this thesis was the establishment of robust stimulation paradigms. Electrical stimulation of either the forepaws or the hind paws is widely used in animal fMRI and induces robust activation in the brain. In our mouse studies, electrical stimulation at different amplitudes led to activation of brain areas considered to be part of the pain matrix: the somatosensory cortices S1 and S2, the thalamus and the insular cortex. Activation in all areas increased with increasing stimulation amplitude, and the BOLD signal change correlated with the stimulation periods. Despite the robust activation patterns elicited by electrical stimulation paradigm, there are also several drawbacks to it. Electrical stimulation is not physiological in the sense that it does not directly activate one of the body's nociceptive systems (touch, heat, chemical) [161]. It is not quite clear what eventually induces the

activation: the current generates an innocuous or noxious sensation which is transmitted by the primary afferents. But electrical current can also directly activate neurons, the signal transmission of which is conveyed electrically along the axon. Therefore, subcutaneous electrical stimulation of the forepaw may activate all nerve fibers present in the paw, including motor fibers, leading to an unspecific brain activation originating from innocuous or noxious sensory, and antidromic motor signal transmission. A further point is the difficulty of discriminating noxious and innocuous stimuli. The stimulation strength depends on the current density, which is determined by the relative placement of the electrodes. This makes it difficult to compare stimulation parameters and their effect across different labs or with literature. A secure identification of the fiber types activated by electrical stimulation using different parameters could be obtained by electrophysiological recording of the different fiber types.

In view of these restrictions we aimed at implementing a more physiological stimulation paradigm, using high temperatures to induce noxious stimulation. The advantages of laser stimulation as used in our studies are well controllable and reliable stimulus parameters, which can be adjusted in terms of intensity, duration, area and frequency. Thermo-sensing receptors are well described and temperature ranges of activation as well as the respective expression on primary afferents have been determined for different receptors. Thermal pain sensations are mediated by Aδ- and C-fibers, depending on the stimulation temperatures used [179, 180]. By stimulating at temperatures of 45-46 °C, predominantly TRPV1 receptors located on C-fibers are activated, leading to a C-fiber-mediated noxious activation which is relayed to the brain via the spinothalamic tract. The two temperatures (45 and 46 °C) applied in the studies of this thesis led to BOLD signal changes that correlated with the intensity of the stimulus. For stimulation at higher temperatures, the parameters of the stimulation paradigm would need to be adapted. The long stimulation period of one minute leads to a large deposition of heat, causing injuries at the affected paws when stimulated at temperatures around 50 °C, impeding longitudinal studies. The thermal stimulation paradigm proved to be a useful tool to investigate nociceptive processing in mice, which can

be applied to study the mechanisms involved in heat transmission and perception under normal and pathophysiological conditions.

7.3 Anesthesia

A crucial point that needs to be considered, also in view of translational studies, is the use of anesthetics in animal fMRI. In contrast to human fMRI studies where the subjects typically are conscious, most animal studies are performed on anesthetized animals in order to reduce motion artifacts and stress. Even smallest movements of the head will lead to image distortions and shifts in signal intensity which can be mistaken for stimulus-induced activation [181]. On the other hand, the imaging conditions (restraint, loud noise, enclosed space) are challenging for conscious animals and likely raise stress levels [81]. Despite these concerns, studies on fully conscious animals have been performed. Acclimation over a couple of days by restraining rats in a dark tube and playing pulse sequences seems to reduce stress levels in the animals as measured by heart rate, corticosterone levels, body temperature and movement. Comparing the data quality to non-acclimated rats, the contrast-to-noise (CNR) ratio is increased, probably by decreased physiological noise caused by motion, increased heart rate and respiration [81]. However, conscious rats, even if acclimated to the fMRI procedure, cannot be used for all fMRI paradigms. Noxious stimulation for instance, or any other stimulation which elicits a motor reflex, is not suitable as it would induce motion artifacts. Another possibility to perform studies on awake animals is to paralyze the animal using neuromuscular blocking agents, leaving the animal fully conscious but unable to move [83]. However, this requires artificial ventilation of the animal, which by itself is probably already quite stressful for a conscious animal and raises ethical issues about the experiment. Different restrainers or surgical interventions to implant a screw on the head are additional possibilities to perform fMRI on conscious animals [182-184], but the stress caused by the entire procedure is still a major concern. Primates such as marmosets or rhesus macaques can be well acclimated to the process without showing major stress syndromes [185, 186]. Still, mice, as used in our studies, are even more anxious and less controllable than rats, and

therefore probably almost impossible to acclimate to a scanning session without strongly restraining them. Any procedure necessary to perform fMRI on fully conscious mice would likely dramatically increase their stress levels, influencing the entire organisms and possibly affect the fMRI readout; potentially even more than under well controlled anesthetic conditions.

Therefore, despite the effects of general anesthetics on neuronal metabolism, CBF, neurovascular coupling or sensory perception [82, 84, 187, 188] we chose to use the inhalation anesthetic isoflurane for our studies, in combination with paralysis of the mice. We reasoned that low concentrations of isoflurane will not influence the neurovascular coupling to an extent that would seriously interfere with the BOLD readout, but instead significantly reduce the stress and discomfort of the animal. This is particularly important in view of the noxious stimulation paradigms applied. The robust and sensitive BOLD signal changes observed confirm the suitability of the applied anesthesia protocols.

7.4 Mouse Models of Pain

The advent of transgenic techniques in the 1980's that allowed altering the function or expression of a specific gene [189-191] has substantially affected pain research. Being able to study the role of individual genes and proteins promised to gain new insight into molecular mechanisms of pain, leading to the discovery of new drug targets. At present time, the Pain Genes Database [192] lists 322 genes published by MEDLINE/PubMed (www.pubmed.org), which have been analyzed using transgenic animals showing a pain-related phenotype. Despite this vast number of pain- or nociception-related genes discovered, translation to humans and development of new effective and safe analgesics remains difficult [193]. The reasons for the limited success are complex and multilayered, one of them being the potential limitations of current animal models of pain. Animal models are important despite the well developed and reliable tools used for self-ratings of pain in human pain studies [194]. Animal models allow a less subjective assessment of the behaviors in response to a noxious stimulus; however, frequently the scored behavior shows a reflex or congenital

behavior, which lacks clinical validity [195]. Pain is a very complex phenomenon containing sensory and discriminative aspects that are largely processed separately from the motivational and affective characteristics [68, 196]. An ideal assay would consider all of these aspects in order to provide a translatable readout. Despite the numerous assays available and still being developed, none of them accounts for all dimensions of pain perception [197]. The use of transgenic animals in pain research holds great potential, but also some aspects which can complicate the interpretation of the results obtained. The most commonly used approach is generating null-mutant (knock-out) mice, where a specific gene is silenced by disrupting its sequence. The critical point lies in the absence of the gene already during development, inducing compensatory mechanisms which influence the phenotype, thereby masking the real changes due to the lack of the gene [198, 199]. To overcome these shortcomings, more advanced techniques allow to spatially and/or temporally control the gene disruption, allowing for more subtle interference with the organisms [200-203].

The nociceptive specific $Na_V1.7$ knock-out ($Na_V1.7R^{-/-}$) used for one of our studies in this thesis is an example of a conditional knock-out mouse where the gene SCN9A encoding for the voltage-gated sodium channel $Na_V1.7$ is disrupted in nociceptors only [94]. Knocking-out SCN9A globally leads to a lethal phenotype, most likely because the pups are unable to feed [204]. The $Na_V1.7R^{-/-}$ in contrast are viable and show a loss of acute mechanical and inflammatory pain [94], which was reflected by a decrease of the BOLD response in our fMRI studies. Only a few years ago, humans suffering from a loss of function mutation of the SCN9A gene, which renders them insensitive to pain, were discovered [50], supporting the phenotype observed in the animals. On the other hand, human gain of function mutations of the SCN9A gene lead to a chronic inflammatory condition called erythermalgia [205]. Voltage-gated sodium channels are crucial for propagation of action potentials in neurons and hence in nociceptors. Mouse k.o.-studies have provided important knowledge about the genes coding for sodium channels [192], revealing three genes encoding for sodium channels only expressed on sensory neurons, presenting potential drug targets.

The other transgenic model used in our studies was a global cannabinoid receptor 1 knock-out mouse ($CB_1^{-/-}$), which does not display any different spontaneous nociceptive thresholds as compared to WT mice [93]. This finding was corroborated by our fMRI experiment which did not show a difference of the BOLD response as compared to the WT animals, indicating that either the CB_1 receptor does not play a critical role in processing of spontaneous nociception, or other systems compensate for the lack of the CB_1 receptor. A recent study showed that global $CB_1^{-/-}$ mice did not develop mechanical sensitization and secondary hyperalgesia induced by capsaicin as compared to WT or nociceptor-specific knock-out (*sns*-$CB_1^{-/-}$) mice [143]. The $CB_1^{-/-}$ were used for our study based upon the supposition by Pernia-Andrade and colleagues, which showed a contribution of endocannabinoids and the CB_1 receptor to heterosynaptic pain sensitization originating from the dorsal horn of the spinal cord [143]. The $CB_1^{-/-}$ in our study indeed did not show the lidocaine-induced hyperalgesia observed in WT mice, a finding which could be reproduced by pretreatment of the WT mice with the selective CB_1 -blocker rimonabant, reinforcing the results obtained with the transgenic animals.

These examples display the potential of transgenic animals in revealing the functions of a certain gene or its role in a specific mechanism; however, they are not real pain models. Common clinical pain conditions are probably too polygenic and complex to be modeled by a (transgenic) animal [195].

Another crucial point that needs to be considered in pain research is the differences resulting from factors such as mouse strain, sex, age and husbandry [206] [207, 208]. C57Bl/6 mice are popular subjects in research mainly due to their good performance in behavioral and cognitive tests [209, 210], but regarding nociception, they show higher sensitivity to nociceptive assays, are relatively resistant to developing thermal hyperalgesia and comparatively insensitive to a number of analgesic compounds as compared to other commonly used mouse strains [207].

Hence, for a more thorough assessment of nociception in mice, a test not only measuring reflexes needs to be chosen, different strains should be compared, and mice of both sexes and

different ages should be used [195]. Of course, such study designs will likely increase inter-subject variability and decrease statistical power, but the results obtained may be more suitable and meaningful for translational research.

By using fMRI with peripheral noxious stimulation, we have a device to access cortical and subcortical processes involved in pain perception. To what extent emotional and associative aspects can be measured still needs to be determined, but in any case fMRI allows getting an overall picture of the brain areas activated upon a stimulus. Being non-invasive, fMRI also allows performing longitudinal studies, in which each animal can serve as its own control, and which enables to monitor functional and structural changes of the brain as a consequence of e.g. injury or chronic pain syndromes. Refinement of existing and development of new techniques will therefore likely render fMRI increasingly important in pain research, hopefully attributing to successful translational research.

7.5 Outlook

Electrical stimulation has been used for many studies in this thesis. Nevertheless, it is still not clearly determined which fiber types are activated upon stimulation, and thus at which point the stimulation turns from innocuous to noxious. Electrophysiological analysis of the activation of the distinct fiber types in response to electrical stimulation would therefore be of great value. Knowing the noxious threshold and involved fiber types would increase the significance of the stimulation paradigm for future studies, e.g. to directly compare innocuous and noxious stimulation.

Thermal stimulation is an ideal tool to study normal or pathological nociception (e.g. heat hyperalgesia) in mice. Future applications could therefore lie in characterization of phenotyping of mouse models displaying different pathologies. For this purpose, the development of further stimulation paradigms would be of use, in order to assess the different forms of nociceptive input (temperature, chemicals, and touch). Complementary to heat stimulation, cold stimulation could be established, e.g. by injecting compounds

activating cold-sensing receptors, such as menthol or icilin [211], since cold allodynia (innocuous cool stimuli induce pain) is a major feature of neuropathic pain [212]. The development of an MR-compatible device for mechanical stimulation would allow for innocuous and noxious stimulation of pressure-sensitive sensory afferents. Application of different modalities would allow for a thorough and distinct characterization of mouse models as it is been done by conventional assays.

Since the major health problem is chronic and not acute pain, this should become a major topic in animal fMRI research. Several mouse models to study chronic pain have been established, particularly to study neuropathic pain. Models for central neuropathic pain are mostly based on spinal cord injury; and a number of animal models have been developed to simulate human peripheral neuropathic pain, most of them based on injuries of or near the sciatic nerve [213]. Different approaches can be used for imaging of chronic pain syndromes. The stimulation paradigms implemented for the present work could be used to assess altered thresholds to acute innocuous or noxious stimuli (allodynia, hyperalgesia). In patients suffering from chronic pain, alterations of brain structures and functional connectivity have been reported [177]. The structural changes could be assessed by high-resolution fMRI of the brain to determine morphological alterations of brain structures and by using diffusion tensor imaging (DTI) [214], which allows to depict fiber tracts of the brain. Functional changes could be assessed using stimulus-induced fMRI, measuring changes in CBF, CBV or BOLD.

Additionally, resting state fMRI could be established to assess default connection networks. Resting state fMRI has been applied to rats [215-217], but to our awareness not yet in mice. Technically, we should be able to implement it on the 9.4 T scanner using the CryoProbe, which significantly enhances sensitivity as measured by SNR [36]. Resting state fMRI applied to models of chronic pain syndromes may give new insights into alterations of functional connectivity and areas active in the absence of a stimulus. Correlation analyses used for evaluation of resting state activity could also be applied for stimulus-induced fMRI in order to assess functional connectivity of brain areas in correlation to a stimulus; a property which

might be changed as well in chronic pain states. Correlation analyses of functional networks may also be a way to assess the affective and emotional aspects of pain perception in mice.

A last point which would be of great interest for pain research is the implementation of spinal cord fMRI in mice. Processes in the spinal cord are equally important in pain research as brain processes, as many pathological pain symptoms have their origin in the spinal cord. It would therefore be appealing to assess activity in the spinal cord elicited by peripheral stimulation. Rat spinal cord fMRI has been implemented [85-87, 218-221] but no studies in mice are, to our knowledge, published as yet. This may be due to two reasons complicating mouse fMRI: 1) The mouse spinal cord is small (1-2 mm); therefore the acquisition needs to be very sensitive combined with high spatial resolution and reasonable temporal resolution. However, even when recording with in-plane spatial resolution of 100 μm^2, there will only be 10-20 voxels across the spinal cord. 2) Physiological noise is greatly enhanced as compared to brain imaging, due to motion artifacts originating predominantly from respiration and heart beat. 3) The anatomical location of the spinal cord with its proximity to massive bone structures will cause susceptibility artifacts in T_2*-weighted images. If these challenges can be overcome, mouse spinal cord fMRI could be a valuable tool to analyze nociceptive processing.

8. References

1. Bloch, F., *Nuclear Induction.* Phys Rev, 1946. **70**: p. 460.
2. Purcell, E.M., H. Torrey, and R.V. Pound, *Resonance Absorption by Nuclear Magnetic Moments in a Solid.* Phys Rev, 1946. **69**: p. 37-38.
3. Ernst, R.R., *Nuclear magnetic double resonance with an incoherent radio-frequency field.* Journal of Chemical Physics, 1966. **45**(10): p. 3845-3861.
4. Lauterbur, P.C., *Image formation by induced local interactions: examples employing nuclear magnetic resonance.* Nature, 1973. **242**: p. 190-191.
5. Mansfield, P., *Multi-planar image formation using NMR spin-echos.* J Phys C: Solid State Physics, 1977. **10**: p. L55 - L58.
6. Bandettini, P.A., et al., *Time course EPI of human brain function during task activation.* Magn Reson Med, 1992. **25**(2): p. 390-7.
7. Kwong, K.K., et al., *Dynamic magnetic resonance imaging of human brain activity during primary sensory stimulation.* Proc Natl Acad Sci U S A, 1992. **89**(12): p. 5675-9.
8. Aiver, M.N., *All you really need to know about MRI*. January 1996 ed. 1996: Rittenhouse Book Distributors. 140.
9. Schild, H.H., *MRI made easy - well almost*. 1 ed. 1990, Berlin: Nationales Druckhaus Berlin, Germany. 105.
10. del Zoppo, G.J., *Stroke and neurovascular protection.* N Engl J Med, 2006. **354**(6): p. 553-5.
11. Raichle, M.E., *Images of the mind: studies with modern imaging techniques.* Annu Rev Psychol, 1994. **45**: p. 333-56.
12. Magistretti, P.J. and L. Pellerin, *Cellular mechanisms of brain energy metabolism and their relevance to functional brain imaging.* Philos Trans R Soc Lond B Biol Sci, 1999. **354**(1387): p. 1155-63.
13. Shulman, R.G., et al., *Energetic basis of brain activity: implications for neuroimaging.* Trends in Neurosciences, 2004. **27**(8): p. 489-495.
14. Sirotin, Y.B. and A. Das, *Anticipatory haemodynamic signals in sensory cortex not predicted by local neuronal activity.* Nature, 2009. **457**(7228): p. 475-9.
15. Heeger, D.J. and D. Ress, *What does fMRI tell us about neuronal activity?* Nat Rev Neurosci, 2002. **3**(2): p. 142-151.
16. Roy, C.S. and C.S. Sherrington, *On the Regulation of the Blood-supply of the Brain.* J Physiol, 1890. **11**(1-2): p. 85-158 17.
17. Barbier, E.L., L. Lamalle, and M. Decorps, *Methodology of brain perfusion imaging.* J Magn Reson Imaging, 2001. **13**(4): p. 496-520.

18. Buxton, R.B., et al., *A general kinetic model for quantitative perfusion imaging with arterial spin labeling.* Magn Reson Med, 1998. **40**(3): p. 383-96.
19. Reese, T., et al., *Regional brain activation by bicuculline visualized by functional magnetic resonance imaging. Time-resolved assessment of bicuculline-induced changes in local cerebral blood volume using an intravascular contrast agent.* NMR Biomed, 2000. **13**(1): p. 43-9.
20. Reese, T., et al., *Impaired functionality of reperfused brain tissue following short transient focal ischemia in rats.* Magn Reson Imaging, 2002. **20**(6): p. 447-54.
21. Sauter, A., et al., *Recovery of function in cytoprotected cerebral cortex in rat stroke model assessed by functional MRI.* Magn Reson Med, 2002. **47**(4): p. 759-65.
22. Mandeville, J.B., et al., *Dynamic functional imaging of relative cerebral blood volume during rat forepaw stimulation.* Magn Reson Med, 1998. **39**(4): p. 615-24.
23. Keilholz, S.D., et al., *BOLD and CBV-weighted functional magnetic resonance imaging of the rat somatosensory system.* Magnetic Resonance in Medicine, 2006. **55**(2): p. 316-324.
24. Kim, Y.R., et al., *Measurements of BOLD/CBV ratio show altered fMRI hemodynamics during stroke recovery in rats.* J Cereb Blood Flow Metab, 2005. **25**(7): p. 820-9.
25. Silva, A.C., A.P. Koretsky, and J.H. Duyn, *Functional MRI impulse response for BOLD and CBV contrast in rat somatosensory cortex.* Magn Reson Med, 2007. **57**(6): p. 1110-8.
26. Ogawa, S., et al., *Oxygenation-sensitive contrast in magnetic resonance image of rodent brain at high magnetic fields.* Magn Reson Med, 1990. **14**(1): p. 68-78.
27. Pauling, L. and C.D. Coryell, *The Magnetic Properties and Structure of Hemoglobin, Oxyhemoglobin and Carbonmonoxyhemoglobin.* Proceedings of the National Academy of Sciences of the United States of America, 1936. **22**(4): p. 210-216.
28. Logothetis, N.K. and J. Pfeuffer, *On the nature of the BOLD fMRI contrast mechanism.* Magn Reson Imaging, 2004. **22**(10): p. 1517-31.
29. Kim, S.G. and K. Ugurbil, *Comparison of blood oxygenation and cerebral blood flow effects in fMRI: estimation of relative oxygen consumption change.* Magn Reson Med, 1997. **38**(1): p. 59-65.
30. Logothetis, N.K., *The underpinnings of the BOLD functional magnetic resonance imaging signal.* J Neurosci, 2003. **23**(10): p. 3963-71.
31. Gati, J.S., et al., *Experimental determination of the BOLD field strength dependence in vessels and tissue.* Magn Reson Med, 1997. **38**(2): p. 296-302.
32. Kruger, G. and G.H. Glover, *Physiological noise in oxygenation-sensitive magnetic resonance imaging.* Magn Reson Med, 2001. **46**(4): p. 631-7.

33. Kruger, G., A. Kastrup, and G.H. Glover, *Neuroimaging at 1.5 T and 3.0 T: comparison of oxygenation-sensitive magnetic resonance imaging.* Magn Reson Med, 2001. **45**(4): p. 595-604.
34. Triantafyllou, C., et al., *Comparison of physiological noise at 1.5 T, 3 T and 7 T and optimization of fMRI acquisition parameters.* NeuroImage, 2005. **26**(1): p. 243-50.
35. Ratering, D., et al., *Performance of a 200-MHz cryogenic RF probe designed for MRI and MRS of the murine brain.* Magn Reson Med, 2008. **59**(6): p. 1440-7.
36. Baltes, C., et al., *Micro MRI of the mouse brain using a novel 400 MHz cryogenic quadrature RF probe.* NMR Biomed, 2009. **22**(8): p. 834-42.
37. Baltes, C., et al., *Increased blood oxygen level-dependent (BOLD) sensitivity in the mouse somatosensory cortex during electrical forepaw stimulation using a cryogenic radiofrequency probe.* NMR in Biomedicine, 2010: p. n/a-n/a.
38. Benson, G.J., J.C. Thurmon, and W.J. Tranquilli, *Lumb & Jones' Veterinary Anesthesia*. 3rd ed. History and outline of animal anesthesia, ed. G.J. Benson, J.C. Thurmon, and W.J. Tranquilli. 1996, Baltimore, MD: Willias and Wilkins.
39. Ueki, M., G. Mies, and K.A. Hossmann, *Effect of alpha-chloralose, halothane, pentobarbital and nitrous oxide anesthesia on metabolic coupling in somatosensory cortex of rat.* Acta Anaesthesiol Scand, 1992. **36**(4): p. 318-22.
40. Mueggler, T., et al., *Compromised hemodynamic response in amyloid precursor protein transgenic mice.* J Neurosci, 2002. **22**(16): p. 7218-24.
41. Abo, M., et al., *Influence of Isoflurane Concentration and Hypoxia on Functional Magnetic Resonance Imaging for the Detection of Bicuculline-Induced Neuronal Activation.* Neurosignals, 2004. **13**(3): p. 144-149.
42. Antognini, J.F., et al., *Isoflurane anesthesia blunts cerebral responses to noxious and innocuous stimuli: a fMRI study.* Life Sciences, 1997. **61**(24): p. PL349-PL354.
43. Lenz, C., et al., *Local Cerebral Blood Flow, Local Cerebral Glucose Utilization, and Flow-Metabolism Coupling during Sevoflurane versus Isoflurane Anesthesia in Rats.* Anesthesiology, 1998. **89**(6): p. 1480-1488.
44. Masamoto, K., et al., *Relationship between neural, vascular, and BOLD signals in isoflurane-anesthetized rat somatosensory cortex.* Cereb Cortex, 2007. **17**(4): p. 942-50.
45. Sommers, M.G., et al., *Isoflurane anesthesia is a valuable alternative for <B>alpha</B>-chloralose anesthesia in the forepaw stimulation model in rats.* NMR in Biomedicine, 2009. **22**(4): p. 414-418.
46. Bosshard, S.C., et al., *Assessment of brain responses to innocuous and noxious electrical forepaw stimulation in mice using BOLD fMRI.* Pain, 2010. **151**(3): p. 655-63.
47. Sydekum, E., et al., *Functional reorganization in rat somatosensory cortex assessed by fMRI: elastic image registration based on structural landmarks in fMRI images and application to spinal cord injured rats.* NeuroImage, 2009. **44**(4): p. 1345-54.

48. Linden, A.v.d., et al., *Current status of functional MRI on small animals: application to physiology, pathophysiology, and cognition.* NMR Biomed, 2007. **20**(5): p. 522-545.
49. Lukasik, V.M. and R.J. Gillies, *Animal anaesthesia for in vivo magnetic resonance.* NMR in Biomedicine, 2003. **16**(8): p. 459-467.
50. Cox, J.J., et al., *An SCN9A channelopathy causes congenital inability to experience pain.* Nature, 2006. **444**(7121): p. 894-8.
51. Miranda, C., et al., *Novel pathogenic mechanisms of congenital insensitivity to pain with anhidrosis genetic disorder unveiled by functional analysis of neurotrophic tyrosine receptor kinase type 1/nerve growth factor receptor mutations.* J Biol Chem, 2002. **277**(8): p. 6455-62.
52. Woolf, C.J., *Pain: moving from symptom control toward mechanism-specific pharmacologic management.* Ann Intern Med, 2004. **140**(6): p. 441-51.
53. Woolf, C.J., *What is this thing called pain?* The Journal of Clinical Investigation, 2010. **120**(11): p. 3742-3744.
54. Schweinhardt, P. and M.C. Bushnell, *Pain imaging in health and disease — how far have we come?* The Journal of Clinical Investigation, 2010. **120**(11): p. 3788-3797.
55. Handwerker, H.O. and G. Kobal, *Psychophysiology of experimentally induced pain.* Physiol Rev, 1993. **73**(3): p. 639-71.
56. Craig, A.D. and M.C. Bushnell, *The thermal grill illusion: unmasking the burn of cold pain.* Science, 1994. **265**(5169): p. 252-5.
57. Campero, M., et al., *Human cutaneous C fibres activated by cooling, heating and menthol.* J Physiol, 2009. **587**(Pt 23): p. 5633-52.
58. Ma, Q., *Labeled lines meet and talk: population coding of somatic sensations.* The Journal of Clinical Investigation, 2010. **120**(11): p. 3773-3778.
59. Basbaum, A.I., et al., *Cellular and molecular mechanisms of pain.* Cell, 2009. **139**(2): p. 267-84.
60. Patapoutian, A., S. Tate, and C.J. Woolf, *Transient receptor potential channels: targeting pain at the source.* Nat Rev Drug Discov, 2009. **8**(1): p. 55-68.
61. Caterina, M.J., et al., *The capsaicin receptor: a heat-activated ion channel in the pain pathway.* Nature, 1997. **389**(6653): p. 816-824.
62. Siemens, J., et al., *Spider toxins activate the capsaicin receptor to produce inflammatory pain.* Nature, 2006. **444**(7116): p. 208-12.
63. Lawson, J.J., et al., *TRPV1 unlike TRPV2 is restricted to a subset of mechanically insensitive cutaneous nociceptors responding to heat.* J Pain, 2008. **9**(4): p. 298-308.
64. Ossipov, M.H., G.O. Dussor, and F. Porreca, *Central modulation of pain.* The Journal of Clinical Investigation, 2010. **120**(11): p. 3779-3787.
65. Tracey, I. and E. Johns, *The pain matrix: reloaded or reborn as we image tonic pain using arterial spin labelling.* Pain, 2010. **148**(3): p. 359-60.

66. Tracey, I. and P.W. Mantyh, *The cerebral signature for pain perception and its modulation.* Neuron, 2007. **55**(3): p. 377-91.
67. Apkarian, A.V., et al., *Human brain mechanisms of pain perception and regulation in health and disease.* Eur J Pain, 2005. **9**(4): p. 463-84.
68. Price, D.D., *Psychological and neural mechanisms of the affective dimension of pain.* Science, 2000. **288**(5472): p. 1769-72.
69. Eippert, F., et al., *Activation of the opioidergic descending pain control system underlies placebo analgesia.* Neuron, 2009. **63**(4): p. 533-43.
70. Adamczak, J.M., et al., *High field BOLD response to forepaw stimulation in the mouse.* NeuroImage, 2010. **51**(2): p. 704-712.
71. Nair, G. and T.Q. Duong, *Echo-planar BOLD fMRI of mice on a narrow-bore 9.4 T magnet.* Magn Reson Med, 2004. **52**(2): p. 430-434.
72. Ahrens, E.T. and D.J. Dubowitz, *Peripheral somatosensory fMRI in mouse at 11.7 T.* NMR in Biomedicine, 2001. **14**(5): p. 318-324.
73. Hess, A., et al., *Imaging of hyperalgesia in rats by functional MRI.* European Journal of Pain, 2007. **11**(1): p. 109-119.
74. Basavaraju G. Sanganahalli, P.H.F.H., *Frequency-dependent tactile responses in rat brain measured by functional MRI.* NMR in Biomedicine, 2008. **21**(4): p. 410-416.
75. Chang, C. and B.-C. Shyu, *A fMRI study of brain activations during non-noxious and noxious electrical stimulation of the sciatic nerve of rats.* Brain Research, 2001. **897**(1-2): p. 71-81.
76. Cho, Y.R., et al., *Refining the sensory and motor ratunculus of the rat upper extremity using fMRI and direct nerve stimulation.* Magn Reson Med, 2007. **58**(5): p. 901-9.
77. Goloshevsky, A.G., et al., *BOLD fMRI and somatosensory evoked potentials are well correlated over a broad range of frequency content of somatosensory stimulation of the rat forepaw.* Brain Research, 2008. **1195**: p. 67-76.
78. Spenger, C., et al., *Functional MRI at 4.7 tesla of the rat brain during electric stimulation of forepaw, hindpaw, or tail in single- and multislice experiments.* Exp Neurol, 2000. **166**(2): p. 246-53.
79. Weber, R., et al., *A fully noninvasive and robust experimental protocol for longitudinal fMRI studies in the rat.* NeuroImage, 2006. **29**(4): p. 1303-1310.
80. Yu, O., et al., *Texture analysis of brain MRI evidences the amygdala activation by nociceptive stimuli under deep anesthesia in the propofol-formalin rat model.* Magnetic Resonance Imaging, 2007. **25**(1): p. 144-146.
81. King, J.A., et al., *Procedure for minimizing stress for fMRI studies in conscious rats.* Journal of Neuroscience Methods, 2005. **148**(2): p. 154-160.
82. Lahti, K.M., et al., *Comparison of evoked cortical activity in conscious and propofol-anesthetized rats using functional MRI.* Magn Reson Med, 1999. **41**(2): p. 412-6.

83. Peeters, R.R., et al., *Comparing BOLD fMRI signal changes in the awake and anesthetized rat during electrical forepaw stimulation.* Magnetic Resonance Imaging, 2001. **19**(6): p. 821-826.
84. Sicard, K., et al., *Regional cerebral blood flow and BOLD responses in conscious and anesthetized rats under basal and hypercapnic conditions: implications for functional MRI studies.* J Cereb Blood Flow Metab, 2003. **23**(4): p. 472-81.
85. Lawrence, J., P.W. Stroman, and K.L. Malisza, *Functional MRI of the cervical spinal cord during noxious and innocuous thermal stimulation in the [alpha]-chloralose- and halothane-anesthetized rat.* Magnetic Resonance Imaging, 2008. **26**(1): p. 1-10.
86. Zhao, F., et al., *BOLD and blood volume-weighted fMRI of rat lumbar spinal cord during non-noxious and noxious electrical hindpaw stimulation.* NeuroImage, 2008. **40**(1): p. 133-147.
87. Zhao, F., et al., *Pain fMRI in rat cervical spinal cord: An echo planar imaging evaluation of sensitivity of BOLD and blood volume-weighted fMRI.* NeuroImage, 2009. **44**(2): p. 349-362.
88. Hutchison, R.M., et al., *Functional Networks in the Anesthetized Rat Brain Revealed by Independent Component Analysis of Resting-State fMRI.* J Neurophysiol, 2010. **103**(6): p. 3398-3406.
89. Kalthoff, D., et al., *Functional connectivity in the rat at 11.7 T: Impact of physiological noise in resting state fMRI.* NeuroImage. In Press, Corrected Proof.
90. Sanganahalli, B.G., et al., *Tactile and non-tactile sensory paradigms for fMRI and neurophysiologic studies in rodents.* Methods Mol Biol, 2009. **489**: p. 213-42.
91. Lilja, J., et al., *Blood Oxygenation Level-Dependent Visualization of Synaptic Relay Stations of Sensory Pathways along the Neuroaxis in Response to Graded Sensory Stimulation of a Limb.* J. Neurosci., 2006. **26**(23): p. 6330-6336.
92. Harvey, R.J., et al., *GlyR alpha 3: An Essential Target for Spinal PGE2-Mediated Inflammatory Pain Sensitization.* Science, 2004. **304**(5672): p. 884-887.
93. Ledent, C., et al., *Unresponsiveness to Cannabinoids and Reduced Addictive Effects of Opiates in CB1 Receptor Knockout Mice.* Science, 1999. **283**(5400): p. 401-404.
94. Nassar, M.A., et al., *Nociceptor-specific gene deletion reveals a major role for Nav1.7 (PN1) in acute and inflammatory pain.* Proc Natl Acad Sci U S A, 2004. **101**(34): p. 12706-11.
95. Caterina, M.J., et al., *Impaired Nociception and Pain Sensation in Mice Lacking the Capsaicin Receptor.* Science, 2000. **288**(5464): p. 306-313.
96. Wilson, S.G. and J.S. Mogil, *Measuring pain in the (knockout) mouse: big challenges in a small mammal.* Behav Brain Res, 2001. **125**(1-2): p. 65-73.

97. Manning, B.H., M.J. Morgan, and K.B. Franklin, *Morphine analgesia in the formalin test: evidence for forebrain and midbrain sites of action.* Neuroscience, 1994. **63**(1): p. 289-94.
98. Davis, K.D., et al., *Functional MRI of pain- and attention-related activations in the human cingulate cortex.* J Neurophysiol, 1997. **77**(6): p. 3370-80.
99. Morrow, T.J., et al., *Regional changes in forebrain activation during the early and late phase of formalin nociception: analysis using cerebral blood flow in the rat.* Pain, 1998. **75**(2-3): p. 355-65.
100. Millan, M.J., *The induction of pain: an integrative review.* Progress in Neurobiology, 1999. **57**(1): p. 1-164.
101. Casey, K.L., *Forebrain mechanisms of nociception and pain: analysis through imaging.* Proc Natl Acad Sci U S A, 1999. **96**(14): p. 7668-74.
102. Mueggler, T., et al., *Age-Dependent Impairment of Somatosensory Response in the Amyloid Precursor Protein 23 Transgenic Mouse Model of Alzheimer's Disease.* J. Neurosci., 2003. **23**(23): p. 8231-8236.
103. Franklin, K. and G. Paxinos, *The Mouse Brain in Stereotaxic Coordinates*. 1997, San Diego: Academic Press.
104. Silva, A.C., et al., *Simultaneous blood oxygenation level-dependent and cerebral blood flow functional magnetic resonance imaging during forepaw stimulation in the rat.* J Cereb Blood Flow Metab, 1999. **19**(8): p. 871-9.
105. Spaeth, N., et al., *Uptake of 18F-Fluorocholine, 18F-Fluoroethyl-L-Tyrosine, and 18F-FDG in Acute Cerebral Radiation Injury in the Rat: Implications for Separation of Radiation Necrosis from Tumor Recurrence.* J Nucl Med, 2004. **45**(11): p. 1931-1938.
106. Wyss, M.T., et al., *A beta-scintillator for surface measurements of radiotracer kinetics in the intact rodent cortex.* NeuroImage, 2009. **48**(2): p. 339-347.
107. Thal, S.C. and N. Plesnila, *Non-invasive intraoperative monitoring of blood pressure and arterial pCO2 during surgical anesthesia in mice.* Journal of Neuroscience Methods, 2007. **159**(2): p. 261-267.
108. Hsu, E.W., L.W. Hedlund, and J.R. MacFall, *Functional MRI of the rat somatosensory cortex: Effects of hyperventilation.* Magnetic Resonance in Medicine, 1998. **40**(3): p. 421-426.
109. Tuor, U.I., et al., *Functional magnetic resonance imaging in rats subjected to intense electrical and noxious chemical stimulation of the forepaw.* Pain, 2000. **87**(3): p. 315-324.
110. Kida, I. and T. Yamamoto, *Stimulus frequency dependence of blood oxygenation level-dependent functional magnetic resonance imaging signals in the somatosensory cortex of rats.* Neurosci Res, 2008. **62**(1): p. 25-31.

111. Staud, R., et al., *Brain activity related to temporal summation of C-fiber evoked pain.* Pain, 2007. **129**(1-2): p. 130-142.
112. Torquati, K., et al., *Nociceptive and non-nociceptive sub-regions in the human secondary somatosensory cortex: An MEG study using fMRI constraints.* NeuroImage, 2005. **26**(1): p. 48-56.
113. Stancák, A., et al., *Desynchronization of cortical rhythms following cutaneous stimulation: effects of stimulus repetition and intensity, and of the size of corpus callosum.* Clinical Neurophysiology, 2003. **114**(10): p. 1936-1947.
114. Terekhin, P. and C. Forster, *Hypocapnia related changes in pain-induced brain activation as measured by functional MRI.* Neuroscience Letters, 2006. **400**(1-2): p. 110-114.
115. Sutherland, M.T. and A.C. Tang, *Reliable detection of bilateral activation in human primary somatosensory cortex by unilateral median nerve stimulation.* NeuroImage, 2006. **33**(4): p. 1042-54.
116. Mohajerani, M.H., et al., *Mirrored Bilateral Slow-Wave Cortical Activity within Local Circuits Revealed by Fast Bihemispheric Voltage-Sensitive Dye Imaging in Anesthetized and Awake Mice.* J. Neurosci., 2010. **30**(10): p. 3745-3751.
117. Ruscheweyh, R. and J. Sandkühler, *Long-range oscillatory Ca2+ waves in rat spinal dorsal horn.* European Journal of Neuroscience, 2005. **22**(8): p. 1967-1976.
118. Maandag, N.J., et al., *Energetics of neuronal signaling and fMRI activity.* Proc Natl Acad Sci U S A, 2007. **104**(51): p. 20546-51.
119. Matta, B.F., et al., *Direct cerebral vasodilatory effects of sevoflurane and isoflurane.* Anesthesiology, 1999. **91**(3): p. 677-80.
120. Corfield, D.R., et al., *Does hypercapnia-induced cerebral vasodilation modulate the hemodynamic response to neural activation?* NeuroImage, 2001. **13**(6 Pt 1): p. 1207-11.
121. Kemna, L.J. and S. Posse, *Effect of respiratory CO(2) changes on the temporal dynamics of the hemodynamic response in functional MR imaging.* NeuroImage, 2001. **14**(3): p. 642-9.
122. Deady, J.E., et al., *Anesthetic Potencies and the Unitary Theory of Narcosis.* Anesth Analg, 1981. **60**(6): p. 380-384.
123. Hansen, T.D., et al., *The role of cerebral metabolism in determining the local cerebral blood flow effects of volatile anesthetics: evidence for persistent flow-metabolism coupling.* J Cereb Blood Flow Metab, 1989. **9**(3): p. 323-8.
124. Torebjork, H.E., R.H. LaMotte, and C.J. Robinson, *Peripheral neural correlates of magnitude of cutaneous pain and hyperalgesia: simultaneous recordings in humans of sensory judgments of pain and evoked responses in nociceptors with C-fibers.* J Neurophysiol, 1984. **51**(2): p. 325-339.

125. Friston, K.J., et al., *Nonlinear Responses in fMRI: The Balloon Model, Volterra Kernels, and Other Hemodynamics.* NeuroImage, 2000. **12**(4): p. 466-477.
126. Buxton, R.B., et al., *Modeling the hemodynamic response to brain activation.* NeuroImage, 2004. **23 Suppl 1**: p. S220-33.
127. Buxton, R.B., E.C. Wong, and L.R. Frank, *Dynamics of blood flow and oxygenation changes during brain activation: the balloon model.* Magn Reson Med, 1998. **39**(6): p. 855-64.
128. Martindale, J., et al., *The hemodynamic impulse response to a single neural event.* J Cereb Blood Flow Metab, 2003. **23**(5): p. 546-55.
129. Stephan, K.E., et al., *Biophysical models of fMRI responses.* Curr Opin Neurobiol, 2004. **14**(5): p. 629-35.
130. Darrasse, L. and J.C. Ginefri, *Perspectives with cryogenic RF probes in biomedical MRI.* Biochimie, 2003. **85**(9): p. 915-37.
131. Doty, F.D., et al., *Radio frequency coil technology for small-animal MRI.* NMR Biomed, 2007. **20**(3): p. 304-25.
132. Edelstein, W.A., et al., *The intrinsic signal-to-noise ratio in NMR imaging.* Magn Reson Med, 1986. **3**(4): p. 604-18.
133. Stollberger, R. and P. Wach, *Imaging of the active B1 field in vivo.* Magn Reson Med, 1996. **35**(2): p. 246-51.
134. Hennig, J., A. Nauerth, and H. Friedburg, *RARE imaging: a fast imaging method for clinical MR.* Magn Reson Med, 1986. **3**(6): p. 823-33.
135. Gruetter, R., *Automatic, localized in vivo adjustment of all first- and second-order shim coils.* Magn Reson Med, 1993. **29**(6): p. 804-11.
136. Mueggler, T., et al., *Bicuculline-induced brain activation in mice detected by functional magnetic resonance imaging.* Magn Reson Med, 2001. **46**(2): p. 292-8.
137. Verhaegen, M.J., et al., *Cerebral autoregulation during moderate hypothermia in rats.* Stroke, 1993. **24**(3): p. 407-14.
138. Nau, C. and G.K. Wang, *Interactions of local anesthetics with voltage-gated Na+ channels.* J Membr Biol, 2004. **201**(1): p. 1-8.
139. Nakamura, T., et al., *The critical role of concentration for lidocaine block of peripheral nerve in vivo: studies of function and drug uptake in the rat.* Anesthesiology, 2003. **99**(5): p. 1189-97.
140. Kindler, C.H., C.S. Yost, and A.T. Gray, *Local Anesthetic Inhibition of Baseline Potassium Channels with Two Pore Domains in Tandem.* Anesthesiology, 1999. **90**(4): p. 1092-1102.
141. Olschewski, A., et al., *Enhancement of delayed-rectifier potassium conductance by low concentrations of local anaesthetics in spinal sensory neurones.* Br J Pharmacol, 2002. **136**(4): p. 540-9.

142. Leffler, A., et al., *The vanilloid receptor TRPV1 is activated and sensitized by local anesthetics in rodent sensory neurons.* J Clin Invest, 2008. **118**(2): p. 763-76.
143. Pernia-Andrade, A.J., et al., *Spinal endocannabinoids and CB1 receptors mediate C-fiber-induced heterosynaptic pain sensitization.* Science, 2009. **325**(5941): p. 760-4.
144. Marsicano, G., et al., *The endogenous cannabinoid system controls extinction of aversive memories.* Nature, 2002. **418**(6897): p. 530-4.
145. Leite, C.E., et al., *Rimonabant: an antagonist drug of the endocannabinoid system for the treatment of obesity.* Pharmacol Rep, 2009. **61**(2): p. 217-24.
146. Lee, K.S., et al., *Sodium current depression by lidocaine and quinidine in isolated ventricular cells.* Nature, 1981. **291**(5813): p. 325-7.
147. Bean, B.P., C.J. Cohen, and R.W. Tsien, *Lidocaine block of cardiac sodium channels.* The Journal of General Physiology, 1983. **81**(5): p. 613-642.
148. Hondeghem, L.M. and B.G. Katzung, *Antiarrhythmic Agents: The Modulated Receptor Mechanism of Action of Sodium and Calcium Channel-Blocking Drugs.* Annual Review of Pharmacology and Toxicology, 1984. **24**(1): p. 387-423.
149. Fioravanti, B., et al., *Constitutive Activity at the Cannabinoid CB1 Receptor Is Required for Behavioral Response to Noxious Chemical Stimulation of TRPV1: Antinociceptive Actions of CB1 Inverse Agonists.* J. Neurosci., 2008. **28**(45): p. 11593-11602.
150. Hermann, H., et al., *Dual effect of cannabinoid CB1 receptor stimulation on a vanilloid VR1 receptor-mediated response.* Cellular and Molecular Life Sciences, 2003. **60**(3): p. 607-616.
151. Endo, T., et al., *Reorganization of sensory processing below the level of spinal cord injury as revealed by fMRI.* Experimental Neurology, 2008. **209**(1): p. 155-160.
152. Catterall, W.A., *From Ionic Currents to Molecular Mechanisms: The Structure and Function of Voltage-Gated Sodium Channels.* Neuron, 2000. **26**(1): p. 13-25.
153. Wood, J.N., et al., *Voltage-gated sodium channels and pain pathways.* Journal of Neurobiology, 2004. **61**(1): p. 55-71.
154. Ritchie, J.M. and R.B. Rogart, *The binding of saxitoxin and tetrodotoxin to excitable tissue.* Rev Physiol Biochem Pharmacol, 1977. **79**: p. 1-50.
155. Waxman, S.G., et al., *Diverse functions and dynamic expression of neuronal sodium channels.* Novartis Found Symp, 2002. **241**: p. 34-51; discussion 51-60.
156. Waxman, S.G., et al., *Sodium channels, excitability of primary sensory neurons, and the molecular basis of pain.* Muscle Nerve, 1999. **22**(9): p. 1177-87.
157. Wood, J.N., et al., *Sodium channels in primary sensory neurons: relationship to pain states.* Novartis Found Symp, 2002. **241**: p. 159-68; discussion 168-72, 226-32.
158. Nagy, I. and H. Rang, *Noxious heat activates all capsaicin-sensitive and also a sub-population of capsaicin-insensitive dorsal root ganglion neurons.* Neuroscience, 1999. **88**(4): p. 995-7.

159. Caterina, M.J., et al., *A capsaicin-receptor homologue with a high threshold for noxious heat.* Nature, 1999. **398**(6726): p. 436-441.
160. Peier, A.M., et al., *A Heat-Sensitive TRP Channel Expressed in Keratinocytes.* Science, 2002. **296**(5575): p. 2046-2049.
161. Arendt-Nielsen, L. and A.C.N. Chen, *Lasers and other thermal stimulators for activation of skin nociceptors in humans.* Neurophysiologie Clinique/Clinical Neurophysiology, 2003. **33**(6): p. 259-268.
162. Yarnitsky, D., et al., *Heat pain thresholds: normative data and repeatability.* Pain, 1995. **60**(3): p. 329-332.
163. Frazier, D.T., T. Narahashi, and M. Yamada, *The site of action and active form of local anesthetics. II. Experiments with quaternary compounds.* J Pharmacol Exp Ther, 1970. **171**(1): p. 45-51.
164. Strichartz, G.R., *The inhibition of sodium currents in myelinated nerve by quaternary derivatives of lidocaine.* J Gen Physiol, 1973. **62**(1): p. 37-57.
165. Cahalan, M.D. and W. Almers, *Interactions between quaternary lidocaine, the sodium channel gates, and tetrodotoxin.* Biophys J, 1979. **27**(1): p. 39-55.
166. Narahashi, T., J.W. Moore, and R.N. Poston, *Anesthetic blocking of nerve membrane conductances by internal and external applications.* J Neurobiol, 1969. **1**(1): p. 3-22.
167. Binshtok, A.M., B.P. Bean, and C.J. Woolf, *Inhibition of nociceptors by TRPV1-mediated entry of impermeant sodium channel blockers.* Nature, 2007. **449**(7162): p. 607-610.
168. Qu, Y., et al., *Molecular determinants of drug access to the receptor site for antiarrhythmic drugs in the cardiac Na+ channel.* Proc Natl Acad Sci U S A, 1995. **92**(25): p. 11839-43.
169. Ries, C.R., et al., *QX-314 Produces Long-lasting Local Anesthesia Modulated by Transient Receptor Potential Vanilloid Receptors in Mice.* Anesthesiology, 2009. **111**(1): p. 122-126 10.1097/ALN.0b013e3181a9160e.
170. Lim, T.K., et al., *The quaternary lidocaine derivative, QX-314, produces long-lasting local anesthesia in animal models in vivo.* Anesthesiology, 2007. **107**(2): p. 305-11.
171. Gavva, N.R., et al., *The vanilloid receptor TRPV1 is tonically activated in vivo and involved in body temperature regulation.* J Neurosci, 2007. **27**(13): p. 3366-74.
172. Lee, S.Y., et al., *Sensitization of vanilloid receptor involves an increase in the phosphorylated form of the channel.* Arch Pharm Res, 2005. **28**(4): p. 405-12.
173. Ahern, G.P., et al., *Extracellular Cations Sensitize and Gate Capsaicin Receptor TRPV1 Modulating Pain Signaling.* J. Neurosci., 2005. **25**(21): p. 5109-5116.
174. Woolf, C.J., et al., *Towards a mechanism-based classification of pain?* Pain, 1998. **77**(3): p. 227-9.

175. Woolf, C.J. and M.B. Max, *Mechanism-based pain diagnosis: issues for analgesic drug development.* Anesthesiology, 2001. **95**(1): p. 241-9.
176. Costigan, M., J. Scholz, and C.J. Woolf, *Neuropathic pain: a maladaptive response of the nervous system to damage.* Annu Rev Neurosci, 2009. **32**: p. 1-32.
177. May, A., *Chronic pain may change the structure of the brain.* Pain, 2008. **137**(1): p. 7-15.
178. Vierck, C.J., P.T. Hansson, and R.P. Yezierski, *Clinical and pre-clinical pain assessment: are we measuring the same thing?* Pain, 2008. **135**(1-2): p. 7-10.
179. Meyer, R.A., J.N. Campbell, and S.R. Raja, eds. *Peripheral neural mechanisms of nociception*. Textbook of pain, ed. P. Wall and R. Melzack. 1994, Churchill Livingstone: Edinburgh. 13-44.
180. Torebjork, E., *Human microneurography and intraneural microstimulation in the study of neuropathic pain.* Muscle Nerve, 1993. **16**(10): p. 1063-5.
181. Hajnal, J.V., et al., *Artifacts due to stimulus correlated motion in functional imaging of the brain.* Magn Reson Med, 1994. **31**(3): p. 283-91.
182. Hagino, H., et al., *Effects of D2 dopamine receptor agonist and antagonist on brain activity in the rat assessed by functional magnetic resonance imaging.* Brain Res, 1998. **813**(2): p. 367-73.
183. Dubowitz, D.J., et al., *Functional magnetic resonance imaging in macaque cortex.* Neuroreport, 1998. **9**(10): p. 2213-8.
184. Ludwig, R., et al., *A dual RF resonator system for high-field functional magnetic resonance imaging of small animals.* J Neurosci Methods, 2004. **132**(2): p. 125-35.
185. Ferris, C.F. and C.T. Snowdon, *Functional magnetic resonance imaging in conscious marmoset monkeys: methods and applications in neuroscience research*, in *The Laboratory Primate: Handbook of Experimental Animals*, W.-C. S., Editor. 2005, Elsevier Science: Amsterdam.
186. Logothetis, N.K., et al., *Functional imaging of the monkey brain.* Nat Neurosci, 1999. **2**(6): p. 555-62.
187. Brammer, A., C.D. West, and S.L. Allen, *A comparison of propofol with other injectable anaesthetics in a rat model for measuring cardiovascular parameters.* Lab Anim, 1993. **27**(3): p. 250-7.
188. Fox, P.T. and M.E. Raichle, *Focal physiological uncoupling of cerebral blood flow and oxidative metabolism during somatosensory stimulation in human subjects.* Proc Natl Acad Sci U S A, 1986. **83**(4): p. 1140-4.
189. Capecchi, M.R., *Altering the genome by homologous recombination.* Science, 1989. **244**(4910): p. 1288-92.
190. Capecchi, M.R., *The new mouse genetics: altering the genome by gene targeting.* Trends Genet, 1989. **5**(3): p. 70-6.

191. Koller, B.H. and O. Smithies, *Altering genes in animals by gene targeting.* Annu Rev Immunol, 1992. **10**: p. 705-30.
192. Lacroix-Fralish, M.L., J.B. Ledoux, and J.S. Mogil, *The Pain Genes Database: An interactive web browser of pain-related transgenic knockout studies.* Pain, 2007. **131**(1-2): p. 3 e1-4.
193. Kola, I. and J. Landis, *Can the pharmaceutical industry reduce attrition rates?* Nat Rev Drug Discov, 2004. **3**(8): p. 711-5.
194. Price, D.D., et al., *The validation of visual analogue scales as ratio scale measures for chronic and experimental pain.* Pain, 1983. **17**(1): p. 45-56.
195. Mogil, J.S., *Animal models of pain: progress and challenges.* Nat Rev Neurosci, 2009. **10**(4): p. 283-294.
196. Braz, J.M., et al., *Parallel "pain" pathways arise from subpopulations of primary afferent nociceptor.* Neuron, 2005. **47**(6): p. 787-93.
197. Mogil, J.S., K. Simmonds, and M.J. Simmonds, *Pain research from 1975 to 2007: a categorical and bibliometric meta-trend analysis of every Research Paper published in the journal, Pain.* Pain, 2009. **142**(1-2): p. 48-58.
198. Mogil, J.S. and J.E. Grisel, *Transgenic studies of pain.* Pain, 1998. **77**(2): p. 107-128.
199. Crawley, J.N., *Unusual behavioral phenotypes of inbred mouse strains.* Trends Neurosci, 1996. **19**(5): p. 181-2; discussion 188-9.
200. Mayford, M., et al., *Memory and behavior: a second generation of genetically modified mice.* Curr Biol, 1997. **7**(9): p. R580-9.
201. Brocard, J., et al., *Spatio-temporally controlled site-specific somatic mutagenesis in the mouse.* Proc Natl Acad Sci U S A, 1997. **94**(26): p. 14559-63.
202. Furth, P.A., et al., *Temporal control of gene expression in transgenic mice by a tetracycline-responsive promoter.* Proc Natl Acad Sci U S A, 1994. **91**(20): p. 9302-6.
203. Gu, H., et al., *Deletion of a DNA polymerase beta gene segment in T cells using cell type-specific gene targeting.* Science, 1994. **265**(5168): p. 103-6.
204. Foulkes, T. and J.N. Wood, *Pain genes.* PLoS Genet, 2008. **4**(7): p. e1000086.
205. Yang, Y., et al., *Mutations in SCN9A, encoding a sodium channel alpha subunit, in patients with primary erythermalgia.* J Med Genet, 2004. **41**(3): p. 171-4.
206. Rice, A.S.C., et al., *Animal models and the prediction of efficacy in clinical trials of analgesic drugs: A critical appraisal and call for uniform reporting standards.* Pain, 2008. **139**(2): p. 243-247.
207. Lariviere, W.R., E.J. Chesler, and J.S. Mogil, *Transgenic Studies of Pain and Analgesia: Mutation or Background Genotype?* Journal of Pharmacology and Experimental Therapeutics, 2001. **297**(2): p. 467-473.
208. Mogil, J.S., et al., *Sex differences in thermal nociception and morphine antinociception in rodents depend on genotype.* Neurosci Biobehav Rev, 2000. **24**(3): p. 375-89.

209. Crawley, J.N., et al., *Behavioral phenotypes of inbred mouse strains: implications and recommendations for molecular studies.* Psychopharmacology (Berl), 1997. **132**(2): p. 107-24.
210. Taylor, B.A., *Genetic relationships between inbred strains of mice.* J Hered, 1972. **63**(2): p. 83-6.
211. Andersson, D.A., H.W.N. Chase, and S. Bevan, *TRPM8 Activation by Menthol, Icilin, and Cold Is Differentially Modulated by Intracellular pH.* J. Neurosci., 2004. **24**(23): p. 5364-5369.
212. Allchorne, A.J., D.C. Broom, and C.J. Woolf, *Detection of cold pain, cold allodynia and cold hyperalgesia in freely behaving rats.* Mol Pain, 2005. **1**: p. 36.
213. Wang, L.X. and Z.J. Wang, *Animal and cellular models of chronic pain.* Adv Drug Deliv Rev, 2003. **55**(8): p. 949-65.
214. Basser, P.J. and D.K. Jones, *Diffusion-tensor MRI: theory, experimental design and data analysis – a technical review.* NMR in Biomedicine, 2002. **15**(7-8): p. 456-467.
215. Lu, H., et al., *Synchronized delta oscillations correlate with the resting-state functional MRI signal.* Proc Natl Acad Sci U S A, 2007. **104**(46): p. 18265-9.
216. Pawela, C.P., et al., *Resting-state functional connectivity of the rat brain.* Magn Reson Med, 2008. **59**(5): p. 1021-9.
217. Zhao, F., et al., *BOLD study of stimulation-induced neural activity and resting-state connectivity in medetomidine-sedated rat.* NeuroImage, 2008. **39**(1): p. 248-60.
218. Brieu, N., et al., *Characterization of the hemodynamic response in the rat lumbar spinal cord using intrinsic optical imaging and laser speckle.* Journal of Neuroscience Methods, 2010. **191**(2): p. 151-157.
219. Lawrence, J., P.W. Stroman, and K.L. Malisza, *Comparison of functional activity in the rat cervical spinal cord during alpha-chloralose and halothane anesthesia.* NeuroImage, 2007. **34**(4): p. 1665-1672.
220. Malisza, K.L. and P.W. Stroman, *Functional imaging of the rat cervical spinal cord.* Journal of Magnetic Resonance Imaging, 2002. **16**(5): p. 553-558.
221. Pórszász, R., et al., *Signal changes in the spinal cord of the rat after injection of formalin into the hindpaw: Characterization using functional magnetic resonance imaging.* Proceedings of the National Academy of Sciences of the United States of America, 1997. **94**(10): p. 5034-5039.

Acknowledgements

Many people have contributed to the success of my PhD thesis in one way or another. I would like to thank everyone that supported me during the past four years. My special thanks go to:

- Prof. Markus Rudin, group leader and my supervisor. Thank you for giving me the opportunity to perform research in a very stimulating environment. I highly appreciated your scientific and personal support during this time. You always encouraged me to follow my ideas and projects, and your enthusiasm and knowledge helped to overcome any difficulties.

- Prof. Hanns Ulrich Zeilhofer and Prof. John N. Wood, co-referees. Thank you for your interest in my scientific work and for taking the time to act as co-referees. I appreciated our scientific discussions and was always thankful for your input.

- Christof Baltes. I was very fortunate to work with and learn from you. Thank you for teaching me physics, electrical engineering and sometimes even biology. I am very grateful for all our scientific and personal discussions and enjoyed our collaborations.

- Thomas Mueggler. Thank you for introducing me to mouse fMRI and teaching me all I needed to know about preparing mice.

- AIC Group. I would like to thank all members of the Rudin-Group at the Animal Imaging Center for the support and nice working atmosphere.

- Bruno Willi, IT services. Thank you for your competent IT support and your emergency operations, which many times prevented my computer from being thrown out the window.

- Markus Küpfer, workshop. Thank you for manufacturing all requested devices and parts which often were crucial for the experiments. I am also very thankful for all the repairs you carried out, ensuring ongoing scientific activities in the lab.

- The project was founded by the National Center of Competence in Research (NCCR) 'Neural Plasticity and Repair'.

- Florian, danke für die vielen Sportstunden und Mittagessen, die immer für die nötige Auflockerung und Ablenkung sorgten.

- Aileen, Birgit, Margarete, Many, Jürg; vielen Dank für die (moralische) Unterstützung, die Ablenkung und die Aufmunterungen, die mich immer wieder neu motivieren konnten.

- René und Christian; das gemeinsame ‚Dampfablassen' beim Klettern sowie Eure unkonventionellen Lösungsansätze waren mir immer sehr wichtig. Vielen Dank für Eure Unterstützung!

- Erich; herzlichen Dank für den musikalischen und geisteswissenschaftlichen Ausgleich den Du mir die ganzen Jahre lang geboten hast, sowie für unsere langen Diskussionen.

- Meinen Eltern Maja und Siegfried Bosshard möchte ich für die kontinuierliche Unterstützung danken.

- Cariño – Graçias!